3 PHYSICAL PROCESSES

Convenor: Dr. Alan Brandt

Toward a Sustainable Coastal Watershed:
The Chesapeake Experiment. Proceedings of a Conference
1-3 June 1994. Norfolk, VA
Chesapeake Research Consortium Publication No. 149

PHYSICAL PROCESSES IN THE CHESAPEAKE BAY AND THEIR BIO-CHEMICAL EFFECTS

Alan Brandt
The Johns Hopkins University

INTRODUCTION AND DISCUSSION

In Chesapeake Bay, as in other bodies of water, a wide range of physical processes exist, ranging from the long-term residual circulation to short- period bursts of turbulent mixing events, lasting minutes or less. When the Bay is stratified, internal waves are present, as are intrusive and frontal processes. Additionally, transient, short-term forcing events, such as storms and the spring runoff, cause rapid changes in the physical dynamics of the Bay. Each of these physical processes can affect the transport, distribution, and dynamics of the Bay's biology and sediment, nutrient, and toxic loadings. For example, the residual circulation results in the upstream transport of plankton biomass while the internal wave field affects the vertical distribution and horizontal density of the biomass.

Efforts to improve the quality of the Bay clearly must focus, as they do, on the bioecological and chemical (nutrient, oxygen, toxics) issues. The role of physical processes, however, is pervasive in that the transport, distribution, and production of the biological and chemical constituents is, to a large extent, controlled by the Bay's physical processes.

The general, tidally averaged circulation of the Bay has been extensively studied and modeled, and used to drive the Bay water quality model that has played a major role in the understanding and determination of the state of the Bay (Linker and Neumiller 1995). The long-term, two-layer transport of plankton, which plays a key role in the ecology of the Bay, is also now well-known and understood (Tyler and Seliger 1978).

Somewhat less known are the nature and role of the supertidal processes, including turbulent mixing, dispersion, internal waves, and surface layer entrainment. These high-frequency and often intermittent events are directly responsible for biochemical mixing, aggregation, and vertical transport and contribute substantially to small-scale plankton-plankton and plankton-nutrient encounter and feeding rates. Figure 1, from our studies of the small-scale, mid-Bay processes (Brandt et al. 1986), illustrates several of these processes: vertical advection by large amplitude internal waves (A); enhanced mixing resulting from the overturning of the internal waves (B); and the enhanced concentration of plankton patches in the convergent regions between internal wave crests (C).

Other important small-scale processes are boundary mixing (Salmun 1995), persistent homogenous layers (Sarabun and Frizzell - Makowski 1995), and tidal fronts (Sarabun 1993).

Our degree of understanding of the plethora of physical, biological, and chemical marine processes has proceeded in stages. The relative compactness of physical processes as compared to the broad diversity of biological species, stages, and biochemical interactions has resulted in a higher degree of quantitative understanding in the physical domain. Nevertheless, as these fields progress, the need for interdisciplinary considerations to further our understanding is clearly increasing. Figure 2 illustrates the evolution of the marine biophysical sciences. At present we are entering the second orders, nonlinear regime, where interdisciplinary biophysical interactions are necessary to further progress.

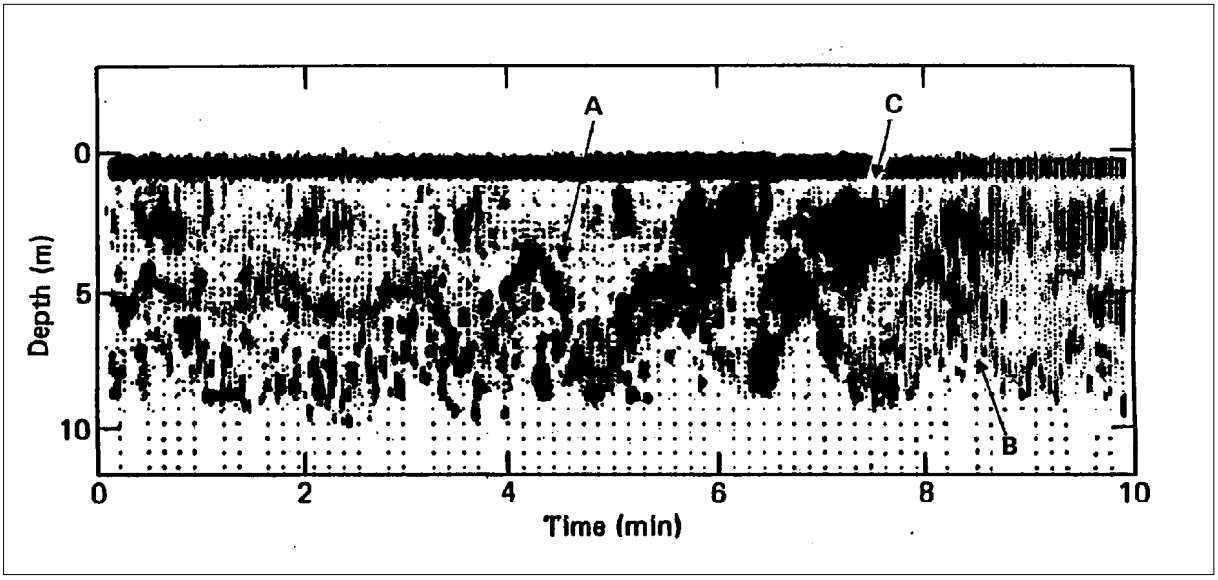

Figure 1. Evolution and overturning of internal waves in Chesapeake Bay. Data obtained from a downward looking 200 KHz acoustic fathometer station 858, just south of the Chesapeake Bay Bridge, 31 May 1984. Maximum wave amplitude is 4 m in water of 15 m depth. Dashed lines have been added to outline observed features from Brandt et al. (1986).

Problem Complexity	Era	Physical Oceanography	Biological Oceanography	Interdisciplinary Interactions
0th Order	Discovery	forces/ conservation laws	discovery/taxonomy	Not required
1st Order	Interactions	kinematics (sources/sinks/evolution)	morphology /food chains	Important
2nd Order	Non-linear	dynamics	???	Essential

Figure 2. Evolution of biophysical marine science.

At this juncture, there are five general issues in the physical domain that appear to be critical to furthering our understanding of the biogeochemical dynamics of the Chesapeake Bay (as well as other estuarine environments). they are:

- Estuary/ coastal ocean exchange.
- Dynamics of shallow water regions.
- Effects of transient events (e.g., storms) on mixing and stratification.
- Air/sea fluxes-particle and gas deposition
- Role of physical processes in plankton and larval ecology.

Aspects of the first issue are addressed by papers by Valle-Levinson (1995) and Wheless (1995). The Papers by Salmun (1995) and Sarabun and Frizzell-Makowski (1995) address the issues of physical mixing as relevant to biophysical interactions.

SUMMARY

In summary, we are entering an era when an understanding of biophysical interactions is necessary for further progress, and thus interdisciplinary cooperation is essential - a challenging and exciting time for estuarine science.

REFERENCES

Brandt, A., C.C. Sarabun, Jr. H.H. Seliger and M.A. Tyler. 1986. The Effects of the Broad Spectrum of Physical Activity on the Biological Processes in the Chesapeake Bay. In: Nihoul, J.C.J., ed. Marine Interfaces Ecohydrodynamics. Amsterdam: Elsevier Sci. Pub., 361-384.

Linker, L, and K. Newmiller. 1995. Transport of consenative traces in the Chesapeake Bay Water Quality Model. In: Toward a Sustainable coastal watershed: The Chesapeake experiment. Proceedings of a conference. Edgewater MD: Chesapeake Research Consortium, CRC publ.No.149

Salmun, H. 1995. Applicability of boundray mixing theory to the Chesapeake Bay. In: Toward a Sustainable coastal watershed: The Chesapeake experiment. Proceedings of a conference. Edgewater MD: Chesapeake Research Consortium, CRC publ.No.149

Sarabun, C.C. 1993. Observation of a Chesapeake Bay Tidal Front. Estuaries 16:68-73.

Sarabun Jr., C.C., and L. Frizzell-Makowski. 1995. Thin homogenous layers in the Chesapeake Bay In: Toward a Sustainable coastal watershed: The Chesapeake experiment. Proceedings of a conference. Edgewater MD: Chesapeake Research Consortium, CRC publ.No.149

Tyler, M.A., and H.H. Seliger. 1978. Annual sub surface transport of a red tide dinoflagellate to its bloom area: Water circulation patterns and organism distributions in the Chesapeake Bay. Limnol and Oceanograp. 23:227-246.

Valle-Levinson, A. 1995 Water exchange in the lower Chesapeake Bay. In: Toward a Sustainable coastal watershed: The Chesapeake experiment. Proceedings of a conference. Edgewater MD: Chesapeake Research Consortium, CRC publ.No.149

Wheless, G. H. 1995. Estuary/Shelf exchange variability due to synoptic-scale wind events and freswaters runoff: Implications for biological recruitment. In: Toward a Sustainable coastal watershed: The Chesapeake experiment. Proceedings of a conference. Edgewater MD: Chesapeake Research Consortium, CRC publ.No.149

Toward a Sustainable Coastal Watershed:
The Chesapeake Experiment. Proceedings of a Conference
1-3 June 1994. Norfolk, VA
Chesapeake Research Consortium Publication No. 149

THE LATERAL VARIATION OF THE SUBTIDAL SURFACE CURRENTS IN THE UPPER CHESAPEAKE BAY

Harry V. C. Wang
U.S. Army Corps of Engineers

Shenn-Yu Chao
Horn Point Environmental Laboratory

Abstract: A three-dimensional hydrodynamic model of upper Chesapeake Bay is used to examine the lateral variation of subtidal current in the middle reaches of the basin. The simulated circulation for the entire year of 1984 shows that surface current intensifies near the eastern boundary. Further investigation reveals that it is not the Coriolis force but the topography that is primarily responsible. The deep ship channel in the east allows the density and tidally induced subtidal currents to intensify over it, producing the eastern intensification. Density-induced forcing is predominantly baroclinic, generating a northward undercurrent in the deep channel and a southward current aloft that attenuates westward. Tidal forcing is mostly barotropic, producing southward mean current in the deep channel and a return flow to the west, resulting in current reversal over the shallow banks. Historical data lend support to these model results.

INTRODUCTION

The upper reaches of Chesapeake Bay (figure 1) are dominated by freshwater input from the Susquehanna River. Tidal forcing is modest, with tidal range rarely exceeding 1 m. Winds are generally episodic, with dominant periods ranging from 2 to 7 days. The region is of scientific interest owing to its large temporal and spatial variabilities resulting from the combined influences of river flux, wind stress, and channel geometry. Furthermore, concerns over the fate of the effluent discharged from the Hart-Miller dredged material containment facility (located at the mouth of the Back River) have raised practical interests in understanding how the current and circulation behave in the region.

Previous studies in upper Chesapeake Bay have been mostly focused on the variability occurred along the channel (longitudinal) direction. For example, Boicourt (1969), Elliott et al. (1978), Najarian et al. (1981), and Hamilton and Boicourt (1984) placed much emphasis on the longitudinal variability, following the classical paradigm that lateral variability may not be as important. However, Grano (1983) pointed out that large lateral variations do exist in the upper Bay. Figure 2, taken from Grano (1983), shows a cross section of subtidal currents in the upper Bay. The southward surface current intensifies over the deep channel to the east and a weak current reversal occurs over the shallow banks to the west. Figure 3, taken from Blumberg et al. (1991), shows the long-term (1977-83) average of near-surface currents in upper Chesapeake Bay. Mean currents of up to 15 cm/sec generally follow the eastern boundary southward. Weak reversals were also observed. The inadequacy of present knowledge in interpreting the nature and the cause of the lateral

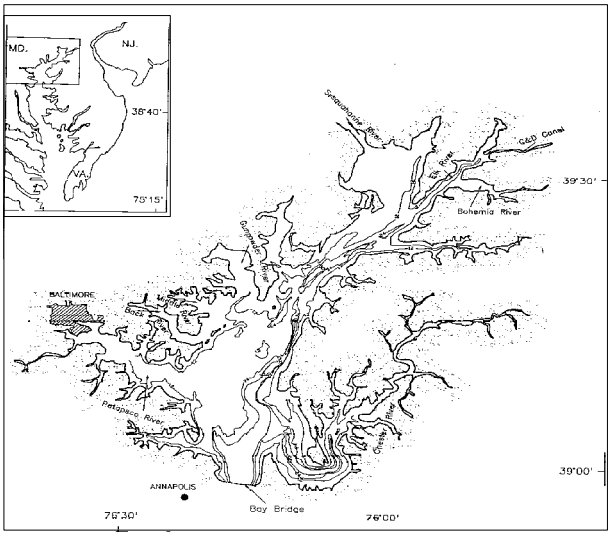

Figure 1. Location and bathymetry of upper Chesapeake Bay. The open boundary to the south is marked by a thick dashed line. Isobaths in feet.

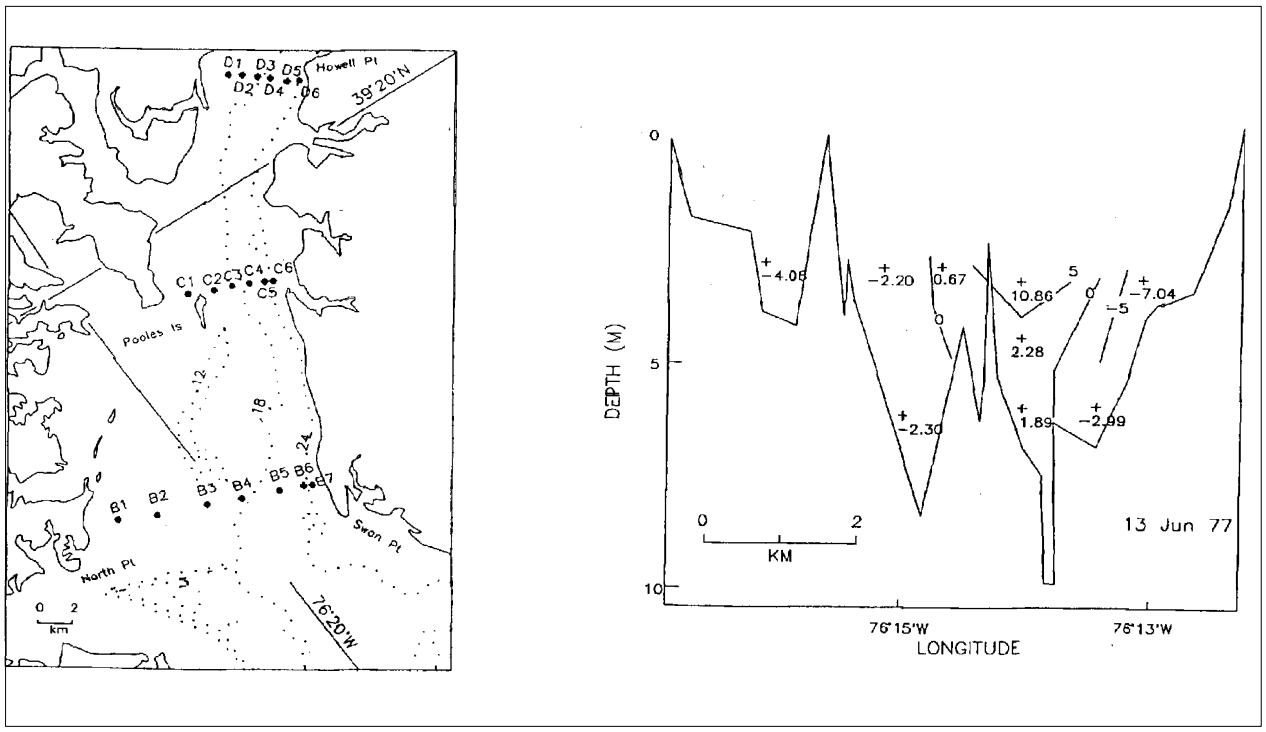

Figure 2. Map of upper Chesapeake Bay showing positions of the mooring station and the depth contour in feet (left column). Measured subtidal velocity (cm/sec) along section C (right column). Positive southward and negative northward. From Grano (1983).

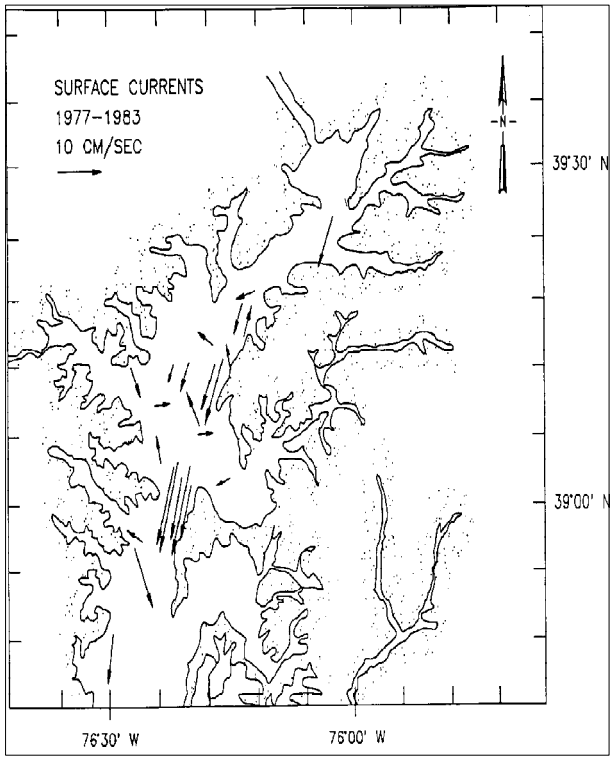

Figure 3. Measured near-surface mean currents averaged from 1977 to 1983. From Blumberg et al. (1991).

variation of the subtidal current motivated us to investigate the subject further.

A three-dimensional hydrodynamic model of upper Chesapeake Bay developed by Johnson et al. (1989) was used to simulate the circulation for the entire year of 1984.

MODEL DESCRIPTION

Under Boussinesq and hydrostatic approximations, the model solves for salinity, sea level elevation, and velocities in three dimensions. Horizontally, the basic equations are cast in a boundary-fitted curvilinear coordinate system to cope with the irregular shoreline configuration and the deep navigation channel. The nonuniform grid spacings generally range from 0.5 km to 2 km. There are up to 12 layers in the vertical with a uniform thickness of 5 ft, except the top layer thickness fluctuates with sea level. The vertical eddy viscosity and diffusivity are computed from mean flow and stratification characteristics using a second-order turbulence closure scheme developed by Donaldson (1973). A quadratic stress is exerted at the bottom, assuming the bottom boundary layer is logarithmic over a bottom roughness height of $z0 = 0.2$ cm.

The model solves external and internal modes

equations separately. The external mode consists of equations for the water surface elevation and vertically averaged flows in two horizontal directions. The internal mode computes vertical shear of horizontal velocities, vertical velocity, and salinity. Time steps for the external and internal modes are both set at 300 sec. The larger-than-normal time step for the external mode is made possible by an implicit solver that relaxes the stringent requirement for small time steps set by Courant-Friedrichs-Levy computational stability criterion. Further, as in many shallow water models with small horizontal grid spacings (e.g., Oey et al. 1985), the model does not require horizontal viscosity and diffusion to achieve computational stability. In our production runs made for 1984, we have set both A_H and K_H equal to 0.

CIRCULATION IN 1984

The model is initialized by the mean observed salinity field in January 1984, assuming a motionless state and no sea level deviation from the mean. Subsequently, the model is driven by hourly wind stress at the sea surface, by daily freshwater discharge from the Susquehanna River, and by hourly salinity distribution and water surface elevation on the southern open boundary. Hourly wind stress data were derived from the meteorological station at Baltimore-Washington International Airport. Daily discharge rate from the Susquehanna River was measured by the U.S. Geological Survey. Hourly salinity profile and water surface elevation on the open boundary were derived from the outputs of a larger-scale hydrodynamic model of the entire Chesapeake Bay (Johnson et al. 1991). The time series results generated by the present model compare quite favorably with several time series of observed salinity and tidal elevation at fixed locations. These comparisons were discussed in Johnson et al. (1989); details are not repeated here.

Figure 4 shows the daily discharge rate from the Susquehanna River for the entire year of 1984. Discharge was generally high from February to May, further enhanced by three isolated peaks of 5-10 days duration, but decreased markedly from June to December.

Figure 5 shows the model results of surface subtidal flow for 1984. When averaged over the last 5 days of each month to remove most of the tidally induced and meteorologically driven currents, the lateral variation in flow fields invariably emerges. Southward currents carry low salinity waters down-estuary and, upon reaching the middle reaches of the basin, intensify over the deep channel along the eastern boundary. Reverse

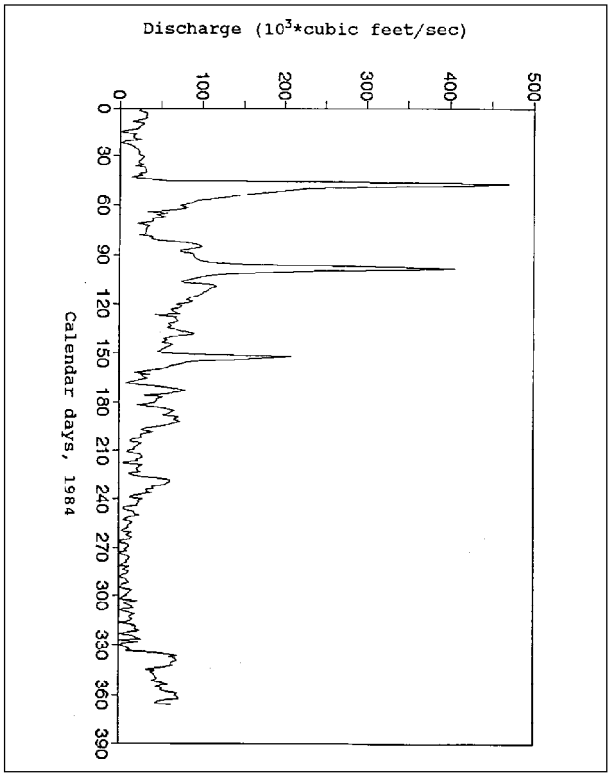

Figure 4. Daily Susquehanna River discharge in 1,000 ft³/sec for 1984.

currents occur over the shallow banks to the west of the deep channel. The eastern intensification over the deep channel and current reversal over the shallow banks are associated with the anticyclonic circulation prevalent in all months of the year. The degree of eastern intensification seems weakly proportional to the monthly discharge rate from the Susquehanna River. In keeping with the Susquehanna discharge rate, the annual march of saline water is southward from December to March, and northward from April to October as the freshwater discharge continues to decline. Figure 6 shows the 5-day averaged flow fields at the end of May and August at 25 ft depth. Up-estuary flow penetrates northward along the deep ship channel. The two-layered mean circulation over the deep channel was observed, and is typical of estuarine circulation dominated by river discharge.

CONCLUSION

A process of elimination has been conducted to identify the cause of the eastern intensification of the surface current in the middle reaches of the basin. Details were reported earlier (Wang and Chao 1995) and are not repeated here. Two mechanisms are identified to be primarily responsible: density-driven flow and tidally induced residual current.

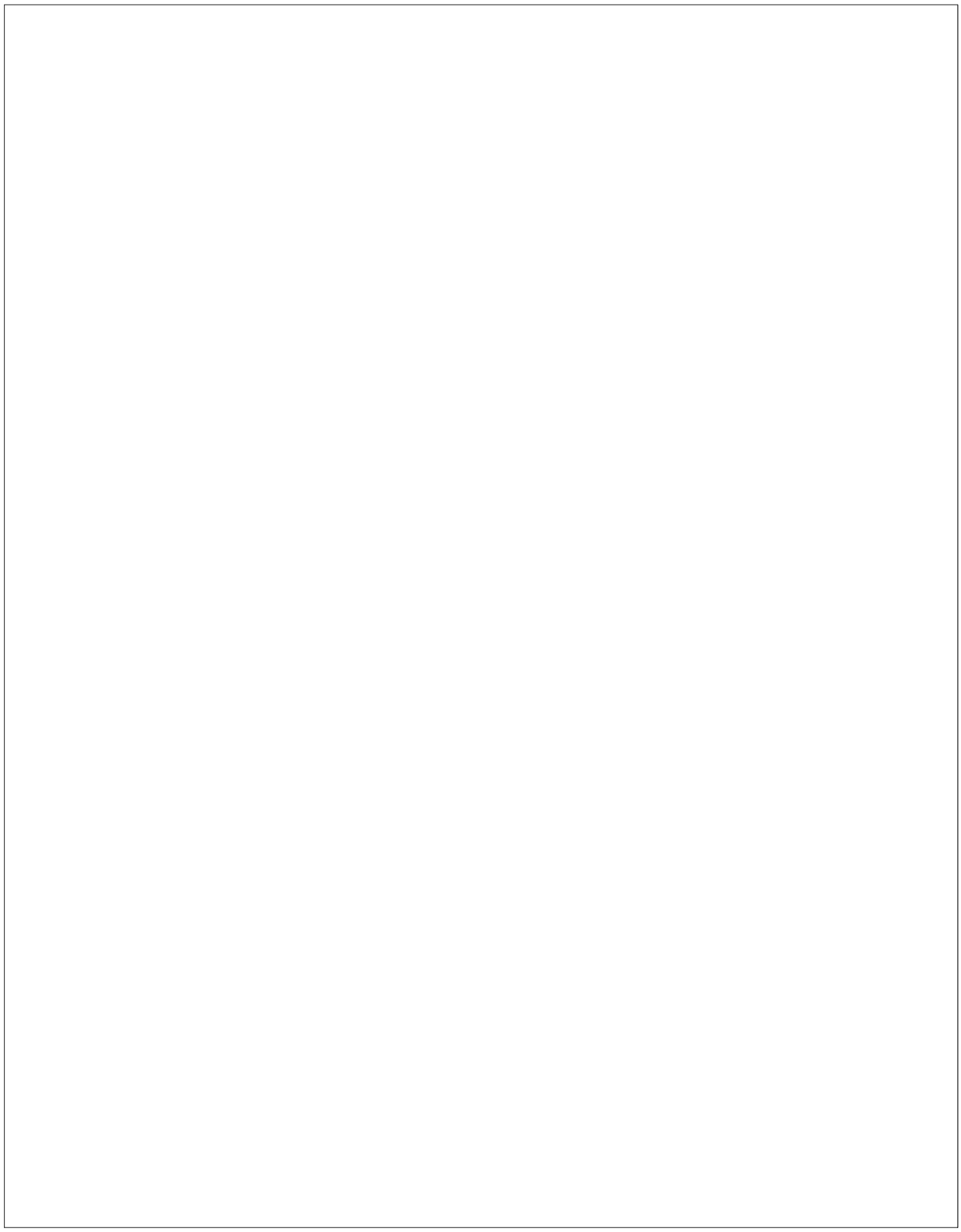

Figure 5. Model results of surface subtidal flow for January through December 1984. 5a. Model-produced near-surface flow over the period January-April 1984; the flow field is averaged over a 5-day period at the end of each month. **5b: May-August 1984. 5c: September-December 1984.**

Figure 5 continued

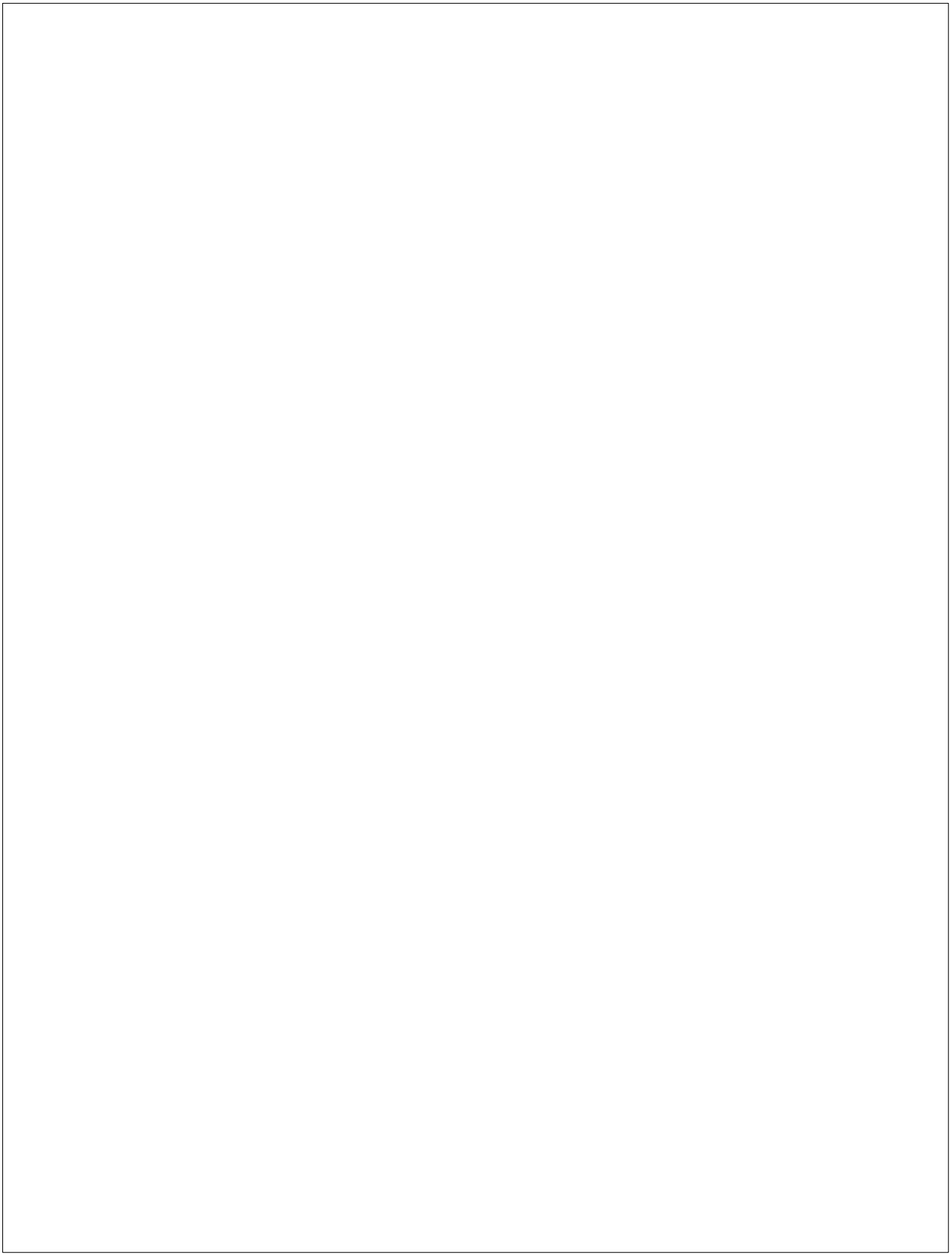

Figure 5 continued

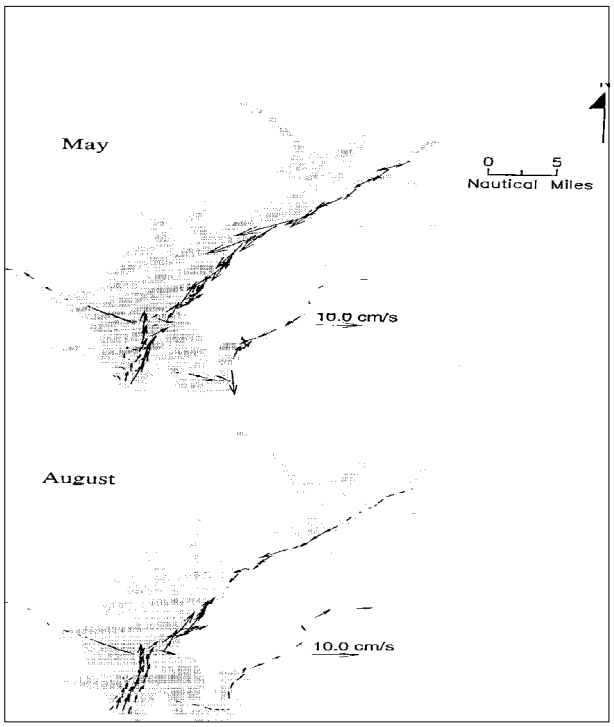

Figure 6. Model-produced 5-day averaged flow fields at 25 ft depth at the end of May (top) and August (bottom) of 1984.

Both enhance the southward mean current over the deep navigation channel along the eastern boundary of the basin. The density-induced pressure force, maintained by the freshwater discharge from the Susquehanna River, is quite baroclinic, inducing a generally southward surface current that intensifies near the eastern boundary and a return undercurrent in the deep channel. Current reversal does not occur over the shallow banks to the west of the deep channel. Tidal forcing, on the other hand, is quite barotropic, inducing a southward mean current in the deep channel and a return current over the shallow banks to the west. Both mechanisms persist in the nonrotating limit, suggesting that the earth's rotation does not play a crucial role.

ACKNOWLEDGEMENTS

H. Wang is indebted to Nauth Panday of the Maryland Department of Environment and Lamere Hennessee of the Maryland Geological Survey for their support in the Hart-Miller Islands environmental impact study. Permission was granted by the Office of Chief of Engineers, U.S. Army Corps of Engineers, to publish this information. S. Yu-Chao was supported by the National Science Foundation under grant no. BSR-8814272 as part of the Land Margin Ecosystem Research.

REFERENCES

Blumberg, A. F., W. H. Johnson, R. H. Heath, B. Hsieh, V. Pankow, K. W. Kim, and H. L. Butler, 1991. Data employed in the development of a three-dimensional, time-varying numerical hydrodynamic model of Chesapeake Bay. Vicksburg, MS: U. S. Army Corps of Engineeres, Waterways Experiment Station, Tech. Rep. No. HL-91-1, 222 pp.

Boicourt, W.C. 1969. A numerical model of the salinity distribution in upper Chesapeake Bay. Chesapeake Bay Insti. Tech. Rep. No. 54, 70 pp.

Donaldson, C. 1973. Atmospheric turbulence and dispersal of atmospheric pollutants. In: Haugen, D.A., ed. AMS workshop on micrometerology. Boston Science Press, 313-390.

Elliott, A.J., D-P Wang, and D.W. Pritchard. 1978. The circulation near the head of the Chesapeake Bay. J. Mar. Res., 36: 643-655.

Grano, V. 1983. On the non-tidal circulation of the Upper Chesapeake Bay. Ph.D. thesis. Baltimore: Johns Hopkins University 356 pp.

Hamilton, P., and W.C. Boicourt. 1984. Long-term salinity, temperature and current measurement in upper Chesapeake Bay. Annapolis: Maryland Dept. of Natural Resources, Power Plant Siting Program, PPRP 87, 106 pp.

Johnson, B. H., R. E. Heath, and K. W. Kim. 1989. Development of a three-dimensional hydrodynamic model of the Upper Chesapeake Bay. Final rep. submitted to Maryland Dept. of Natural Resources, Tidal Water Administration, 73 pp.

Johnson, B. H., R. E. Heath, B. B. Hsieh, K. W. Kim, H. L. Butler. 1991. Development and verification of a three-dimensional numerical hydrodynamic, salinity, and temperature model of Chesapeake Bay. Vicksburg, MS: U.S. Army Corps of Engineers, Waterways Experiment Station Tech. Rep. HL-91-7, 43 pp.

Najarian, T. O., D.P. Wang, and M.L. Thatcher. 1981. Upper Chesapeake Bay salinity study. Annapolis, Maryland, Dept. of Natural Resources, Power Plant Siting Program, PPRP-51, 42 pp.

Oey, L.-Y., G.L. Mellor, and R.I. Hires. 1985. A three-dimensional simulation of the Hudson-Raritan estuary. Part I: Description of the model and model simulations. J. Physical Oceanog15: 1676-1692.

Wang, H.V., and S.Y. Chao. 1995. Intensification of subtidal surface currents over a deep channel in the upper Chesapeake Bay. Estuarine, Coastal and Shelf Science (in press).

Toward a Sustainable Coastal Watershed:
The Chesapeake Experiment. Proceedings of a Conference
1-3 June 1994. Norfolk, VA
Chesapeake Research Consortium Publication No. 149

Recovery of Circulation and Forcing in Chesapeake Bay by Assimilation of Tide Gauge Observations

Y. H. Spitz and J. M. Klinck
Old Dominion University

Abstract: The recovery of the circulation in Chesapeake Bay is investigated by assimilating tide gauge observations into a vertically integrated, two-dimensional, shallow-water model. As part of the assimilation, the surface wind stress and bottom drag coefficients are adjusted to improve agreement with the data.

The data assimilation technique used for the parameter estimation is the variational method, which consists of minimizing the "distance" between the model and the sea level observations(i.e., the cost function). The computation of the gradient of the cost function, which is required by the considered minimization algorithm (i.e., the quasi-Newton method), is done using the adjoint of the forward model. In our case, the Fortran code of the adjoint model is directly obtained from the code of the linear version of the forward model. This technique has two main advantages: (1) it reduces the complexity of the construction of the adjoint model, and (2) it avoids the inconsistency that can arise from the derivation of the adjoint model followed by its discretization.

Several twin experiments using the model solutions as observations were done with a realistic bathymetry of Chesapeake Bay. These experiments also addressed the question of how many data points are needed around the Bay in order to recover the wind stress, the bottom friction, and the surface elevation in the interior of the domain.

Toward a Sustainable Coastal Watershed:
The Chesapeake Experiment. Proceedings of a Conference
1-3 June 1994. Norfolk, VA
Chesapeake Research Consortium Publication No. 149

APPLICABILITY OF BOUNDARY MIXING THEORY TO THE CHESAPEAKE BAY

Haydee Salmun
The Johns Hopkins University

Abstract : Boundary mixing theories have elucidated the manner in which mixing processes occuring near sloping boundaries can determine the flow structure in these active boundary regions. Namely, boundary processes drive secondary and tertiary recirculating flows that affect the stratification of the surrounding areas, enhance the effectiveness of the mixing, and provide a dynamic, framework for the analysis of transport phenomena. Boundary mixing has been investigated in experimental and modelling studies. Advances in the observations have also contributed to a more clear picture of the possible contributions of these processes to the overall state of mixing in large bodies of fluid. Recent works on boundary mixing that use a two-dimensional model, for example, have been able to derive an expression for the overall effective vertical diffusivity that yields the well-known values for oceanic and lake situations when realistic field parameters are considered. Although these estimates are derived somewhat indirectly, they strongly suggest the potential importance of boundary mixing and of pursuing such studies further.

The applicability of boundary mixing theories to the Chesapeake Bay environment is discussed. Results from a two-dimensional model for boundary mixing are reviewed and an oceanic application presented. This model is adapted to represent more closely the geophysical situation of an idealized cross section of an estuary, and is made time-dependent. The objective of these types of studies is to understand the boundary processes in themselves and to assess in more direct ways the consequences of small-scale motions and mixing processes on the hydrodynamics of the entire estuary.

INTRODUCTION AND DISCUSSION

The exchange of mass and properties across isopycnal surfaces, or vertical mixing, has a prominent role in the hydrodynamics of estuaries not only because it is an important element in the small-scale, turbulent processes but also because of its importance to the gyre-scale distribution of water properties. As water is exchanged between the surface and bottom layers, the potential energy of the system increases and horizontal differences in density and presure are generated. These differences, which drive the global circulation, are greater when the fluid is stratified.

Mixing can take place anywhere, and to some extent does, if the conditions are conducive. This is possible wherever inhomogeneities are encountered in the fluid body. For instance, mixing (horizontal and vertical) will occur in the middle of a lake if the fluid in the upper layer becomes colder and denser than the fluid immediately below, or in areas where internal waves can break. But the most vigorous and sustained mixing will take place in those regions of the fluid body where the flow is turbulent. This again may be anywhere given the appropriate conditions, but it is most certainly the case in the areas near boundaries, because in most geophysically relevant situations the flow around those areas is characteristically turbulent.

Mixing processes have been studied extensively, theoretically and experimentally. Yet, there have been few reported cases of field confirmation of a particular mechanism of vertical mixing in stratified fluids, and the applicability of modeling theory and laboratory descriptions of mixing processes occurring in nature has not yet been properly tested.

Mixing processes are small-scale and fast acting, so that they are indeed difficult to measure directly. Much of the information about them, by necessity, derives from extrapolation from laboratory experiments, inference, and process studies.

In a large, partially mixed estuary such as Chesapeake Bay, mixing may be

- Attributable to turbulence caused primarily by surface winds effects. This may result in deepening of the surface water layer by erosion as turbulence generated at the surface propa gates downward to the pycnocline leading to entrainment of the denser water in the quies cent layer below. Alternatively, wind effects at the surface generate a mean flow shear at the pycnocline and shear-induced instabilities lead to turbulence and local mixing there.
- Attributable to turbulence caused primarily by tides and secondarily by climatic conditions.
- Actively occuring across a salt-wedge interface;
- Local, owing to breaking of internal waves.
- Occurring along the bottom and side boundaries, that is, where the flow is most likely always turbulent.

The energy to drive the mixing near boundaries can, in fact, derive from some of the mechanisms mentioned above. The most immediate example is the tides generating the turbulence along boundaries; also, internal waves impinging on the boundaries, being reflected or breaking there, provides enough energy to drive boundary mixing. Gravity currents can drive these processes. Alternatively, wind effects plus rotation will drive lateral currents in the water that can be upwelling-favorable or downwelling-favorable to the dynamics of the boundary regions, and this seems to affect the mixing processes and the way that, in turn, these processes affect the surrounding areas (Trowbridge and Lentz 1991). We stress here that so far no conclusive field confirmation of these mechanisms has been obtained.

In the case of Chesapeake Bay, for instance, we can read in the *Mid-Atlantic Research Plan*, a comprehensive report developed by the Mid-Atlantic Regional Marine Research Program (1993), that "Mixing occurs by turbulence caused primarily by tidal action and secondary by climatic conditions."

On the other hand, an investigation using wind, current, and salinity data obtained over large areas of the Bay during the fall of 1981 and 1983 and the spring time of 1983 (Goodrich, et. al. 1987) indicated that wind-induced, not tide-induced, top-to-bottom mixing is a process occuring over large areas in the Bay and that it occurs frequently during fall, winter, and spring. The authors concluded that "In terms of mixing energy, wind stress appears to be the major time-dependent source in the Mid-Chesapeake and may be the dominant absolute source."

The first statement does not say much about the details of the mixing mechanisms but it clearly indicates that the energy driving the mixing is attributable to the tides, hence bottom effects are dominant in this picture, while the second attributes the generating mechanism to surface processes driving the mixing via shear instabilities at the pycnocline. Here we would wish to argue that so far a convincing argument about the persistent dominance of either mechanism/effect, everywhere at least, has not been made and to propose the exploration of alternatives.

Because of the difficulties with direct measurements and the resolution of these small-scale processes in comprehensive models, the emphasis has been on trying to parameterize the exchange coefficients of mass and momentum transfer in terms of bulk quantities. One such quantity is the Richardson number, Ri, which in shear flow is a relative measure of the destabilizing effects of shear (turbulence) and the stabilizing effects of the stratification in the fluid. It is possible to define more than one Ri number for the same fluid system, but these are always defined in terms of mean flow values (mean density and velocity gradients) and this effect blurs the distinction between the processes contributing to mixing, as different processes may result in similar averaged mean flows. The mean gradients of density and velocity may not be appropriate in many situations, and this should be kept in mind. Also, the emphasis of most of the work done on estuaries has been mainly on understanding the tidally averaged longitudinal circulation. Research indicates that the topographic interaction with the flow is capable of producing very variable (in time and space) mixing within the tidal cycle. In fact, the major mixing may be caused by processes acting over a relative small part of the tidal cycle and within a small part of the estuary, and attention should be devoted to these considerations.

In a review of tidally generated mixing in estuaries (Dyer 1988), it is stated that, after mixing in localized areas, "Advective processes could then carry the resulting salinity structure throughout the estuary. Consequently, alteration of the estuarine topography in one or two crucial areas may affect processes in the whole estuary, such as flushing and dispersal of pollutants and sedimentation patterns."

Although no mention is made about mixing at the boundaries, or about the advecting mechanism, it is implicit in the statement. And this is at the heart of boundary mixing theories: that localized, vigorous mixing can make an important contribution to the global state of mixing in estuaries and to estuarine dynamics, not just a localized impact as it would appear first. These ideas have been tested and pursued since 1966, after Walter Munk, (1966) firstly advanced them in an oceanographic context.

Munk's hypothesis has been explored in several studies that include field observations (Wunsch 1972, Armi 1978, Hogg, et al. 1978, Gregg and Sanford 1980, Lentz and Trowbridge 1991, and many others), laboratory experiments (Ivey and Corcos 1982, Thorpe 1982, Phillips, et al. 1986, Ivey 1987, Salmun and Phillips 1992, and others), and analytical and numerical studies (Thorpe 1987, Garrett 1991, Woods 1991, Salmun, et al. 1991, Imberger and Ivey 1992). Mixing at the boundaries may be the result of interactions between mean flows and the rough bottom or owing to the reflection of internal waves. When these waves are reflected off sloping boundaries the vertical shear is enhanced, leading to possible shear flow instabilities and wave breaking, providing significant amounts of energy to drive the mixing (Cacchione and Wunsch 1974, Stigebrant 1976, Garrett 1979b, Eriksen 1985, Ivey and Nokes 1989, and several others). Many other studies have concentrated also on the importance of boundary layer mixing in accounting for the overall mixing observed in estuaries, lakes, and fjords (Caldwell, et al. 1978, Marmorino, et al. 1980). Finally, the unsteady aspects of boundary mixing have only recently received attention (MacCready and Rhines 1991). When rotation is included, boundary mixing influences the interior velocity field as well. The temporal variability of mixing is clear in some recent field observations (Thorpe, et al.1990).

Boundary layer mixing may be an important process in accounting for the overall vertical mixing observed in estuaries, lakes, and near fjords. Probably the most important mechanism in lakes of small and medium size is that of boundary mixing (Fisher, et al.1979, Imberger and Patterson 1990.). In lakes, the boundary mixing is likely to be driven by either internal seiching or inflows. In a study of the thermal structure of Lake Tahoe (Caldwell, et al. 1978), it was observed that as the lake shore was approached, the profiles of temperature with depth exhibited an increased step-like structure, indicating an increased mixing of heat closer to the boundaries, a similar observation as that described in previous oceanographic studies. Analysis of a series of profiles of temperature with depth taken in Lake Michigan (Marmorino, et al.1980), showed that the data resembled the oceanic thermal structure observed previously and believed to be associated with warm-water intrusions. From this study, it was concluded that intrusive layers of anomalously warm or cold water with a vertical extent of 10 meters or less are common in Lake Michigan and are responsible for rather abrupt changes in the vertical profiles at one location.

Estuaries are shallow, confined bodies of fluids that are generally characterized by significant mean or tidal flows. Studies such as that of Partch and Smith (1978) however, have shown that a significant fraction of the tidally averaged vertical mixing may occur over a small portion of the tidal cycle and may be limited in spatial distribution. As mentioned earlier, vertical mixing in estuaries may be driven by boundary processes such as tidal interaction with the bottom or/and by surface effects such as mixing driven by the action of the wind. In addition, under appropriate conditions, internal vertical shear may be important (Goodrich et al.1987). These processes result in two layered systems in the case of top or bottom boundary mixing, or near-homogeneity in the vertical at some times of the year when wind-driven internal shear may be a more effective mechanism of inducing vertical overturning, hence destratification in the estuary. In the late spring under the influence of Susquehanna River flow, however, there is a homogeneous upper and lower layer separated by a pycnocline approximately 3 m thick. Under these conditions, mixing along the gradually sloping bed in the region where the pycnocline intersects the boundary and quasi-horizontal advection of mixed fluid along isopycnals may be at least as important as the other mixing mechanisms described above.

The Physical Mechanism

Consider the sketch shown in figure 1a. When a stably stratified fluid is bounded on the sides by a sloping boundary, there will be a net flow upslope right along the boundary because isopycnals, which are horizontal through the bulk of the fluid, must bend to meet the boundary at right angles, otherwise the condition of no normal flow through a rigid boundary would be violated. As isopycnals bend to meet the boundary, local lateral variations

of buoyancy are generated and it is in response to these variations, namely to balance them, that the net up-slope flow is set up (Phillips 1970). When the mixing is confined near boundaries, as is the case when the growth of a turbulent layer is limited by the stratification of the ambient fluid, the flow becomes bidirectional, again because of the local imbalance in buoyancy, with fluid near the wall moving up while fluid near the outer edge of the boundary layer moves downward. This is a shear-type flow inside the boundary layer that increases the dispersive characteristics of the flow beyond that attributable to turbulence alone, and while important because of this capacity to enhance dispersion and thus to help spread isopycnals apart inside the boundary layer, gives rise to a seconday circulation that is confined to the areas of the boundary layer and cannot "discharge" into the ambient fluid.

As heavier fluid is dispersed upward along the slope and lighter fluid downward, an overall buoyancy imbalance with the interior fluid is created, and this is even more so when the ambient stratification is significant, so that in the mean the fluid in the upper part of the boundary layer becomes heavier than the fluid in the interior at the same level while the boundary layer fluid in the lower areas becomes lighter than that in the interior at the same level. In an attempt to restore stratification, then, boundary fluid above the pycnocline tends to develop a slow downward motion while that in the lower parts moves slowly upward in the mean. This "tertiary" component of the circulation drives a convergent flow: fluid converges at about the level of the original pycnocline and intrudes into the interior (figure 1b), spreading the isopycnals apart there and producing the same effect as if local diffusion had been taking place. This is a very possible way in which mixing at boundaries can contribute to vertical mixing away from them. We note that the necessary condition for the tertiary circulation is that the density flux is divergent in the direction of the slope. This can occur when the stratification in the fluid departs significantly from the linear type, when the source of turbulence is inhomogeneous in the slope direction, or when the slope varies significantly over the domain of interest, to name only the most frequently encountered conditions in real situations.

It is clear now that the importance of boundary mixing is attributable to (1) the effect on the vertical distribution of density and other fluid properties in the interior of the fluid, away from

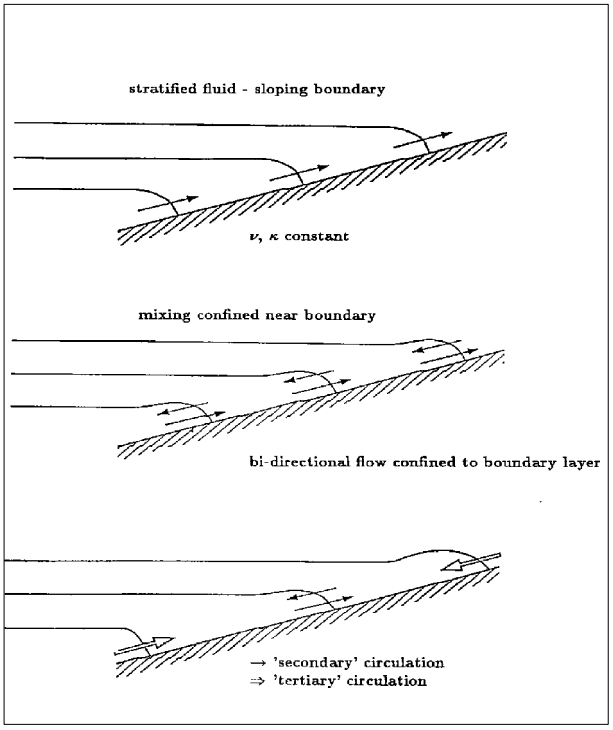

Figure 1a. Schematic of the distortion of isopycnals and resulting "secondary" flow near a sloping boundary for a uniformly, stably stratified fluid (top two panels) and "tertiary" flow for a variable interior stratification (bottom panel).

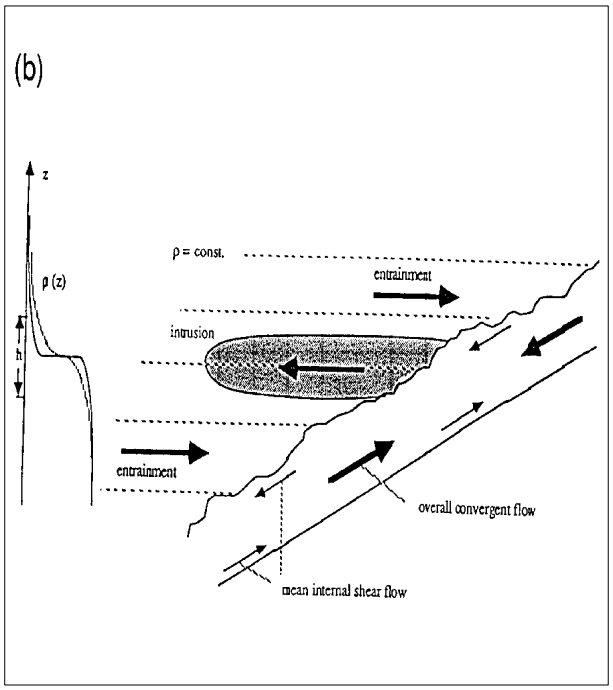

Figure 1b. A schematic diagram of the flow inside the boundary layer and the stratified ambient regions (from Salmun and Phillips 1992).

boundaries; (2) to the fact that it may be a process that tends to drive an interior circulation directly, not only indirectly via its contribution to vertical mixing; and (3) that its study may help understand and elucidate the mean flow in boundary regions, hence the associated transport phenomena there.

The Mathematical Model

Consider the turbulent boundary layer above a bed with constant slope 0 with respect to the horizontal, outside which the ambient fluid is stratified with p = p(z), as in figure 2. We assume that the internal time scales characteristic of the turbulence in the boundary layer are small compared to the characteristic time scales for the changes in both the ambient stratification and the flow generating the turbulence, and that the mechanism generating the turbulence is uniform along the slope. Then the induced mean flow in the turbulent boundary layer can be considered steady and two-dimensional in the (x,y) plane of figure 2.

Let the region of significant stratification in the ambient fluid extend over a vertical distance h, so that the distance up and down the slope over which the turbulent boundary layer modifies this stratification is L~h/sin 0 and the distance normal to the slope over which this stratification extents is Ly ~ h/cos 0. The boundary layer thickness scale is represented by H so that we can define the two ratios

$$E = \frac{H}{L} \sim \frac{H}{h} \sin 0 \ , \ A = \frac{H}{Ly} \sim \frac{H}{h} \cos 0.$$

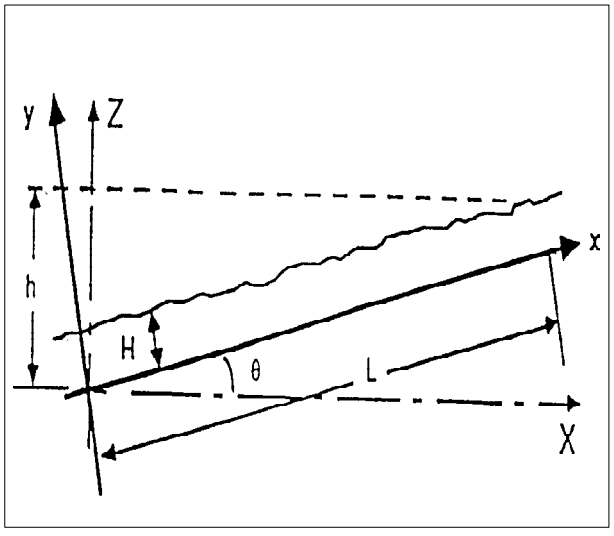

Figure 2. Definition of coordinate system for a two-dimensional model of boundary mixing.

E is the aspect ratio of the region which, for relatively small slopes, is « 1 but A is not necessarily small even for small slopes because H and h may be comparable. We assume that the turbulent fluxes of momentum and buoyancy can be expressed in terms of an eddy viscosity and an eddy diffusivity k that will be considered constant inside the boundary layer. In the regions surrounding the boundary layer, referred to as ambient or interior regions, the stratified fluid is not turbulent and the flow there is in essence inviscid and non-diffusive so that š, k = 0 when y > H. Let u and v denote the mean velocity components in the directions of the bed and normal to it and w the mean vorticity of the flow in the axial (or z direction) direction defined as usual by

$$w = \frac{n}{x} - \frac{u}{y}$$

By virtue of the incompressibility condition $.u = 0$, we can define the stream function y for the mean flow such that

$$u = \frac{y}{y} \ and \ v = -\frac{y}{x} \ and \ then \ w = - \ ^2 y \ .$$

The total mean buoyancy distribution, defined asB = -g(p -po)/po where po is the reference density, will be represented as the sum of two components B(x,y) = B(Z) + b(x,y) where b(x,y) represents the mean perturbation introduced in the basic field by the turbulence and B(Z) is the ambient buoyancy distribution. For the quasi-steady, two-dimensional mean flow in the boundary layer, we can then reduce the equations of motion to two: an equation for the mean vorticity and another for the mean buoyancy, which, with the assumptions and simplifications stated above, are

$$- y_{\ y}(\ ^2 y)_x + - y_{\ x}(\ ^2 y)_y = \cos 0 \, b_x - \sin 0 \, b_y - v \ ^4 y \ ,$$

$$y_{\ y} (n^2 \sin 0 + b_x) - y_{\ x} (N^2 \cos 0 + b_y) = k (n_z^2 + \ ^2 b)$$

where the subindex indicates partial differenciation and the buoyancy frequency N(Z) is given by N^{2} = Bz. These equations constitute a well-defined problem to be solved for ψ and b subject to the appropriate boundary conditions and a given ambient stratification N(Z). The boundary conditions are derived from requiring (a) no slip and no mass flux through the rigid boundary and from (b) integral considerations at the boundary determined by the outer edge of the boundary layer. These

conditions require (b1) continuity of the normal velocity component at the interface, (b2) continuity of the buoyancy flux across the turbulent boundary layer, and (b3) continuity of the tangential stresses across the interface between the turbulent and nonturbulent regions. The boundary conditions add the necessary six equations to close this system. When the set of equations is nondimensionalized using the characteristic scales for this flow, the resulting set contains two nondimensional parameters, E and A (defined above). The smallness of E allows for the neglect of all terms of O(E) or less while terms of O(A) are kept. This simplifies the problem, making it more tractable mathematically while keeping the major characteristics of the problem intact. To solve the problem, we assume that the background stratification (nondimensional) can be taken as a constant to leading order with a small perturbation. This choice of "forcing" term simplifies the problem further in that it allows the use of Fourier methods in the independent variable x, the direction of the slope. A detailed derivation and discussion of the equations, nondimensionalization, methods of solution, and results can be found in Salmun and Phillips (1992) and Salmun et al. (1991). Here, some of the salient results from this two-dimensional model are briefly summarized.

Figure 3 shows typical results obtained with this model where secondary and tertiary circulations inside the boundary layer can be appreciated. Figure 3a gives contours of the forcing function used in this run, one representing closely a two-layer type of stratification. Figure 3b shows contours of the stream function, which indicates that the circulation is indeed dominated by the secondary circulation although the slow overall convergent flow is clearly represented by the negative contour. The effect of this convergent flow, the tertiary circulation, is depicted in figure 3d, where the profile of the velocity component
normal to the slope shows two regions of inflow (fluid from the interior enters the boundary layer) above and below the level of maximum forcing, pycnocline level, and a region of outflow of boundary fluid at about the level of the pycnocline. Finally, figure 3c shows the contours of the buoyancy distribution b inside the boundary layer. These contours show that in all cases fluid near the wall gains buoyancy while fluid near the outer edge loses it; the asymmetry with respect to the original pycnocline level in the figure indicates the variation of b in the slope direction. All fluid near the wall gains buoyancy but it gains more above the pycnocline level than below it, and correspondingly, all fluid loses buoyancy at the edge of the layer but less buoyancy is lost by the fluid above the pycnocline level than by that below it. In other words, the isopycnals spread apart unevenly as one moves in the slope direction, and this is the basic mechanism that drives the tertiary circulation: the divergence of the density flux in the slope direction.

Figures 4 and 5 stress the qualitative agreement between laboratory experiments (Salmun and Phillips 1992) and model results. (Originally, data obtained in the numerical experiments were handled differently than data obtained from the laboratory experiments. As a result, plots of equivalent quantities look slightly different in both works. To facilitate visual comparison, the figures drawn from the model's results were inverted here so that they physically represent the same space as that in the laboratory setting but the labels on the axes of the figures are difficult to read.). The qualitative agreement is very good, especially considering the significant differences between the laboratory settings and the physical system addressed by the model. Figure 4 contrasts the measured buoyancy fluxes associated primarily with the secondary circulation in the laboratory case with the computed advective buoyancy flux. The qualitative agreement between the computed curve and the envelope of the point measurements is excellent. The plot shows that the downward transport of buoyancy increases with depth to a maximum at about the pycnocline level and decreases below this level, as does the vertical gradient of buoyancy. It is interesting to note that the model yielded a curve that depicts the same asymmetry about the level of maximum forcing; there is a weak transport below, but far away from the pycnocline, without a counterpart in the region above. Figure 5 compares values of volume flux measured in the experiments with a computed curve of WI(Z) that is proportional to the boundary layer volume flux in the model formulation, in that

$$WI(Z) \quad a \int_{H} y / \ _{y})dy = y(H).$$

The laboratory studies computed volume flux from measurements of the evolution of the ambient density (shown at the top of the figure). The volume flux thus measured is equal in magnitude but of opposite sign to the volume flux in the boundary layer, which is what is computed in the model. In figure 5, the level Z = 0 in the bottom plot corresponds to the level Z = Zo in the laboratory notation of the top plot. The qualitative agreement is depicted by the linearity of

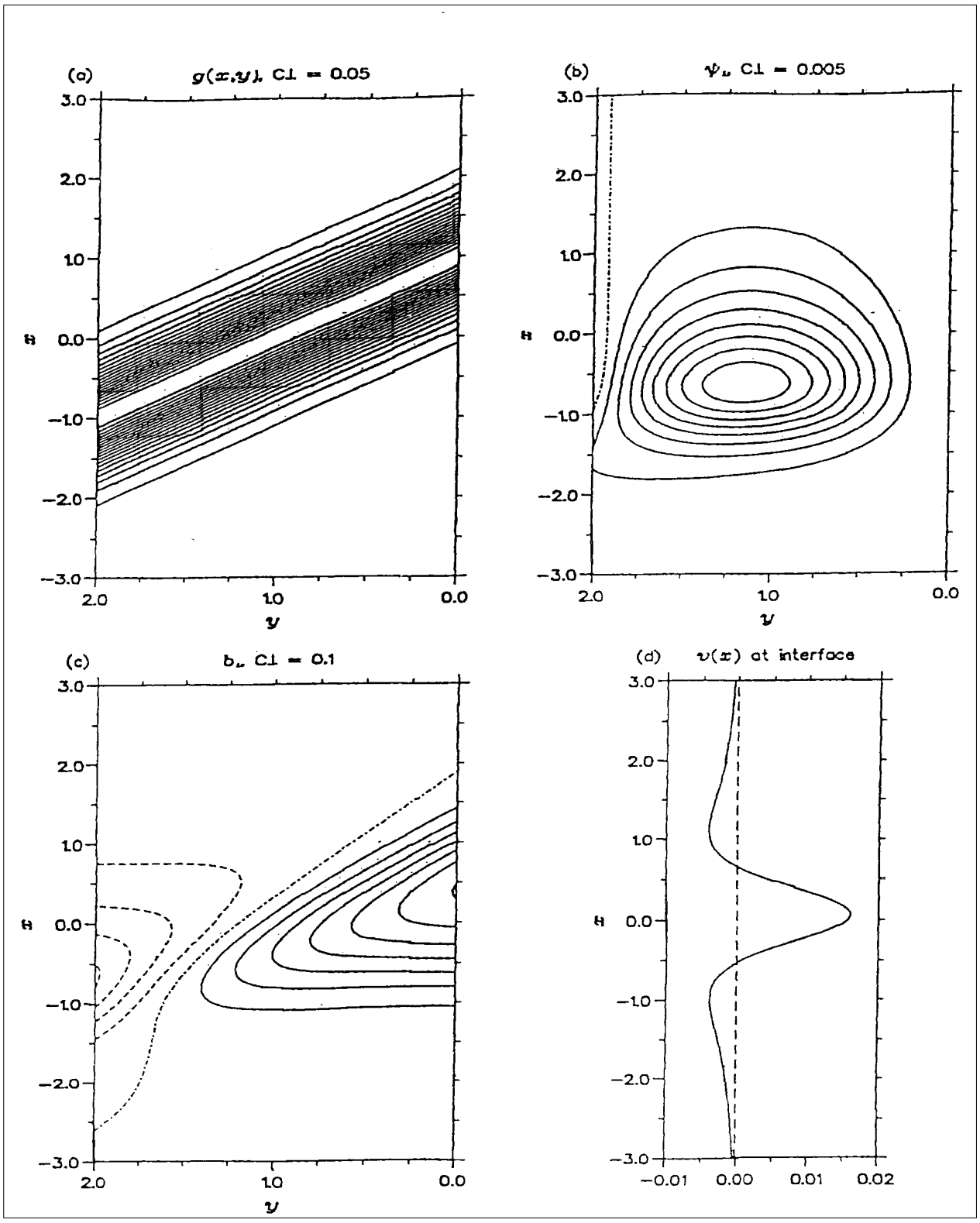

Figure 3. Typical results obtained with the model described in the text. (A) contours of the forcing function, which corresponds to a two-layer interior stratification; (B) contours of the perturbation stream function; (C) contours of the mean perturbation buoyancy field; and (D) the normal velocity field at the interface between the boundary layer and the ambient fluid (from Salmun, et al.1991).

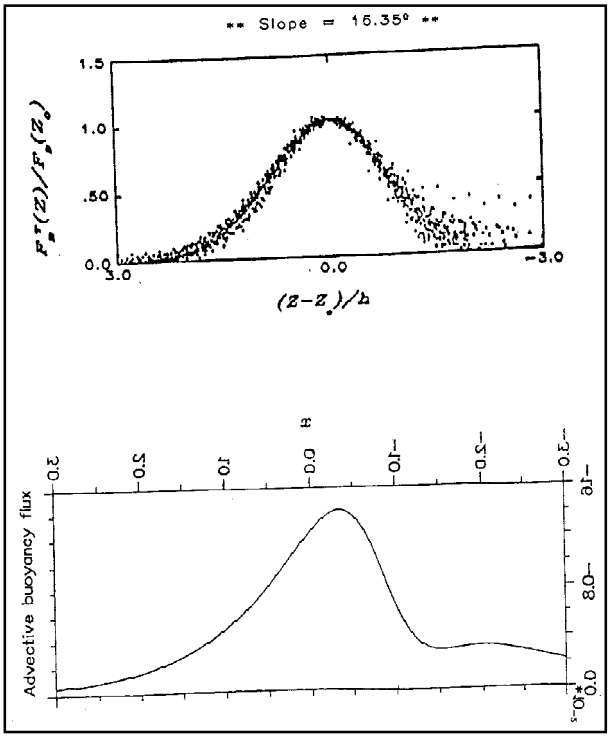

Figure 4. Buoyancy fluxes: Qualitative comparison between typical data from laboratory experiments (top panel) and characteristic model's results (lower panel). These sets represent the contribution to the mean buoyancy transport from turbulent dispersion in the boundary layer. A note about the inversion of the axis can be found in the text.

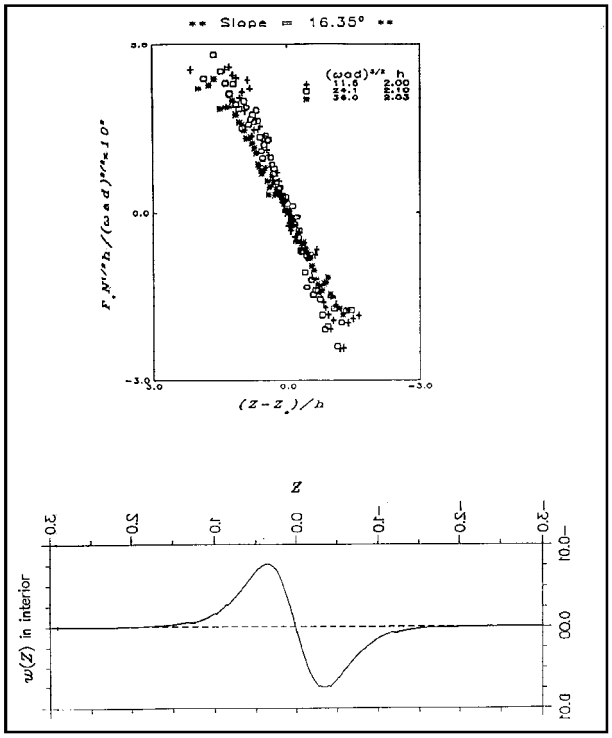

Figure 5. Volume fluxes: Qualitative comparison between typical data from laboratory experiments (top panel) and characteristic model's results (lower panel) stressing the vanishing of the volume flux at the pycnocline midlevel and its linearity with depth over the pycnocline region in both cases. A note on the axis labels can be found in the text.

WI(Z) which Z over the range that corresponds to the laboratory pycnocline and the vanishing of the volume flux at about the level where the forcing in the model has a maximum, in exact agreement with experimental results. Away from the level Z = 0, for distances slightly less than 1 in the figure, the model curve must diverge from the measurements because of the periodicity in the boundary conditions at large values of x considered in the model, and comparisons beyond |Z| larger than about 0.5 are not pertinent.

We now ask the question, Can the movement of water in an interior of finite size be interpreted as an interior diffusivity KI? The answer is directly related to the application of the theory and model results, and it is summarized as follows. Consider a basin of typical horizontal width LI at whose boundaries turbulent boundary layers produce horizontal inflow or outflow to the interior of magnitude UI. Conservation of mass flux requires that there is a simple relationship between this horizontal flow and the velocity field in the boundary layer, that is $U_I \; a \; n_{b1}$, where n_{b1} is obtained from solving the problem above. In such a basin, the effects of inflow or outflow must induce a vertical as well as horizontal motion in the interior and conservation of mass yields a relationship between UI and the vertical speed WI (the speed at which the ambient isopycnals spread apart also) of flow; this is WI a UI. The interior density will now change in time as a result of the vertical advection of density by the WI field against the basic preexisting stratification N²; this is the rate of change of p, a, w. Finally, an observer of this process may interpret the rate of change of p_I as owing to a diffusive process, namely as proportional to an overall diffusivity k_I times the vertical variation of the local vertical flux. In summary, we have arrived at the desired relation between boundary processes and interior changes because we have linked k_I *to* n_{bi} where $n_{bl} \; a$ function of boundary

parameters. This procedure yields

$$K_I = \frac{H^9 N^4 \sin^3 0 \cos^2 0.}{L_{IK}^3}$$

It is encouraging to note that this formula was also obtained using a two-dimensional model with a slightly different emphasis on the initial force balance and using a more general expression for the interior stratification than the two-layer type used in this study (Imberger and Ivey 1993). The formula was then applied to lake measurements obtained in Western Australia and yielded the realistic value of KI $10^{-6} m^2 s^{-1}$. Consider an oceanographic context, with typical values LI ~ 4000km; h ~ 500m; H ranges from 10 to 70 m with an average of 50m; N ~ 10^{-3} s^{-1} : and 0 is very small, 0 (10^{-3}) k-10^{-4} $m^2 s^{-1}$. Then the formula for KI yields Munk's canonical value of K ~ $10^{-4} m^2 s^{-1}$.

Applicability to Chesapeake Bay

The task is now to adapt this model of boundary mixing to a case that can be applied more directly to an estuarine environment such as Chesapeake Bay. To adapt and extend the two-dimensional model, we proceed roughly as follows:

- Consider the sloping boundary to be of a finite extent, thus two horizontal boundaries one at the top and another at the bottom of the domain are included.
- Add the time dependence.
- Consider the slope of the boundary explicitly in the equations of motion, so that the slope dependence can be investigated as well as the effects of possible realistic slope variations that are expected to occur in the field.
- Include the (continuous) variation of the turbulent exchange coefficients with distance from the boundary.

A schematic of the model geometry and a definition of the coordinate system are shown in figure 6. The nondimensionalization of the equations is achieved as follows. Consider characteristic scales based on the stratification of the fluid, which is assumed to be known, and the characteristics of the turbulence field, such as the intensity of the turbulence. For instance, let hbe the characteristic vertical length scale over which the initial stratification in the ambient fluid changes significantly, and V_{01} K_{01} of the same order, be the characteristic values of the eddy coefficients at the boundary. The

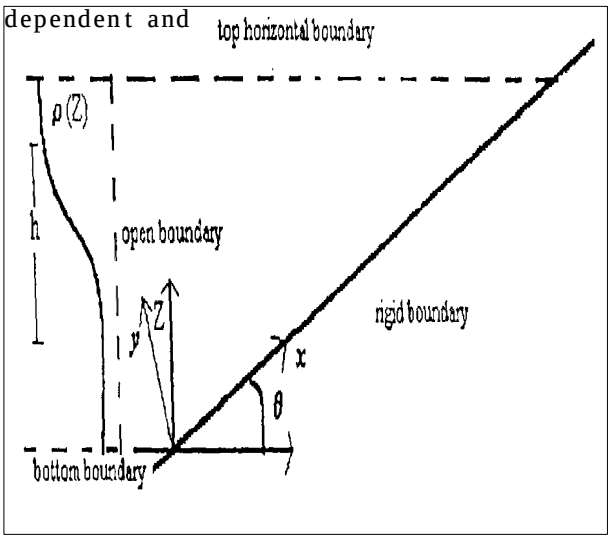

Figure 6. A schematic diagram of the adapted model geometry and coordinate system.

independent variables are then scaled as follows:

$$x, y \sim h,\ u, v, \sim v_o / h\ ,\ v, k, \sim v_0, k_o\ ,\ w \sim v_o / h.$$

Let t_s be the characteristic time scale, which requires further consideration, but for a start can be considered as the "diffusive" time scale owing to the turbulence over the entire depth h, so that it is defined as $t_s = h^2 / V_0$. Finally, two nondimensional numbers appear in these equations; they are the eddy Prandtl number Pr and the Grash of number Gr defined as

$$P_r = \frac{v_o}{k_o} \quad and \quad G_r = \frac{g(\Delta p / p_o)h^3}{v_2^0}.$$

The nondimensional equations for the mean vorticity and the mean buoyancy are as given in figure 7. All quantities are as defined previously and, as before, the continuity equation allows for the definition of the mean stream function y so that the velocity and vorticity field can be expressed in terms of it and the mathematical problem is reduced to solving the above two equations for y and B. To solve these equations, we need to specify initial and boundary conditions, and the functional form of v (y) and k (y). In principle, for a given geometrical domain, it is possible to attempt a numerical solution of this problem, and some progress in this direction has been made.

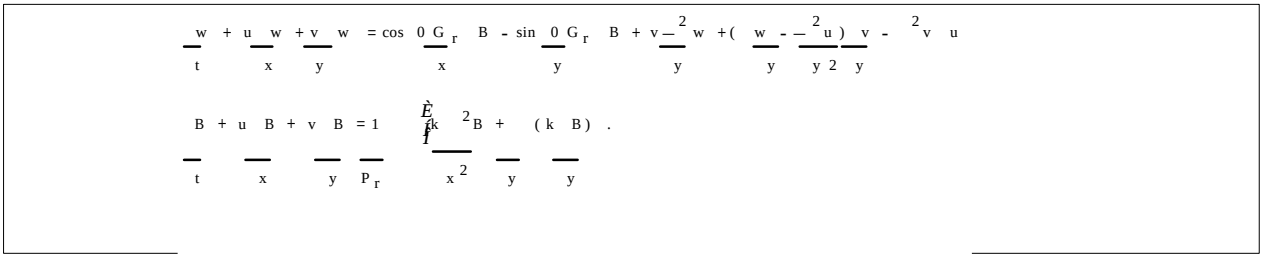

$$\frac{\partial w}{\partial t} + u\frac{\partial w}{\partial x} + v\frac{\partial w}{\partial y} = \cos\theta\, G_r \frac{\partial B}{\partial x} - \sin\theta\, G_r \frac{\partial B}{\partial y} + \nu\frac{\partial^2 w}{\partial y^2} + \left(\frac{\partial w}{\partial y} - \frac{\partial^2 u}{\partial y^2}\right)\nu - \nu^2 u$$

$$\frac{\partial B}{\partial t} + u\frac{\partial B}{\partial x} + v\frac{\partial B}{\partial y} = \frac{1}{P_r}\left(\frac{\partial^2 B}{\partial x^2} + \frac{\partial}{\partial y}\left(k\frac{\partial B}{\partial y}\right)\right).$$

Figure 7. Nondimensional equations for mean vorticity and mean buoyancy.

The equations for the mean flow in the turbulent boundary layer, under suitable assumptions, are the same as those that describe the classical convection problem in a viscous fluid, with the molecular coefficients replaced by the turbulent exchange coefficients. A model describing convection patterns and the associated heat transfer in a triangular domain was developed (Salmun, 1995) and can now be adapted to study the present problem. If the eddy coefficients are assumed constant over the depth of the boundary layer, the equations of both models only differ in the explicit inclusion of the slope, as it appears in equation (3). As a first step in approximating the physical situation describing an estuarine geometry, we consider a wedge-like region contiguous to another of rectangular shape as depicted in figure 6, and the procedure of adapting the numerical model is then straightforward. The sloping boundary is considered a rigid boundary of finite extent, and at the two horizontal boundaries the boundary conditions are those of lines of equal density where flux conditions are required. Finally at the open boundary (that opposed to the sloping bed), conditions that simulate a flow that gradually develops owing to boundary processes are implemented. This point, which may be relatively straightforward to implement numerically, requires some attention; in this model, the local stratification is slowly and continously changing due to boundary mixing processes, and this change has an effect on the boundary processes themselves. This interaction, in turn, constitutes one of the most interesting, and perhaps challenging, aspects to be accounted for in this model that of the two time scales involved: the slow time scale over which the initially imposed stratification changes owing to boundary mixing processes that occur over the faster time scale associated with turbulence. At this stage, we have tentatively chosen the latter as the time scale, the cases of variable turbulent coefficients are being considered, and the numerical sensitivity and stability of the model to the different parameters and parameter ranges are being tested. Preliminary results are encouraging and seem to indicate that the numerical model will be amenable to long and more realistic integrations.

An alternative approach to this kind of modelling is to study basic processes using simpler models, for example one-dimensional models (Salmun and Phillips 1992). These process studies are complementary to the approach presented here, and they are used as a first step to gain insight into the nature of the characteristic scales relevant to the model, particularly the time scale, the nature and functional form of the spatial variation of the eddy coefficients, and how that variation affects the basic circulation.

CONCLUSION

Vertical mixing and boundary layer dynamics are crucial to the global and local dynamics of estuaries. Boundary mixing processes in theory may contribute significantly to both aspects of estuarine hydrodynamics. In recent years there have been advances in the observations and modeling of boundary processes, which also have contributed to a more clear picture of the complexities associated with the problem of boundary mixing, the structure and variability of these boundary layers in the field and to some understanding of many of the individual processes involved in boundary mixing as well as the possible application of these studies to real problems. There are, unfortunately, few direct observations that may help establish the importance of boundary mixing, confirm the importance of a particular mechanism of mixing, or even describe the structure of benthic boundary layers on a slope.

This paper has reviewed and summarized the physics and mathematical modeling of boundary mixing and argued that this mechanism is a potentially important alternative to other mechanisms, such as mixing owing to shear at an interface, in accounting for overall vertical mixing. There is a reasonable amount of theory, laboratory, and modeling studies of these processes that gives confidence in its application to a field situation, and it is clear that observational feedback is lacking. It is the goal of the extension of the work presented here that a program of data acquisition, data analysis, and model validation will develop following guidelines from the modeling studies. We propose, and anticipate, to take some steps towards answering such questions as:

- Is boundary mixing a mechanism responsible for the actual observed state of mixing and stratification in Chesapeake Bay?
- How much of the state of the Bay is caused by boundary mixing, hence can be explained by it, and how much is owed to local internal mixing?
- Is boundary mixing important everywhere (along the boundaries) in the Bay?, and if not, then where is it important?
- Under what conditions may boundary mixing be more effective?; for example Are the effects of boundary mixing seasonally dependent?

We also anticipate that, in turn, analysis of field data will serve as a test of the validity and accuracy of the existing models, and furthermore help to improve them. The hope is that general flow models of the Bay can use results of these type of studies to correctly parameterize the small-scale, sub-grid, processes that are important to problems of transport of sediments, pollutants, and other important constituents.

REFERENCES

Armi, L. 1978. Some evidence for boundary mixing in the deep ocean. J. Geophys. Res. 83:1971-1979.

Cacchione, D., and Wunsch, C. 1974. Experimental study of waves over a slope. J. Fluid Mech. 66:223-229.

Caldwell, D.R., J.M.Brubaker, and V.T. Neal, 1978. Thermal microstructure on a lake slope. Limnol. Oceanogr. 23:372-374.

Dyer, K.C. 1988. Tidally generated estuarine mixing processes. In: Kjerfve, B., ed. Hydrodynamics of estuaries.Volume I. Estuarine physics. CRC Press, 41-57.

Eriksen, C.C. 1985. Implications of ocean bottom reflection for internal wave spectra and mixing. J. Phys. Oceanogr. 15:1145-1156.

Fisher, H.B., E.J. List, R.C.Y Koh, I. Imberger, and N. H. Brooks, 1979. Mixing in inlands and coastal waters. New York: Academic Press.

Garrett, C. 1979. Mixing in the ocean interior. Dyn. Atmos. Ocean 3:239-265.

Garrett, C. 1991. Marginal mixing theories. Atmosphere-Oceans 29:313-339.

Goodrich, D. M., W. C. Boicourt, P. Hamilton, and D. W. Pritchard 1987. J. Phys. Oceanogr. 17:2232:2240.

Gregg, M.C., and Sanford, T.B. 1980. Signatures of mixing from the Bermuda slope, the Sargasso Sea and the Gulf Stream. J. Phys. Oceanogr. 10:105-127.

Hogg, N. G., E.J. Katz, and T. B. Sanford, 1978. Eddies, islands and mixing. J. Geophys. Res. 83:2921-2938.

Imberger, J. and G.N. Ivey, 1993. Boundary mixing instratified reservoirs. J. Fluid Mech. 248:477-491.

Imberger, J. and J.C. Patterson, 1990. Physical limnology. Adv. Appl. Mech. 27:303-475.

Ivey, G.N. and G.M. Corcos, 1982. Boundary mixing in a stratified fluid. J. Fluid Mech. 121:1-26.

Ivey, G.N. 1987. Boundary mixing in a rotating, stratified fluid. J. Fluid Mech. 183:25-44.

Ivey, G.N., and R.I. Nokes, 1989. Vertical mixing due to the breaking of critical internal waves on sloping boundaries. J. Fluid Mech. 204:479-500.

Lentz, S. J., and J.H. Trowbridge, 1991. The bottom boundary layer over the Northern California Shelf. J. Phys. Oceanogr. 21:1186-1201.

MacCready, P., and P.B. Rhines, 1991. Buoyant inhibition of Ekman transport on a slope and its effect on stratified spin-up. J. Fluid Mech. 223:631-661.

Marmorino, G.O., S.C. Danos, and J.S. Maki, 1980. Temperature fine structure of Lake Michigan hypolimnion. Limnol. Oceanogr. 25:680-699.

Munk, W. 1966. Abyssal recipes. Deep-Sea Res. 13:107-175.

Partch, E. N., and J.D. Smith, 1978 Time dependent mixing in a salt wedge estuary. Estuarine Coastal Shelf Sci. 6:3-19.

Phillips, O. M. 1970. On flows induced by diffusion in a stably stratified fluid. Deep-Sea Res. 17:435-443.

Phillips, O.M., J.H. Shyu, and H. Salmun, 1986. An experiment on boundary mixing: mean circulation and transport rates. J. Fluid Mech. 173:473-499.

Salmun, H. 1995. Convection patterns in a triangular domain. Int. J. Heat & Mass Transfer, 38(2):351-362.

Salmun, H. and Phillips, O.M. 1992. An experiment on boundary mixing. Part 2. The slope dependence at small angles. J. Fluid Mech. 240:355-377.

Salmun, H., P.D. Killworth, and J.R. Blundell, 1991. A two-dimensional model of boundary mixing. J. Geophys. Res. 96:18,447-18,474.

Stigebrant, A. 1976. Vertical diffusion driven by internal waves in a sill fjord. J. Phys. Oceanogr. 6:486-495.

Thorpe, S.A. 1982. On the layers produced by rapidly oscillating a vertical grid in a uniform stratified fluid. J. Fluid Mech. 124:391-409.

Thorpe, S.A. 1987. Current and temperature variability on the continental slope. Philos. Trans. R. Soc. London, Ser. A 323: 471-517.

Thorpe, S.A., P. Hall, and M. White, 1990. The variability of mixing on the continental slope. Philos. Trans. R. Soc. London, Ser. A 331:183-194.

Trowbridge, J. H., and S. J. Lentz 1991. Asymmetric behavior of an oceanic boundary layer above a sloping bottom. J. Phys. Oceanogr. 21:1171-1185.

Woods, A.W. 1991. Boundary driven mixing. J. Fluid Mech. 226:625-654.

Wunsch, C. 1972. Temperature microstructure on the Bermuda Slope with application to the mean flow. Tellus 24:350-367.

Toward a Sustainable Coastal Watershed:
The Chesapeake Experiment. Proceedings of a Conference
1-3 June 1994. Norfolk, VA
Chesapeake Research Consortium Publication No. 149

WATER EXCHANGE IN THE LOWER CHESAPEAKE BAY

Arnoldo Valle-Levinson
Old Dominion University

Abstract: Observations of intratidal flow and interannual density fields in Lower Chesapeake Bay are compared to numerical simulations to investigate possible mechanisms of water exchange in this area. Salinity observations in the lower Bay during the months of low freshwater discharge show relatively low values over the Hampton Roads area of a cross-bay transect parallel to the Chesapeake Bay Bridge-Tunnel. Relatively high salinity water is commonly found in the deep reaches of the navigational channels and over the central portion of the transect, off the Delmarva peninsula. This density distribution can be partially explained with a mean flow derived from acoustic Doppler current profiler measurements obtained in early fall of 1993. This shows outflow throughout the water column off Hampton Roads; bottom inflow over the channels; and near-surface outflow at the northern end of the transect. The near-surface low salinity and the outflow associated with it are explained, with simplified numerical simulations, as the natural tendency of the buoyant flow attributable to the geometry of the lower Bay. During high freshwater discharge, observations and simulations show near surface buoyant outflow across the entire transect and near bottom inflow. Moored current meters in the summer of 1993 show that summer patterns should be expected to vary monthly with a predominant near barotropic exchange. Simulations also suggest that outflow increases with increased freshwater discharge, thus hindering inflow. Inflow is further hindered by decreased ambient coastal southward flow.

INTRODUCTION

In lower Chesapeake Bay, where oceanic dissolved and suspended materials, as well as crab and fish larvae, enter the estuary from the adjacent ocean, appropriate boundary conditions for numerical models of the entire Bay need to be established. The lower Bay has been the focus of increased research activities in recent years as it represents the pathway to nursery grounds for many species of ecological and commercial importance. Studies of water exchange between the lower Bay and the coastal ocean are crucial to understanding the mechanisms related to larvae and postlarvae transport..

Forcing agents such as wind stress, river runoff, bathymetry, and spring-neap variations in tidal stirring affect the properties of the water exchange and play an important role in determining the fate of dissolved and suspended matter in coastal areas. The purpose of this study is to describe the monthly variability in water exchange in lower Chesapeake Bay, and to assess the effects of altering estuarine and oceanic flows and of bathymetry on volume exchange. This is done with a combination of current velocity and hydrographic data, and process-oriented numerical simulations.

Estuarine and oceanic waters mix during both flood and ebb tides and through episodic wind events. The degree of water column stratification is determined by the relative intensity of river discharge and of tidally and wind-induced stirring, which tend to destratify the water column and to alter the characteristic gravitational circulation. Spring-neap variations in tidal stirring modulate the stratification and affect the inflow / outflow of water and materials. The development of horizontal density driven circulation through modulation in stirring has been demonstrated experimentally by Linden and Simpson (1988). Further, Nunes-Vaz et al. (1989) suggest that mass flux through an estuary varies with turbulence modulations over a variety of time scales. This confirms the importance of the spring-neap stirring cycle in determining the

long-term mass balance in partially mixed estuaries such as Chesapeake Bay.

Several studies have shown that the lower Bay responds barotropically to local winds and coastal Ekman flux (Wang and Elliott 1978, Wang 1979a,1997 b) producing inflows / outflows larger than those produced by the estuarine circulation and river discharge. Goodrich (1987, 1988) proposed that these wind-induced exchanges in the lower Bay are superposed on the gravitational circulation. The flow observations described herein show that Goodrich's speculations are valid but also that oceanic water tends to intrude near the bottom during neap tides, as described in the next section.

Flow Monthly Variability

This section describes the monthly variability of nontidal flows as obtained by two current meter moorings. The moorings, stations 1 and 2 (figure 1), were located approximately 200 m seaward of the Chesapeake Bay Bridge-Tunnel (CBBT). A tide gauge and meteorological station maintained by the National Oceanic and Atmospheric Administration (NOAA) on a pier off the CBBT (figure 1) provided sea level, wind,

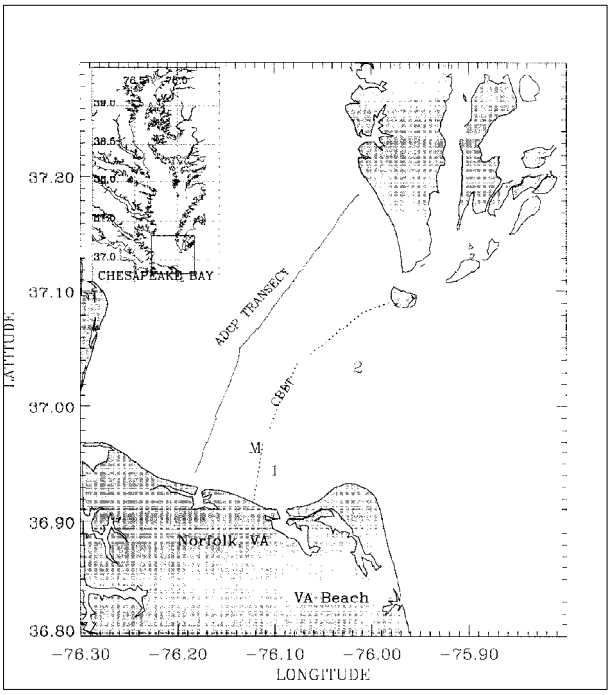

Figure 1. Lower Chesapeake Bay showing locations of current meter moorings stations 1 and 2, just seaward of the Chesapeake Bay Bridge-Tunnel (CBBT). The tide gauge and meteorological station is marked with an M. The ADCP transect is also shown landward of the CBBT.

and barometric pressure data throughout the period of current velocity measurements. Each mooring was deployed in approximately 10 m of water with instruments placed about 3 m from the surface and the bottom. The current meters employed were *SensorData* model SD-2000, which record water temperature and water current speed and direction. The instruments at both moorings began recording on 21 July 1993. The instruments at mooring 1 recorded through 13 September 1993 and at mooring 2 through 31 July 1993. The instruments of mooring 2 did not cover a period long enough to identify monthly variations. Thus the flow description for monthly variability is restricted to station 1. The sampling interval for the current meters was 20 min and for the instruments at NOAA's station was 6 min. All records were reduced to 1hr intervals.

The nontidal flow behavior was described with the low-pass filtered records of water temperature, decomposed current velocity, wind stress, sea level, and complex demodulated amplitude of sea level (to denote tidal phase). The filter consisted of a Lanczos filter with a half-power of 35 h to remove diurnal, semidiurnal, and other high-frequency fluctuations.

The current velocity was decomposed into principal axis and cross-principal axis component.s. The orientation of the principal axis was determined from the semi-major axis of the M_2 ellipse. At station 1, this angle was 138°T near the surface, and 146°T near the bottom. At station 2, it was 164°T and 159°T for near surface and near bottom, respectively. This principal axis distribution suggests flow nearly parallel to the coast in this area. The wind stress or momentum flux is parameterized with the "quadratic law." The east-west, t_{sx}, and north-south, t_{sy}, components of the wind stress are given by

$$t_{sx} = r_a C_D W_{x10} |W_{10}|$$
$$t_{sy} = r_a C_D W_{y10} |W_{10}|$$

where r_a is the air's density (1.2 kg / m^3); $|W|$ is the wind magnitude (m / s) with components [W_x, W_y]; C_D is a nondimensional drag coefficient and equals (0.49 + 0.065 W_{10}) X 10^{-3} for $W \geq 10$ m / s, and 1.14 X 10^{-3} for $W < 10$ m / s (Large and Pond 1981). The subscript 10 denotes wind values at an elevation of 10 m above the sea surface.

The surface net flow at station 1 was directed seaward during the observation period, except on September 6 (figure 2). Bottom flow was also dominantly seaward but exhibited periods of net inflow. Neap tide periods corresponded with landward bottom flow (i.e., intrusion of oceanic waters). This was corroborated by the temperature

records, which showed a decrease in bottom temperature and little change in surface temperature during neap tides. This behavior during neap tides suggests increased thermal stratification induced by near-bottom inflow of oceanic waters that are cooler than Bay waters during this time of the year. The bottom inflow on 1-2 August occurred after southward wind piled water up against Norfolk's coast. The other two bottom inflow events (5-6 August and 6 September) developed after the cessation of the two strongest northward wind events during the observation period, 1-5 August and 2-5 September

The meteorological data show a clear relation between wind stress variations and sea level fluctuations (figure 2). South to southwestward wind corresponds with rising sea level, and north to northeastward wind coincides with dropping sea level. The strongest northward wind events mentioned above caused the greatest sea level drops, which drove water out of the estuary. Once the outflow-producing force weakened, the estuary recovered the water loss through barotropic inflow as seen in the near-surface flow record. On 5-6 August, flow was weakly seaward in contrast to the strong outflow before and after that period. On 6 September after the most energetic wind event of the observation period and the greatest sea level drop, barotropic inflow was strong enough to reverse the near-surface tendency for outflow. These two barotropic inflow events caused water temperature declines at both near-surface and near-bottom sites, in contrast to the baroclinic inflow events of neap-tide periods and of 1-2 August when only bottom temperature decreased.

Hurricane Emily passed near the study area on 30-31 August , causing the greatest sea level increase of the sampling record (~ 0.30 m). The passage of the hurricane also produced decreased outflow at both levels measured and a short period of very weak net bottom inflow (~0.01 m / s) with the brief southwestward winds of 30 August . The effect of the passage of the hurricane was not as dramatic as other events in the year (e.g, winter northeasters) owing to the transitional character of these hurricane winds.

The barotropic response of the lower Chesapeake Bay flow to meteorological forcing has already been described. The study of Wang (1979b) examined data obtained during late fall when the winds are stronger than during the summer. In addition to the barotropic response, the summer data analyzed here suggest a

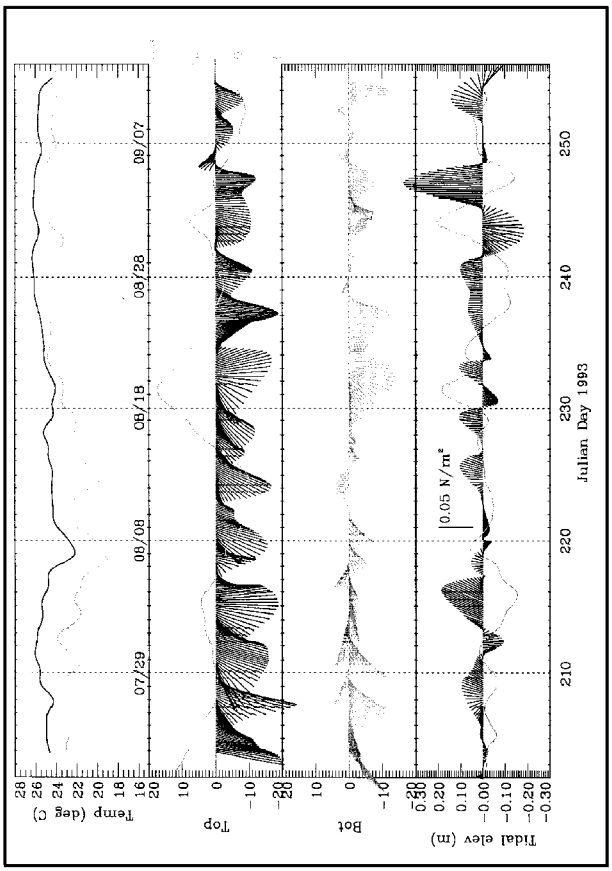

Figure 2. Low-pass filtered records during the period of study. The four panels from top to bottom are: near-surface temperature (bold) and near-bottom temperature (gray); surface flow (stick diagram [cm / s] - positive [negativ] values denote flow into [out of] the estuary) and complex demodulated sea level amplitude (m) to show tidal phase (in gray); bottom flow (stick diagram); and wind stress (N / m^2) (stick diagram - oceanographic convention) and low-passed sea level (m) (in gray). A clear correspondence between wind stress variations and sealevel fluctuations is readily seen. South to southwestward wind corresponds with rising sealevel, and north to northeastward wind coincides with dropping sealevel.

baroclinic response that becomes evident during neap tides. Goodrich (1988) suggested that, in addition to meteorological flushing, other processes operate at the estuary mouth. He speculated that an oscillatory wind-driven circulation could be superposed on a low-amplitude gravitational circulation in lower Chesapeake Bay, also causing a baroclinic response.

The baroclinic response is investigated here through the calculation of the residual flow vertical shears. Low shear values represent

unidirectional, barotropic flow. High shear values indicate tendencies for gravitational circulation and baroclinicity. The difference between near-bottom and near-surface low-passed flows, which represents the vertical shear, tends to increase during neap tides and to decrease during spring tides (figure 3). This suggests the development of baroclinic (barotropic) exchanges during neap (spring) tides. The high shears on 2 August occurred after a southward wind piled up water against Norfolk's coast and induced bottom inflow. The spring neap modulation of water exchange is consistent with studies in other estuaries (e.g, Haas)1977, Griffin and LeBlond 1990 Geyer and Cannon, 1982). However, the modifications to estuarine and oceanic flows that cause the estuary to recover its lost water or to hinder flows into (or out of) it are not well understood. In the next section, two-such modifications: suppression of seaward barotropic estuarine flow, and suppression of ambient coastal ocean flow are explored through process-oriented numerical simulations.

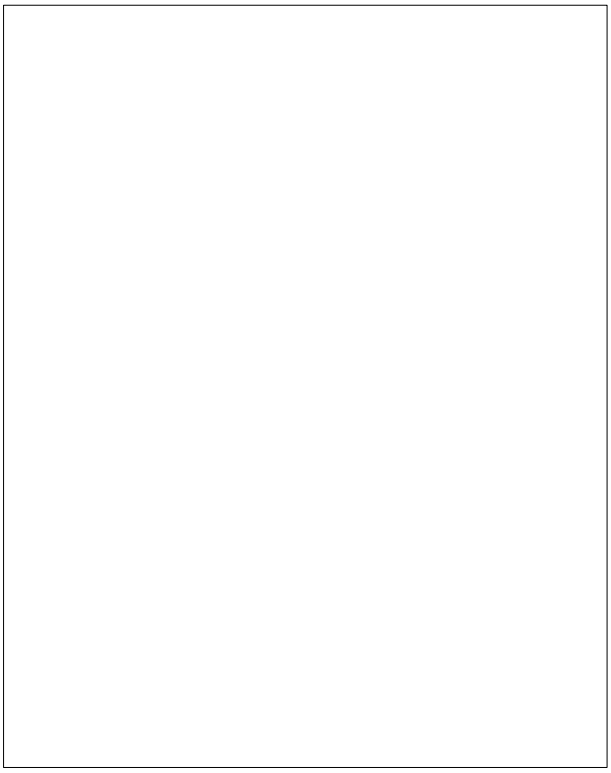

Figure 3. Vertical difference between near-surface and near-bottom residual flows (principal axis component). The complex demodulated sea level amplitude is shown in gray as reference to the tidal phase. The vertical shear of the residual flow increases during neap tides and decreases during spring tides, suggesting the development of baroclinic (barotropic) exchanges during neap (spring) tides.

Modifications to Chesapeake Bay and Coastal Ocean Flows

Two numerical model experiments are presented here to look at the effects of interrupted (or pulse-like) seaward barotropic flow in Chesapeake Bay and of suppressed southward coastal ambient flow on volume exchange at the mouth of the estuary. The former effects can be thought of as those produced after the cessation of a wind event that drives water out of the Bay, such as the events described on 5-6 August and1 September in 1993. The latter effects are analogous to northward winds or weakened longshore pressure gradients in the coastal ocean that tend to hinder the advection of the southward ambient coastal flow in the area off the Bay mouth. A third experiment represents the baseline to which the other two are compared. The baseline experiment, consisted of a flow adjustment subject to rotation, with prescribed seaward barotropic flow at the landward boundary, and southward ambient flow at the northern open boundary of the domain (figure 4). The domain consisted of a flat-bottom (10 m deep) geometry similar to that of the lower Bay. In, experiment 2 a pulse-like seaward flow was prescribed at the landward estuarine boundary. In experiment 3 , the ambient coastal flow was suppressed.

The numerical model solves the full set of momentum and salt balances, as well as continuity, and is described in Valle-Levinson et al. (1994). The initial salinity field consists of a prescribed step of 5 psu located 24 km from the landward boundary (figure 4). This salinity configuration yields a gravity current speed, $c_g = 0.5(g'H)^{1/2}$ (where g' is the reduced gravity gDr/r_o, Dr is the initial density contrast, ro is a reference density, and H is the total water depth), of 0.32 m/s and an internal radius of deformation ($R_d = 2c_g/f$, where f is the Coriolis parameter) of ~7 X 103 m. Since the channel width and the opening at the mouth of the estuary are ~2.4 X 103 m, the earth's rotation is expected to influence the adjustment of the initial salinity field.

Surface and bottom salinity fluxes, as well as surface (wind stress) momentum fluxes, are set equal to zero. Bottom momentum flux (bottom stress t_b) is parameterized linearly as $t_b = r u_b$, where r is a friction parameter that equals 4×10^{-4} m/s and u_b is the bottom velocity vector. At the cross-shore southern boundary, the momentum transport is radiated out of the domain using an Orlanski-type condition as described by Miller and Thorpe (1981). Salinity is extrapolated

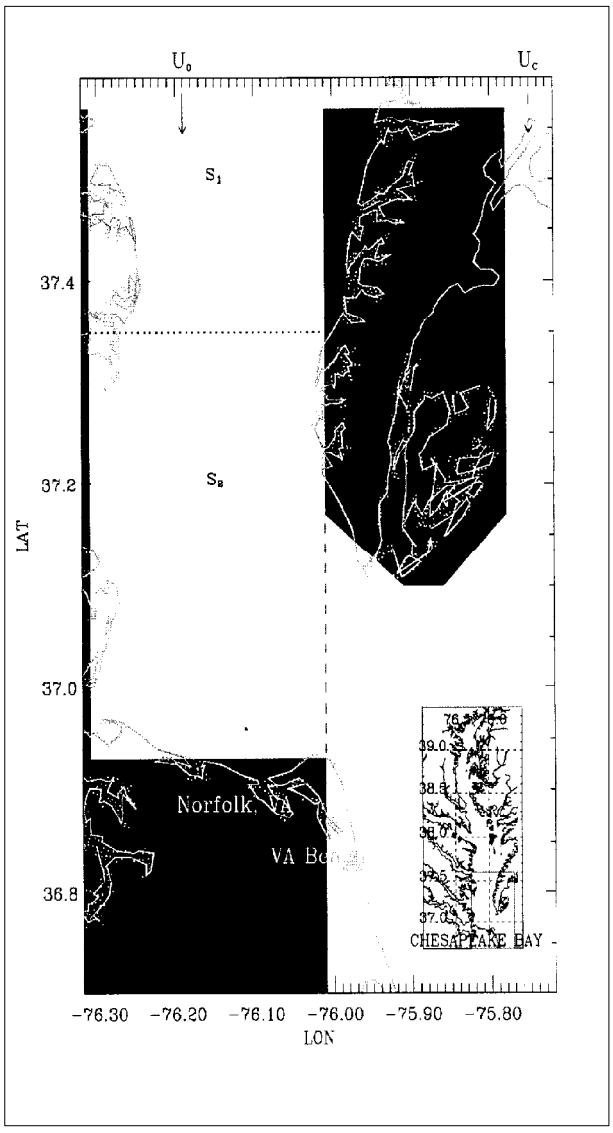

Figure 4. Domain of the numerical experiments performed. The dimensions are drawn from those of lower Chesapeake Bay as shown in the figure. The numerical model has four levels over a flat bottom of 10 m depth and a horizontal grid resolution of 1.5 km by 1.5 km. The dotted line represents the position of an initial salinity step. Landward of (above) the discontinuity, the salinity ($s_1 = 0$) is lower than seaward of (under) it ($s_2 = 5$). The dashed line shows the position of the cross section at the entrance to the estuary (from the northern to the southern capes) referred to in the text. The western (eastern) boundary is at longitude 76.31° (76.01°). The seaward barotropic flow at the landward boundary (U_O) is 0.02 m / s for the baseline experiment. The southward ambient flow (U_C) is prescribed to 0.10 m / s.

to the boundary for both inflows and outflows. Extrapolation is carried out through an advective condition similar to the aforementioned condition for momentum (Orlanski-type). The transports at the open ends are normal to the boundaries. At the northern open boundaries, within the estuary (U_O) and on the coastal ocean (U_C), the momentum transports are prescribed as $U_O = 0.02$ m / s and $U_C = 0.10$ m / s (vertically uniform), respectively, for experiment 1. These boundary values decay exponentially in the transverse direction over a distance equivalent to the Rossby radius (sqrt(gH) / f). For experiment 2, $U_O = 0.02$ (0) m / s during (after) 10 days of simulation. For experiment 3, $U_C = 0$ m / s.

Baseline Experiment

The initial salinity discontinuity is advected out of the estuary at different rates across the domain owing to the development of a near-surface boundary current along the western boundary and a "nose" along the eastern boundary (figure 5). The boundary current moves at ~0.19 m / s, whereas the nose moves at ~0.03 m / s. The near-surface outflow and salinity fields show similar patterns as those described by Weaver and Hsieh (1987), Chao (1988), and Oey and Mellor (1993) over the coastal ocean: a plume limited by an anticyclonic front and a meandering coastal current. The width of the boundary current and the outflow around the southern cape is approximately R_d near the surface and decreases with depth.

In the cross section at the entrance to the estuary shown in figure 4 inflow occurs over most of the section at very low rates (< 0.05 m / s) with higher salinities found in the middle of the section at day 10 (figure 6). Outflow is well-defined around the southern cape reaching to the bottom and it also starts to develop around the northern cape near the surface. At day 20 and through day 30, inflow is confined to the bottom and outflow appears almost throughout the entire near-surface section. The positive values that appear near the surface in the middle of the section on day 20 are associated with the undulating nature of the front located in this area (figure 5). The increased outflow with respect to inflow that develops by day 30 is associated with the seaward translation of the front, related to the initial salinity discontinuity, past the transect sampled at the mouth.

Effects of Suppressing Estuarine Seaward Barotropic Flow

The flow and salinity fields are the same as the previous experiment (no. 1) during the first 10

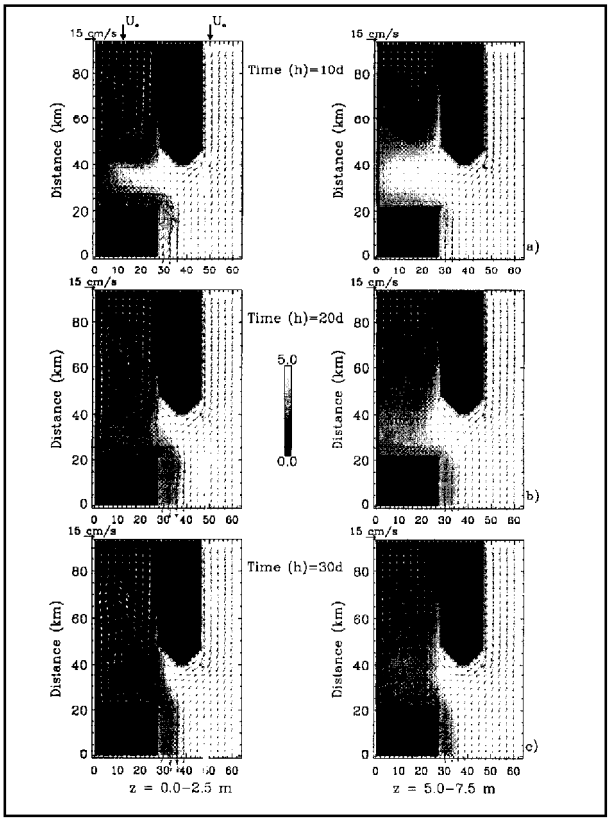

Figure 5. Flow (vectors) and salinity fields for experiment 1: DS = 5, bottom friction.; (a) 10 days; (b) 20 days; and (c) 30 days. Left panels show the surface level (0-2.5 m) and right panels represent the third level (5-7.5 m). Each velocity vector starts at every second grid point of the domain.

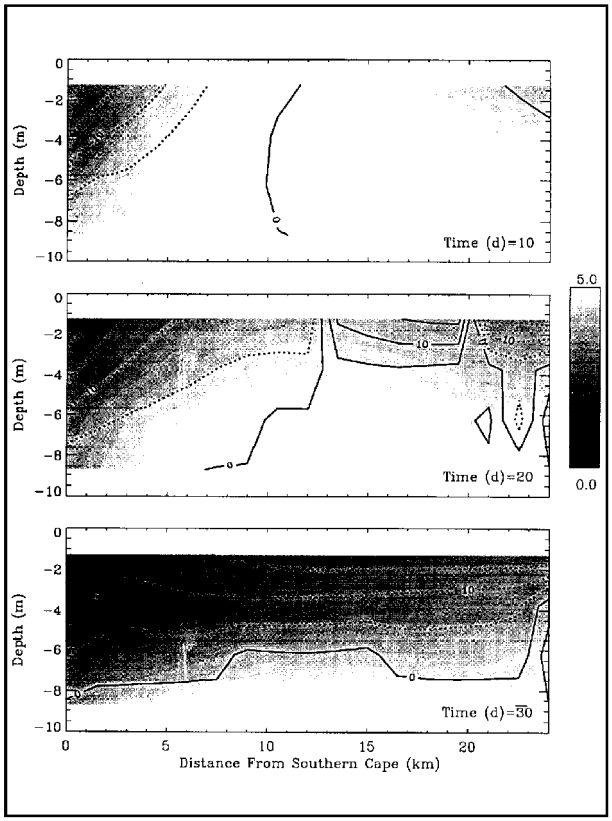

Figure 6. Cross sections of the salinity and flow (contours in cm/s) fields for experiment 2 at 10, 20, and 30 days at the entrance to the estuary. Contour interval is 5 cm / s. Volume inflows (outflows) for each panel are 0.2 (0.5), 0.5 (1.0), and 0.2 (1.7) X 10^4 m^3 / s.

days. After U_O becomes zero, inflow into the estuary increases throughout the water column at the northern end of the cross section sampled (figure 7). The volume exchange shifts from outflow dominated, during the first 10 days, to inflow dominated at 20 and 30 days. Volume inflow is greater than experiment 1, where U_O is constant throughout the experiment. The response time at the estuary entrance for the reversal of volumetric inflow is less than 1 day after cessation of U_O. Hence, time variations of freshwater discharge at the estuarine landward boundary are expected to influence the volumetric exchange at the entrance to the estuary. A similar effect should be expected after cessation of a period of continuous outflow generated by a strong (> 10 m / s) southwesterly wind event. The estuary will tend to "bounce back" with a subsequent period of volume inflow as presented in the current meter observations.

Effects of Suppressing Coastal Ambient Flow

The importance of the coastal flow on determining the direction of the outflow was first suggested by Zhang et al. (1987). The southward coastal flow in the area off the Chesapeake Bay mouth can be weakened or suppressed by northward winds and / or by reduced longshore pressure gradients in the coastal ocean. Suppression of the coastal ambient flow (U_C = 0) allows the outflow at the entrance to the estuary to extend farther offshore than in the previous experiments (figure 8). This is noted after 10 days in the flows inside and out of the estuary. By day 20, the outflow develops a well-defined turning region outside the estuary. By day 30, near-surface outflow occupies practically the entire mouth of the estuary. Near the bottom, the flow is in the opposite direction to the surface, thus causing strong baroclinicity.

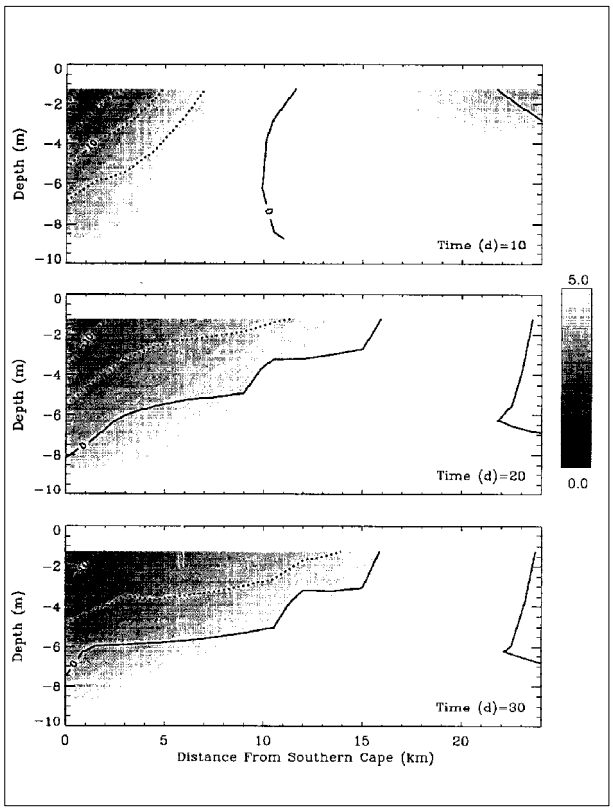

Figure 7. Same as in figure 6 but for experiment 2: DS = 5, with a pulse of barotropic discharge at landward boundary in the estuary. Volume inflows (outflows) for each panel are 0.2 (0.5), 0.5 (0.4), and 0.5 (0.5) X 10^4 m^3 / s.

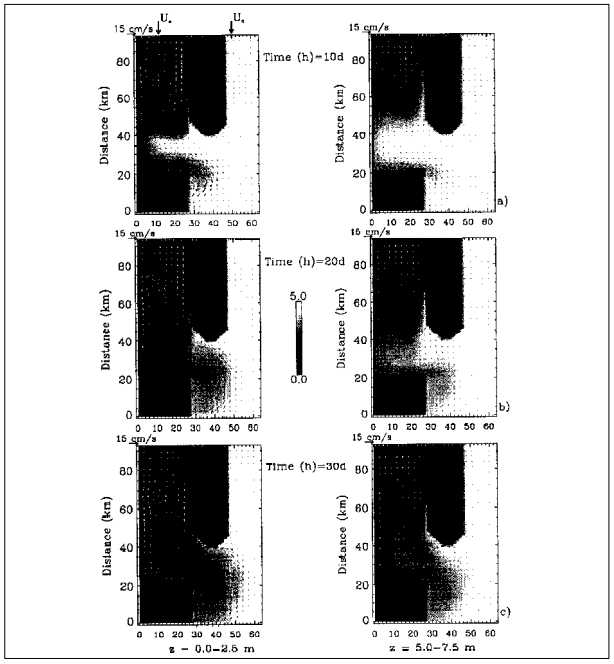

Figure 8. Same as in Ffgure 5 but for experiment 3: DS = 5, with no coastal ambient flow.

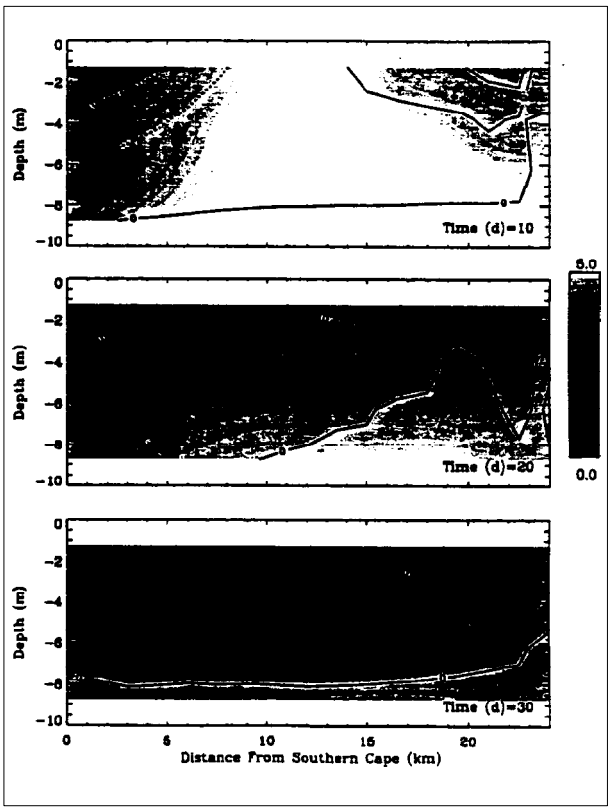

Figure 9. Same as in figure 6 but for experiment 3. Volume inflows (outflows) for each panel are 0.2 (0.6), 0.2 (1.2), and 0.1 (1.0) X 10^4 m^3 / s.

In the section across the entrance to the estuary, outflow starts to develop at the northern cape by day 10 (figure 9) and occupies the near-surface region throughout the section by day 20. The weak inflow on day 30 is confined to the middle of the section and to a small band, approximately 2 m thick, near the bottom. Overall it is clear that the inflow of saline waters is drastically hampered by the suppression of the southward coastal flow. This is corroborated by the volumetric transports at this section, which show large asymmetry between volume outflow and inflow on days 20 and 30, related to the front passage past the transect sampled.

The two scenarios depicted in experiments 2 and 3 act in opposition,(i.e., one enhances volume inflow and the other hampers it). These have been described as mechanisms that generate some of the water exchange variations observed in the current meter records. Other agents such as salinity gradient, tidally and wind-induced vertical mixing, and bathymetry will alter the nature of the volume exchange in lower Chesapeake Bay and are part of on-going research efforts. Among those, the effects of bathymetry are also presented here.

Bathymetry Effects on Volume Exchange

The role of bathymetric features such as navigational channels in determining the transport of salt and water in lower Chesapeake Bay was investigated with high-resolution measurements obtained with an acoustic Doppler current profiler. These measurements were carried out along a lower Chesapeake Bay transect (figure 1) during neap tides on 6-7 October 1993. The data obtained did not offer a synoptic representation of the flow field as it took approximately 3 hours to complete each of eight repetitions of the transect.

The amplitude and phase of the M_2 tidal constituent and the background, or de-tided, flow were obtained for a grid of stations separated 250 m in the horizontal and 0.5 m in the vertical using least-squares fitting of eight observations at each grid point. The de-tided flow was used to characterize regions of net inflow and outflow across the Bay entrance and to calculate net volume inflow and outflow. Wind and sea level data from the station at CBBT were used to explain the imbalance between net volume flows.

The de-tided flow shows that inflow occurs in and over the navigational channels and outflow over the shoals (figure 10a). This flow pattern differs from the theoretical picture of a gravitational flow affected by the earth's rotation, but is consistent with hydrographic observations (Miller and Valle-Levinson, in preparation) and the numerical simulations presented here. The sea level and wind data from the CBBT show a mean sea level increase of between 0.05 and 0.10 m (difference between observed and predicted) caused by winds of easterly component during the period of observations (figure10b). This would result in net volume inflow into the estuary.

In an estuary, mean outflow should be generally greater than inflow by a volume equal to the freshwater discharged, assuming no net loss. During our sampling period, net outflow and inflow should be approximately balanced owing to the wind-induced net barotropic inflow. Residual outflow was 0.7×10^4 m^3/s and inflow was 1.3×10^4 m^3/s. This imbalance was produced by the barotropic inflow (0.3×10^4 m^3/s resulting from a ~0.01 m/s mean inflow over the area of the cross section, i.e., 3.6×10^5 m^2) and the outflow unaccounted for in the upper 2.5 m of the water column (0.3×10^4 m^3/s caused by a mean outflow of ~0.04 m/s throughout the 3.2×10^4 m of the cross section).

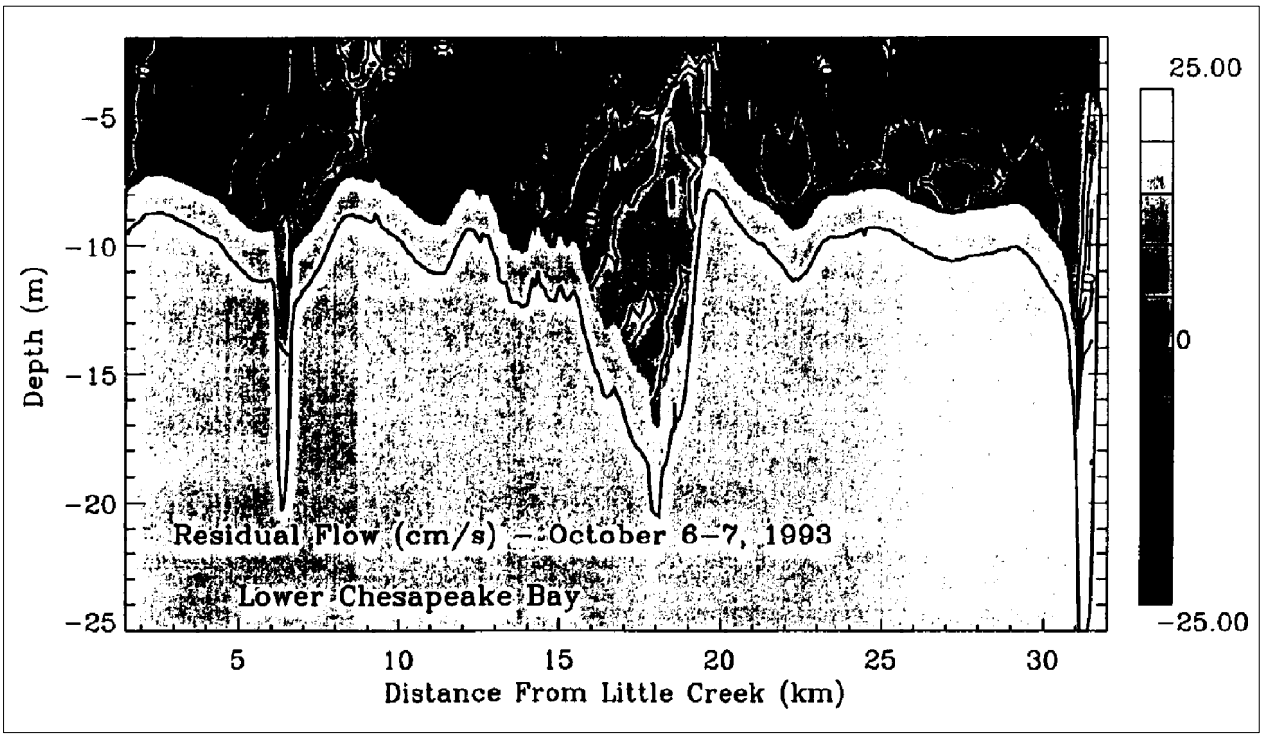

Figure 10a Mean flow (in cm/s) during the period 6-7 October 1993. Positive (negative) values indicate flow into (out of) the estuary. Net inflow occurs in the navigational channels and net outflow appears over the shoals. The navigational channels from left to right are Thimble Shoal, Chesapeake, and Beach.

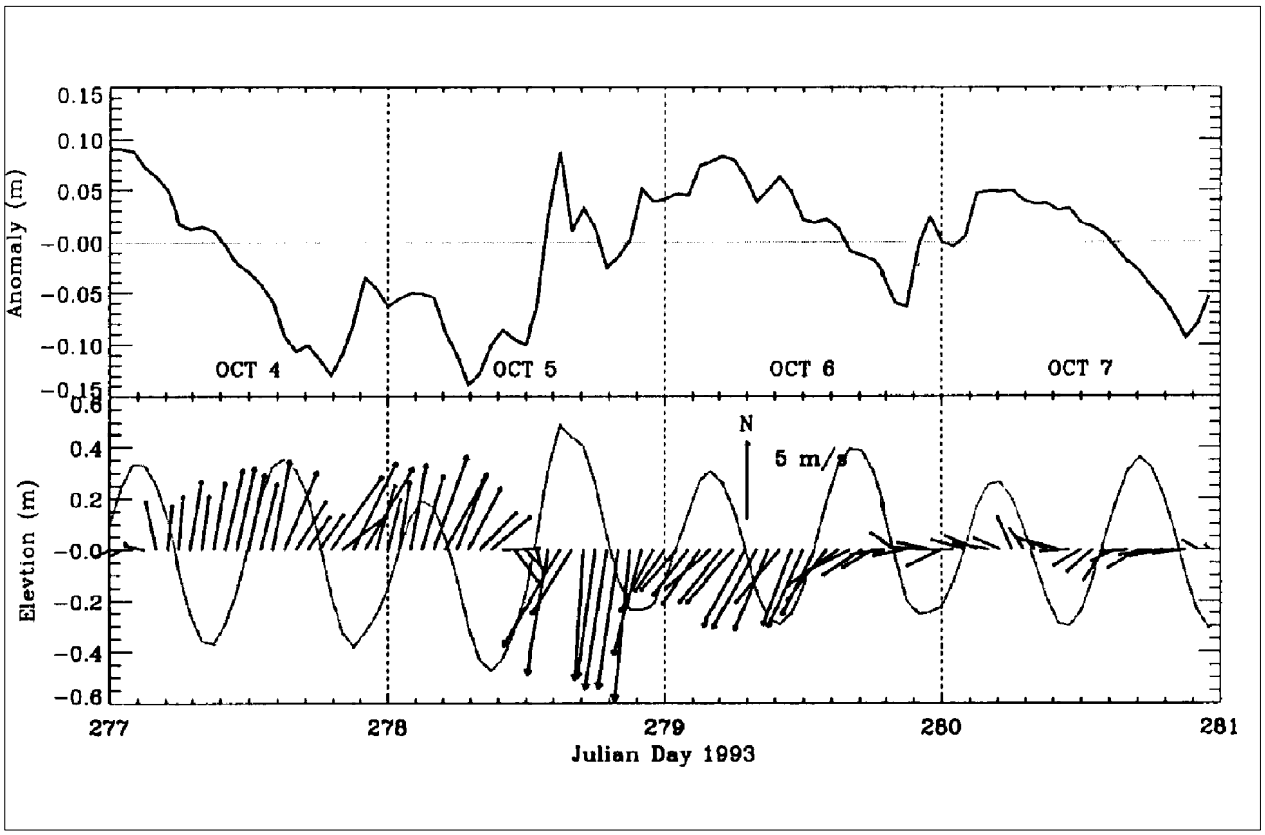

Figure 10b. Wind and sea level from station at CBBT. Tidal anomaly (upper panel) shows the difference between observed and predicted sea level (in meters). Wind velocity (in m/s) and variations around mean sea level (in meters) (lower panel) show westward winds during the ADCP observation period and slight increase in mean sea level owing to the wind forcing.

SUMMARY

A combination of current velocity measurements and process-oriented numerical simulations is used to describe the variability of water exchange between Chesapeake Bay and the adjacent coastal ocean and the response of the lower Bay to different forcing scenarios and to bathymetric effects. Records from moored current meters indicate a general trend for near-surface and near-bottom net outflow at a station south of Thimble Shoal channel. Near-bottom net outflow is reversed by three different mechanisms: during periods of neap tides, which are when decreased tidal stirring allows the development of gravitational circulation; after the cessation of seaward barotropic pulses caused by relatively strong (> 10 m/s) northeastward winds; and by baroclinic effects caused by southward winds that pile up water against the coast of Norfolk. Near-surface net outflow is hindered and can be reversed by the second mechanism.

Numerical simulations over a flat-bottom geometry drawn from the lower Bay confirm the restoring of water into the estuary after a pulse of barotropic outflow. This happens within 1 day after cessation of the outflow. The simulations also show the importance of the southward coastal ambient flow in enhancing volume inflow and in altering the shape and extension of the outflow into the coastal ocean. Variations of this coastal flow, caused by wind stress changes in direction and by longshore pressure gradients fluctuations, will cause volume exchange variability.

Bathymetric effects on volume exchange in the lower Bay are illustrated with high-resolution acoustic Doppler current profiler observations along a transect. Net inflows are restricted to the deepest regions of the transect, over the navigational channels. Net outflows appear over the shoals, even in the portion of the transect where theory predicts net inflow. This net flow pattern suggests the importance of bathymetric features in distributing materials into and out of the estuary.

REFERENCES

Chao, S.-Y. 1988. River-forced estuarine plumes. *J. Phys. Oceanogr.* 18:72-88.

Geyer, R.W., and G.A. Cannon. 1982. Sill processes related to deep water renewal in a fjord. *J. Geophys.Res.*87(C10): 7985-7996.

Goodrich, D. M. 1987. Nontidal exchange processes at the Chesapeake Bay entrance in Ragan, R., ed. *Hydraulic engineering 1987*, New York: American Society of Civil Engineers, 493-498.

Goodrich, D.M. 1988. On meteorologically induced flushing in three U.S. East Coast estuaries. *Estarine, Coastal and Shelf Sci.* 26: 111-121.

Griffin, D.A., and P.H. LeBlond. 1990. Estuary ocean exchange controlled by spring-neap tidal mixing. *Estuarine, Coastal and Shelf Sci.* 30: 275 -305.

Haas, L.W. 1977. The effect of the spring-neap tidal cycle on the vertical salinity structure of the Ames, York,and Rappahannock Rivers, Virginia,USA, *Estuarine, Coastal and Shelf Sci.* 5, 485-496.

Linden P.F., and J.E. Simpson. 1988. Modulated mixing and frontogenesis in shallow seas and estuaries. *Continental Shelf Res.* 8(10):1107-1127.

Miller, M.J., and A.J. Thorpe. 1981. Radiation conditions for the lateral boundaries of limited-area numerical models. *Q.J.R. Meteorol. Soc.* 107: 615-628.

Nunes Vaz, R.A., G.W. Lennon, and J.R. Samarasinghe. 1989. The negative role of turbulence in estuarine mass transport. *Estuarine,Coastal and Shelf Sci.*361-377.

Oey, L.Y., and G.L. Mellor. 1993. Subtidal variability of estuarine outflow plume, and coastal current: A model study. *J. Phys. Oceanogr.*, 23: 164-171.

Valle-Levinson, A., J.M. Klinck, and G. Wheless. 1994. Baroclinic exchange in the lower Chesapeake Bay. Submitted to *Continental Shelf Res.*

Wang, D.P. 1979a. Subtidal sea level variations in Chesapeake Bay and relations to atmospheric forcing. *J Phys. Oceanogr.* 9: 413-421.

Wang, D.P. 1979b. Wind driven circulation in the Chesapeake Bay, winter 1975. J. *Phys. Oceanogr.* 9: 564-572.

Wang, D.P., and A.J. Elliott. 1978. Nontidal variability in the Chesapeake Bay and Potomac River: Evidence for nonlocal forcing *J. Phys. Oceanogr.* 8: 225-232.

Weaver, A.T., and W.W. Hsieh. 1987. The influence of buoyancy flux from estuaries on continental shelf circulation. *J. Phys. Oceanogr.* 17:2127- 2140.

Zhang, Q.H., G.S. Janowitz, and L.J. Pietrafesa 1987. The interaction of estuarine and shelf waters: A model and applications. *J. Phys. Oceanogr.* 17: 455-469.

Toward a Sustainable Coastal Watershed:
The Chesapeake Experiment. Proceedings of a Conference
1-3 June 1994. Norfolk, VA
Chesapeake Research Consortium Publication No. 149

THIN, PERSISTENT, HOMOGENEOUS LAYERS IN THE UPPER CHESAPEAKE BAY

Charles C. Sarabun, Jr. and Linda Frizzell-Makowski
The Johns Hopkins University ,Applied Physics Laboratory

Abstract: Measurements obtained in the upper Chesapeake Bay in late spring show the occurrence of thin (1-3 m thick) layers of homogeneous water that persist for periods of about 30 minutes to several hours. These layers have been observed frequently in thermistor chain data over the period from 1984 to 1993. Vertical profile data showing temperature, salinity, chlorophyll fluorescence, and optical transmissivity and backscatter are presented for events observed in 1991 and 1993. Additional measurements using a static, vertical thermistor chain and acoustic Doppler current profiler(s) are also shown. The combined 1991 and 1993 data sets show the physical, optical, and biological characteristics and persistence of the layers. Spatial measurements of two layers observed in 1993 were made from a Zodiac-deployed conductivity-temperature-depth-fluorescence profiler. The data shown are consistent with two potential source mechanisms for the layers sinking tributary water and surface layers overrun by advancing estuarine fronts.

INTRODUCTION

The general decline in the health of Chesapeake Bay is a major problem facing the region today. The problem stems, for the most part, from the increasing stress of population growth and exploitation demands that are commercial, municipal, and recreational. The problem of course, is not unique to Chesapeake Bay. It is clear that the anthropogenic stresses will always exist. The task is to find the means to manage the stress to maintain a healthy, even if not pristine, Chesapeake Bay environment. Knowledge of the physical transport and mixing mechanisms is fundamental to understanding and managing the complex biological and chemical systems of Chesapeake Bay.

Since 1984, The Johns Hopkins University Applied Physics Laboratory (APL) has been fielding a suite of instrumentation specifically designed to study high- frequency mixing and transport mechanisms along with the interaction of these mechanisms with the biological and chemical regime in the upper Chesapeake Bay. The mechanisms include estuarine surface fronts, high-frequency internal waves, and subsurface layering. This paper discusses subsurface layers and, in particular, two specific events - one from spring 1991 and one from spring 1993.

BACKGROUND

The objective of the APL research program has been to investigate small-scale circulation and mixing processes and their relationship to larger scale flows and to mixing and transport of scalars in the estuarine environment. In Chesapeake Bay in the spring, freshwater runoff from tributary rivers establishes a two-layer system with warm, freshwater overlying cold, salty water. These two relatively well-mixed layers are separated by the pycnocline in which density (temperature and salinity) changes rapidly with depth. Mixing and dispersion in the estuary, and across the pycnocline, may be driven by the gravitational circulation, wind events, tides, and a number of smaller-scale, higher-frequency features such as fronts, shear instabilities, and breaking internal waves. Our focus has been on defining the characteristics of higher -frequency features and

their role in mixing and dispersion in the upper Chesapeake Bay (Sarabun et al. 1985, Sarabun and Dubbell 1990).

The initial focus of the APL program was the study of large-amplitude, high-frequency internal waves. The ongoing studies of internal waves generated many long time-series of thermistor chain data. In reviewing those data, the frequent occurrence of thin layers, or intrusions, was observed. These layers had vertical extents of 0.5 to 2.5 m and "lifetimes" of a few tens of minutes to a few hours (note that the vertical resolution of the chains limited observation to layer thicknesses of ž 0.5 m). Vertical temperature and salinity profiles have shown a great deal of "steppiness", repeating layers of well-mixed water, with vertical scales of a few tens of centimeters. Recent field work by APL has focused on the study of these layers as significant transport mechanisms in Chesapeake Bay. It is the results of these most recent investigations of intrusion-like features that are discussed below, in addition to the previously collected data examined for layering in the upper Bay.

Before we can determine if such features are important to mixing and transport in the Bay, there are several of questions that must be answered. First, do such features appear often enough and have a large enough spatial extent, and do they last long enough to play a significant role in transport and mixing?

If the layers are very short-lived, are spatially very limited, or rarely occur, then their net effect in the Bay will be small. However, if these features occur frequently, last for some time, and have a significant volume, then they have the potential to become significant transport pathways.

Secondwhat are the potential sources for these laminae? Are their chemical, biological characteristics different from the overlying and underlying water masses? There are a number of possible source mechanisms for such layers. In cases where the layers are formed locally, their impact is primarily on vertical exchange. Layers formed as a result of nonlocal mechanisms have the potential to transport scalars (toxic materials, nutrients, etc.) significant distances without appreciable dilution and thus may play an important role in the redistribution of scalars in the Bay.

METHODS

The instrumentation used to investigate intrusion events include several vertical thermistor chains, a 600 kHz acoustic Doppler current profiler (ADCP), a high-resolution vertical profiler and pumped-water sampler, and a high-accuracy GPS navigation system. Additional instrumentation furnished by ship's personnel or other investigators included a Conductivity-temperature-depth-fluorescence (CTDF) profiler, a profiling current meter, meteorological instrumentation, and Niskin bottles for volume water samples.

The ADCP is an RDI system operated with a vertical resolution of 0.25m. Both the current velocity and backscatter intensity were recorded.

The principal thermistor chain is 8 m long and consists of sixteen thermistors spaced at intervals of 0.5m and two pressure transducers located at the top and bottom. The system is faired to reduce drag and to reduce hydrodynamic (flow) disturbances that may alias the data. The resolution of the thermistors is 0.007½C, and their response time is 20 msec. The accuracy of the thermistor sensor is 0.05½C using a 5-point calibration and a second-order fit. The pressure transducers (Stratham or Entran were used on different experiments) have a resolution of 0.01 m. The thermistor and pressure sensors are interfaced to a Metrobyte 16-channel multiplexer extension (EXP-16) board. Digitizing of signals is performed by a Metrobyte 16-channel analogue-to-digital conversion board (DASH-16G2). The digitized output from the Metrobyte board is transferred to a Compaq 386 PC, which uses Labtech Notebook as the control software. Data for all channels were sampled at 4 Hz using an analogue prefilter of 1 Hz. Data were stored on 20 MB Bernoulli hard disks. The thermistor chain was generally deployed from a ship in a static mode and weighted at the lower end; however, this system can also be towed up to a maximum boat speed of 5 knots. The thermistor data were displayed in real time using the Labtech Notebook data acquisition software package. After the conclusion of each experiment, the data were transferred to a DEC VAX 3500, where they were edited and transformed into engineering units for analysis.

The high-resolution vertical profiler (HRVP) system measures the following parameters: temperature, conductivity, depth, *chlorophyll a* concentration, optical beam attenuation, backscatter, and bioluminescence potential. Table 1 lists the specifications of the sensors. The vertical profiler is a modified General Oceanics Model 1015-24-5l rosette multibottle array. The deck unit, a shipboard HP 9826 computer system, handshakes asynchronously with a HP 9920 computer, which provides averaged data profiles and quick-look

Table 1. Vertical profile instrument specifications.

Parameter	Sensor type	Range	Resolution	Absolute accuracy	Response time (s)
Water temperature (°C)	Sea-Bird Electronics SBE-3 thermistor thermometer	0–35	0.001	0.01	0.07
Conductivity (S/m)	Sea-Bird Electronics SBE-4 conductivity cell	0.05–6	5×10^{-5}	1×10	0.17
Depth (m)	Parascientific quartz pressure sensor	0–633	0.05	0.63	0.07
Chlorophyll-a concentration (µg/L)	APL fluorometer	0.04–30	0.04	1% FS	0.7 (estimated)
Beam Attenuation coefficient (% transmission)	APL transmissometer	0–100	0.01	1.0	1.4
Bioluminescence potential (photons/s)	APL bathyphotometer	50–10^6	1.0	10	0.08

FS = full scale.

graphics. The data from all sensor systems on the vertical profiler were collected at a 12 Hz sampling rate. This vertical profiler system was deployed during the 1991 and 1993 Chesapeake Bay field tests. Data were collected every hour during the on-station period (along with the ship's CTDF and ADCP). At the onset of a front or intrusion, the profiler system was deployed every 15 to 20 min. Water samples were also collected. Species enumeration and *chlorophyll a* fluorescence measurements were made on board the ship. After the conclusion of the experiment, data were transferred to a DEC VAX 3500, where they were edited and post-test calibrations were applied.

A battery-operated profiling system was also deployed in 1993 from a Zodiac. The system included CTD, chlorophylla fluorescence and optical backscatter. Data were acquired and displayed in real time using a Compac notebook computer and a Blue Earth A/D system. The Zodiac was deployed to measure the spatial extent of the layer. Positioning of the Zodiac was done using a portable GPS navigation system.

Observations

The data discussed below were acquired during field tests in the spring of years 1984-93. During these tests, several standard stations were occupied for a minimum of 25 hours, during which time the ship was anchored fore-and-aft to minimize contamination in the chain data as a result of the ship swinging at anchor. Figure 1 shows the locations of our standard stations.

We have observed the regular occurrence of thin (1 - 2 m thick) laminae in the time series of the ship-moored thermistor chain data (Frizzell-Makowski et al. 1994). These features have been observed to persist for periods of 10 minutes to several hours. Figure 2 shows the onset of one such event at 1013 in the time series from a thermistor chain moored at station 838 of figure 1. The well-mixed water of the intrusion is colder than the overlying water and warmer than the underlying water. Thus, in the time series, the onset of the event is seen in the temperature drop in thermistor T6 as it encounters the relatively colder water of the well-mixed intrusion. Thermistors T3 and T4 rise in temperature instead as they encounter the relatively warmer water of the intrusion. Because the spacing between thermistors was 50 cm, this

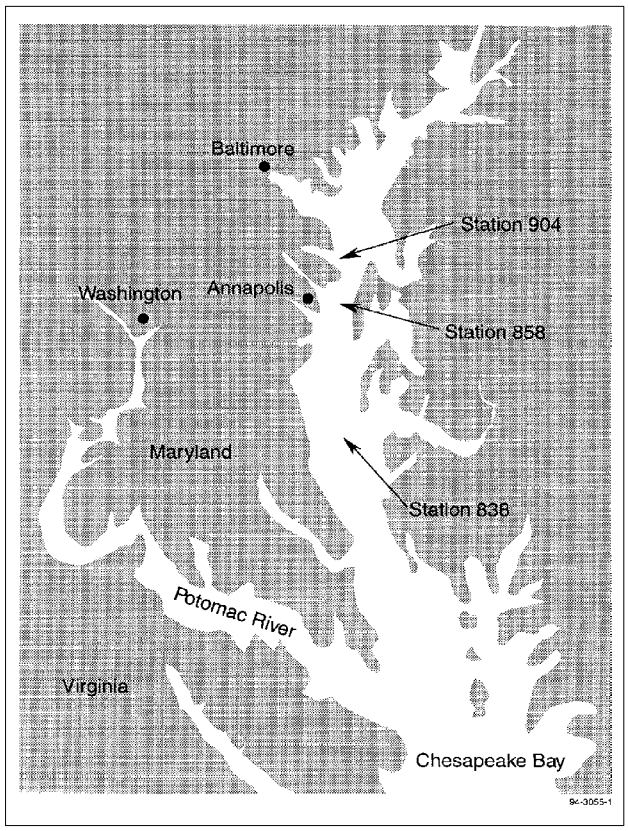

Figure 1. Standard locations of stations 838, 858 and 904 located in the upper Chesapeake Bay.

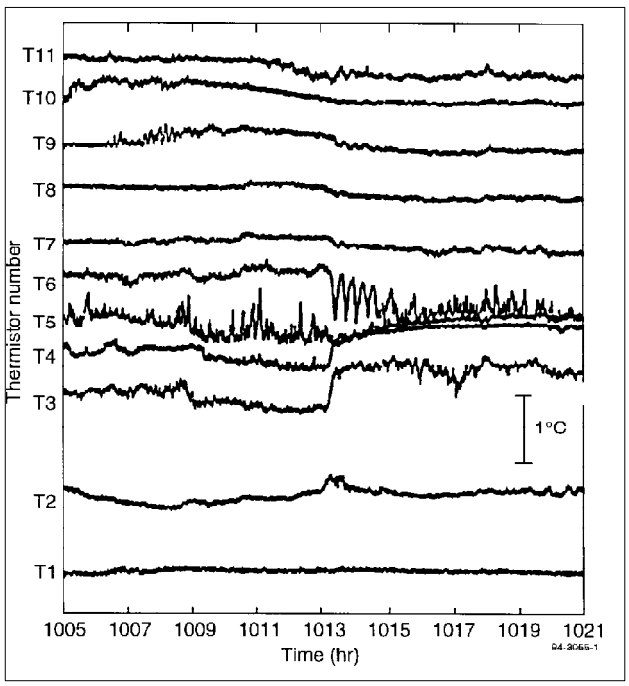

Figure 2. Thermistor chain time series obtained in 1986 at station 838. Note the temperature drop in T6 and the temperature rise in T3 and T4, and the internal waves on the upper, leading edge on T6 at 1013.

event represented an intrusion event of about 1.5 to 2 m in thickness. Note the internal wave activity on the upper, leading edge of the intrusion (T6) beginning at about 1013.

While the thermistor chain data obtained during the 1980s were not processed for intrusion-like events, a preliminary review of those data show that events were observed in each year of historical data reviewed. In addition, layers were observed at all of the station locations shown in figure 1. During the spring 1986 field test, three stations, 906, 838 and 858 were each occupied for a 25 hr period. This data set provided a cursory look at the prevalence of such features. The variability in observed events ranged from 3 to 8 events. The duration of the events are split into three time intervals as shown in table 2. The vertical thickness of these features varied from 0.5m to 2.5m. Frequently, but not always, the thinnest layers existed for the shortest duration. Data obtained from a five tidal cycle station at station 858 (figure 1) in 1993 are summarized in table 3. These data show that such layers do occur frequently.

Table 2. Intrusion-like events observed at three stations during spring 1986.

Station	906	858	838
Hours on Station	25	25	25
Number of Intrusions	7	3	8
Duration			
< 0.5 hr			
0.5 -1.0 hr	3	2	2
< 1.0 hr	2	1	2

Table 3. Preliminary results from CBX field study.

Number of Intrusions	Duration (hr)	Thickness (m)
1	< 0.5	0.5
5	0.5 to 1.5	0.5 to 2.0
2	> 2.0	0.5 to 2.5

In 1993 the Zodiac-based system was used to make concurrent measurements of spatial extent of layers. Once an event triggered more rapid profiling at the R/V *Cape Henlopen* station, the Zodiac would begin a series of profiling runs operating along a line perpendicular to the current direction. Thus, the time series at the station gave an estimate of along-current linear dimension, while the Zodiac provided an estimate of the lateral, or cross-current, dimension. Figure 3 shows the cross-current spatial extent of one event to be on the order 1 km and the current speed times the length of time the layer was observed gave an estimate of 2 km for along-current spatial extent. Thus, it would appear that such features do indeed appear often enough and have a large enough spatial extent to be potentially significant transport pathways.

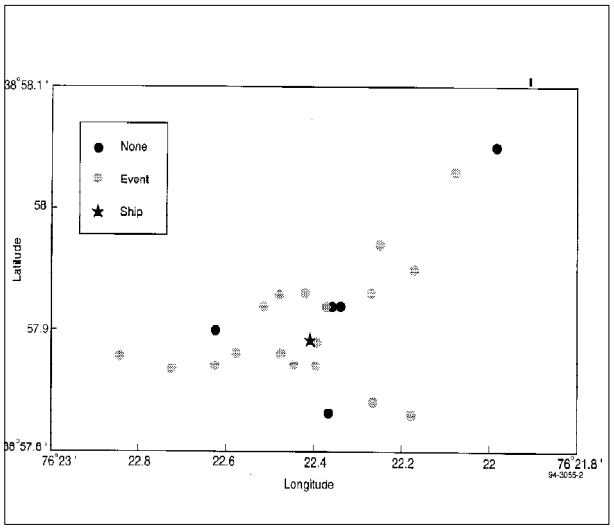

Figure 3. Spatial distribution of intrusion event 2, June 1993.

The question of importance of these features in transport and mixing in the upper Chesapeake Bay depends in part upon the origin of such features and their chemical and biological characteristics relative to water masses above and below. There are a number of potential source mechanisms. Turbulent mixing of two water masses and mixed region collapse following overturning of large internal waves are both plausible source mechanisms, but both generate thin layers of water with characteristics intermediate between the upper and lower local water types. Thus, while physically interesting, these features need not be significant transport mechanisms. Other sources include boundary layer mixing as suggested by Phillips et. al. (1986), and sinking tributary water as suggested by Tyler (1984). These features import into an area water whose chemical and biological makeup is different from that of the local water. These features can act as important transport pathways, moving distinct water types significant distances without appreciable mixing.

In spring 1991, a several-day field test was conducted specifically to begin the study of intrusions seen in thermistor chain data from previou years. While the test was interrupted by strong winds, one intrusion-like event was observed at station 858 prior to the onset of the wind event. A 1 hr time series of the thermistor chain data during which the event occurred is shown in figure 4. Just prior to 0500, thermistor 6 shows a sudden dip in temperature. While not as strong a signature as those seen in figure 2, the appearance of such a feature precipitated more frequent vertical profiling with the *Cape Henlopen* CTDF and the APL HRVP (every 15-20 min rather than hourly). A series of APL HRVP temperature profiles collected before and during the passage of the intrusion are shown in figure 5. Note the distinct, well-mixed layer between 7 and 8 m in 0500 and subsequent temperature profiles. The 0400 profile collected prior to the intrusion event during regular hourly operations does not show a homogeneous layer at that depth. Notice also that the layer is evident in the corresponding *chlorophyll a* fluorescence profiles as a fluorescence deficit. The layer was tracked for 2 hours in the CTDF and HRVP profiles until high surface winds forced abandonment of the station.

After station 858 was abandoned, the R/V *Cape Henlopen* began a series of single-profile stations

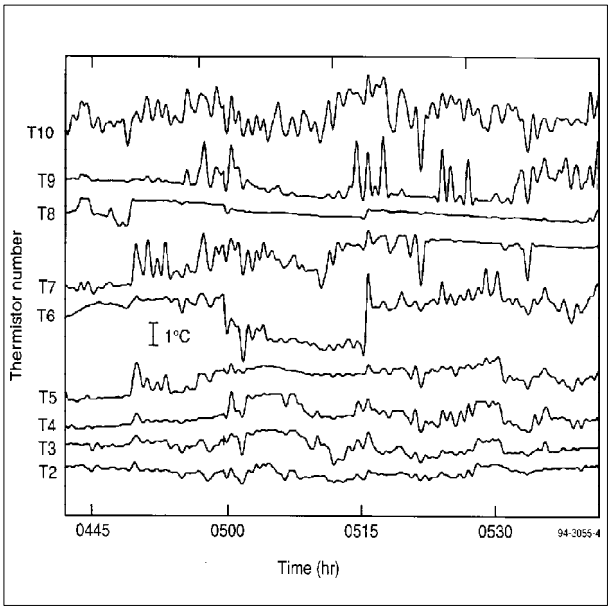

Figure 4. Thermistor chain time series obtained in 1991 at station 858. The dip in temperature in thermistor T6 marks the onset of the event.

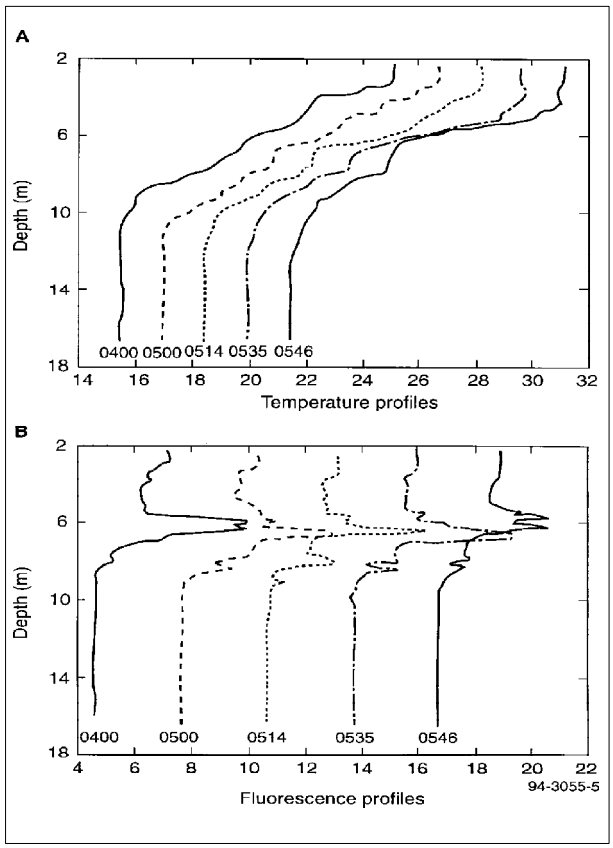

Figure 5. Temperature *chlorophyll a* fluorescence profile series obtained with the high-resolution profiler from before the intrusion at 0400 and during the intursion event (0500 on). Note the step at ca. 7-8 m in the temperature profiles from 0500 on, and the corresponding feature in the fluorescence profiles.

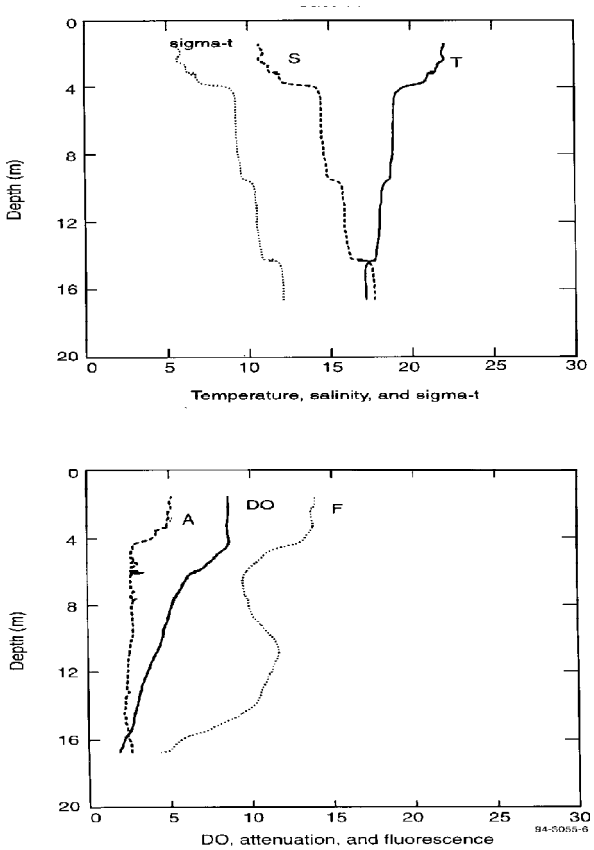

Figure 6. Vertical profiles of temperature (T), salinity (S), sigma-t, fluorescence (F), beam attenuation (A), and dissolved oxygen (DO) at the mouth of Eastern Bay.

ranging from the Chester River to Eastern Bay to several tributaries on the Western Shore of the main stem of the Bay. If the observed layer was sinking tributary water, as suggested in the data presented by Tyler (1984), then the chemical, optical, biological, and physical characteristics of the intrusion should most closely resemble those of one of the tributaries. Figure 6 shows a profile taken at the mouth of Eastern Bay. Note the four distinct layers seen in the physical data. A cluster analysis using temperature, salinity, dissolved oxygen, chlorophyll fluorescence, optical backscatter, and optical beam attenuation showed that the water in the layer observed at station 858 most closely resembled that of the upper layer at the mouth of Eastern Bay when compared to the four layers of figure 6 and the water above and below the layer at station 858. The results, while not conclusive, do suggest that sinking tributary water may account for some of the layers observed in our data.

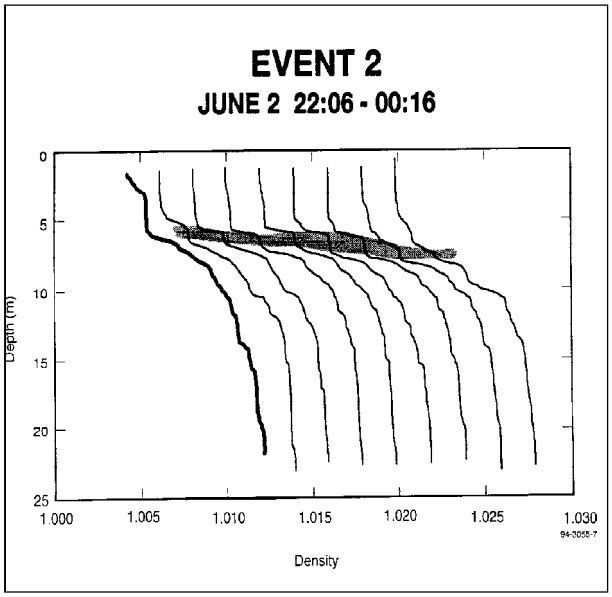

Figure 7. Time series of density profiles from event 2, June 1993. The shaded area highlights the layer of interest.

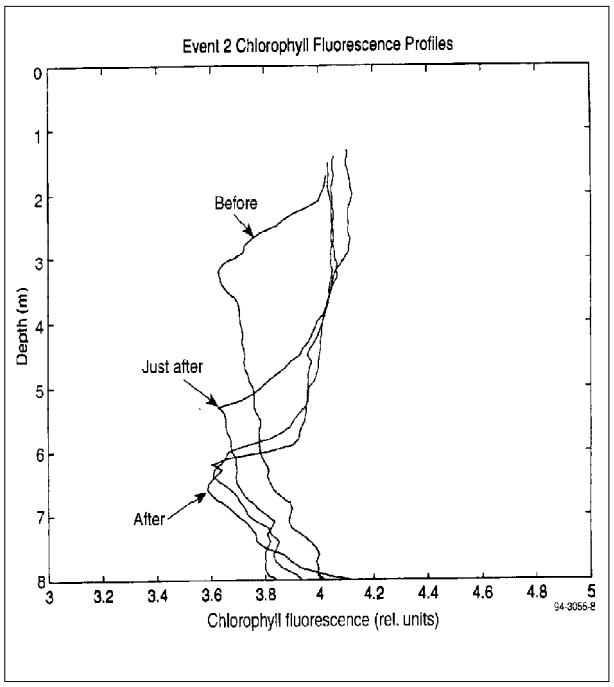

Figure 8. Expanded view of the upper water column chlorophyll fluorescence during event 2, June 1993. The figure shows profiles from before, during, and after the first layer appearance. Note that from figure 6 the layer depth is 6-7 m.

In June 1993, station 858 was occupied for five consecutive tidal cycles to continue the study of the intrusion-like events. As shown in table 3, a number of layer events were observed. Figure 7 shows a series of sigma-t profiles in which an event was observed. The first profile does not show the layer, while it is clearly evident in later profiles. Notice that the layer progressively deepens with time. Figure 8 shows chlorophyll fluorescence profiles of the near-surface region. Notice that at the depth of the layer, the post-appearance profiles clearly show a different chlorophyll signature than the pre-appearance profile. Notice also that the chlorophyll signature could not be the result of mixing of water above and below the observed layer. Thus the layer observed clearly represents a different water type. However, when examining the thermistor chain time series, (see figure 9), the characteristic intrusion signature shown in figure 2 is absent.

A comparison of thermistor chain data and profile data with data presented in Sarabun (1993) suggests that tidal frontal activity is responsible for the appearance of this layer. Figure 10 shows the thermistor chain timeseries for a front observed in 1986 at station 858. In both figures, the thermistor temperatures are seen to rise following the passage of the frontal interface. A comparison of sigma-t profiles from before and after the front passes, (see figure 11), shows clearly the similarity in the near-surface profile. The assertion that the event seen in the 1993 data is attributable to frontal passage is further reinforced by figure 12, which shows gray scale-encoded acoustic backscatter intensity. The light-water pool following the surface front is evident as the light-colored mass that begins at about 2145 hrs. Of more interest is the dark band that starts at the surface prior to the arrival of the light-water pool and gradually deepens to about 5.5 m as the light-water pool migrates through the station. Referring again to figure 7, note that the depth of the layer progressively deepens over time as would be the case if the layer had been formed as a result of an overriding lighter-water pool. Reexamining figure 8,

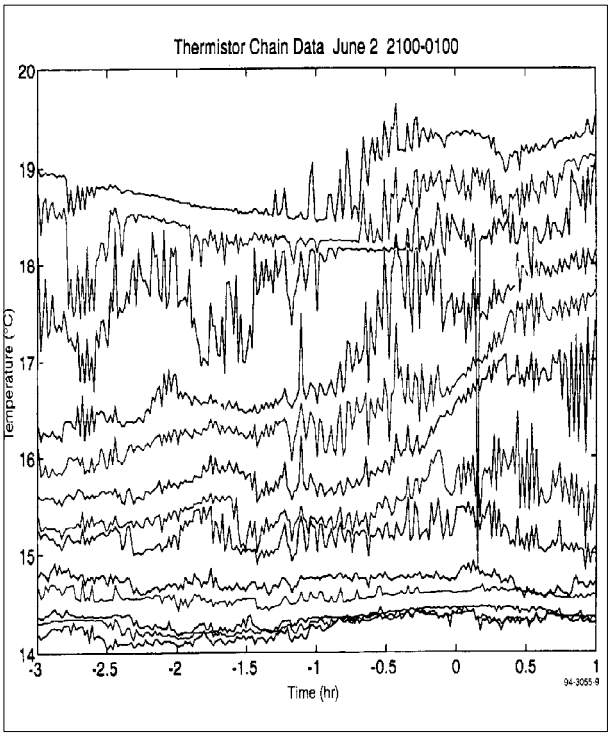

Figure 9. Thermistor chain timeseries from event 2, June 1993. The event onset occurs at about -1.5 hrs.

note that the fluorescence values in the layer are more consistent with the very near surface value in the profile prior to the appearance of the layer. The aggregated data show that the layer clearly had an origin different from the water both above and below it. The data suggest that the layer was formed as a result of the light- water pool behind a tidal front overriding surface water to create the thin layer below the light-water pool. This mechanism produces distinct layers in a manner similar to the sinking tributary water.

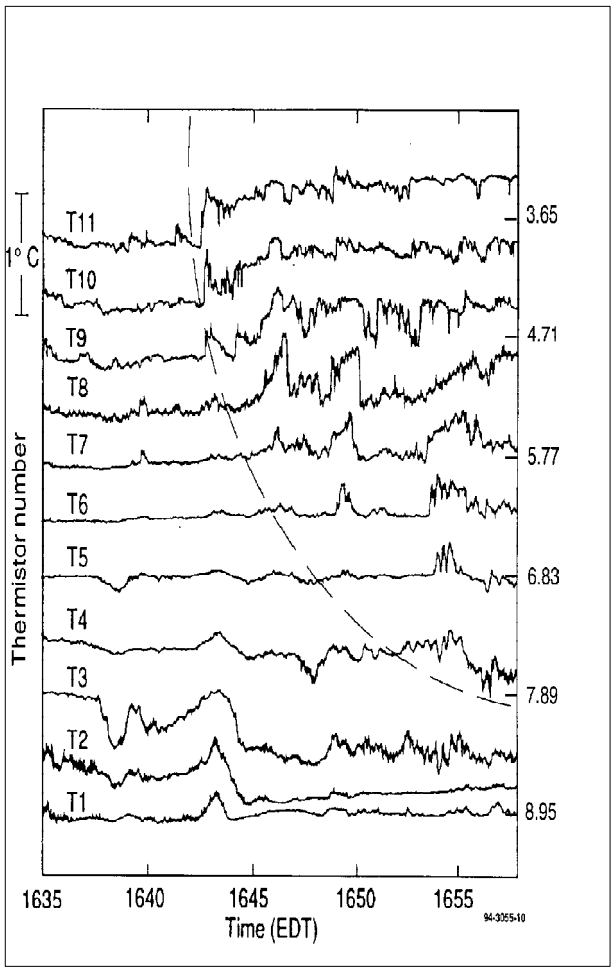

Figure 10. Thermistor chain time series from a frontal passage in June 1985. The dotted line shows the location of the frontal interface. The frontal passage is seen as a series of temperature increases in successively deeper thermistors. Note also the increase in high- frequency activity following frontal passage.

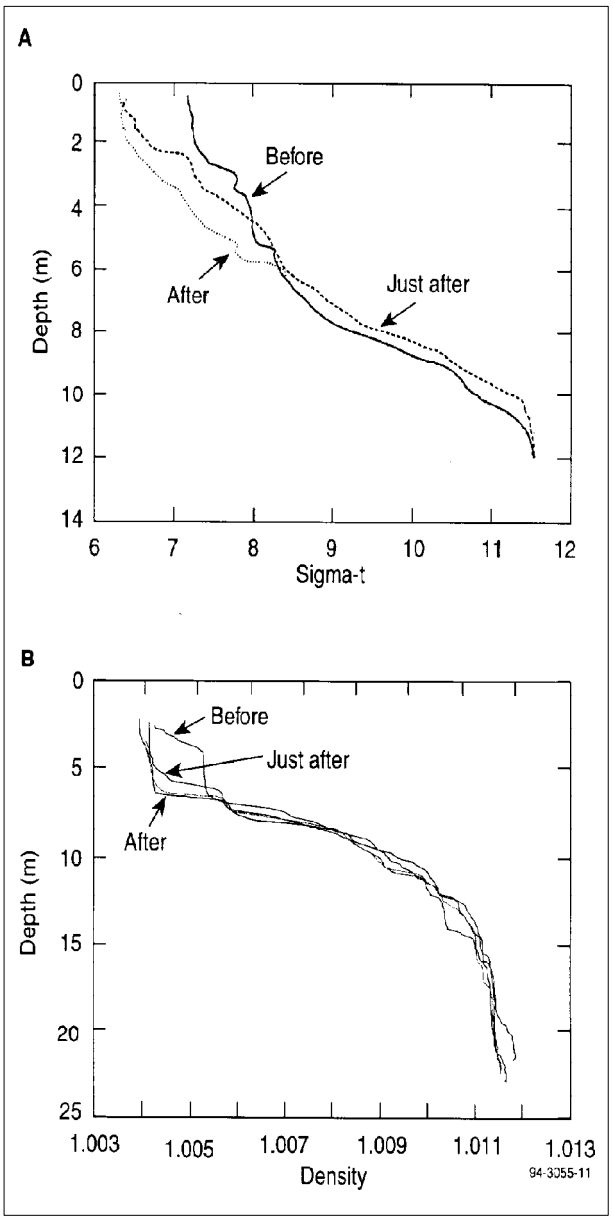

Figure 11. Sigma-t profiles in 1985 and 1993. A: Series of sigma-t profiles before and after frontal passage in 1985. B: Series of sigma-t profiles before and after the onset of event 2, June 1993. In both cases, the sigma-t traces clearly show the surface light-water pool following frontal passage.

CONCLUSION

Our historical data clearly show that the layers we have observed are a frequent occurrence and that they can be persistent in time, which suggests a significant spatial extent. Subsequent data obtained in 1993 show that some layers may indeed have a significant horizontal size, 1 km by 2 km in the example shown. Our historical chain data do not, however, provide sufficient information to determine the origin of such features. There are a number of possible source mechanisms, all of which may be active at one time or another. In this paper we have presented two data sets, one from 1991 and one from 1993. In both cases the data suggest that the layers were not formed as a result of local mixing processes. The data also showed that the layers did have significantly different characteristics from the water above and below. This evidence suggests that such thin, persistent layers could be very important transport pathways capable of conveying passive scalars such as nutrients or toxic materials significant distances (both horizontally and vertically) from the point of origin before appreciable mixing occurs.

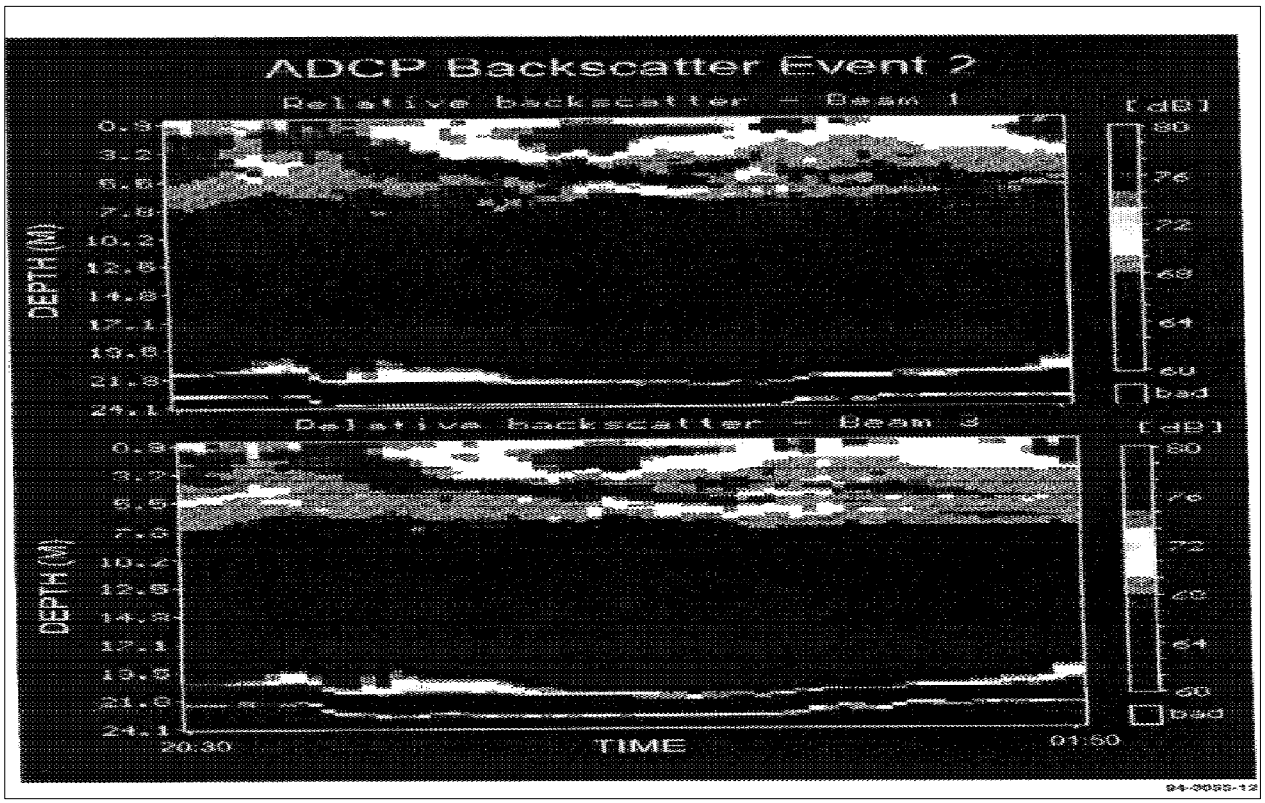

Figure 12. Gray scale-encoded acoustic backscatter intensity during the time of event 2, June 1993. The light-water pool after the surface front is the near-surface, light-colored region. Note the thin, dark layer extending from the surface before the time of event 2 to a depth of about 5.5 m below the light-water pool.

ACKNOWLEDGEMENTS

Ship time for APL Chesapeake Bay work was provided by Dr. Robert Biggs, Dr. Howard Seliger, Dr. Mary Altalo, Dr. Lawrence Harding, The U.S. Naval Academy, and APL. Co-investigators have included Alan Brandt, Dan Dubbell, and Dan Ondercin. The APL project has been supported by Joe Hopkins, Kevin Fleagle, Jim Velky, and Rob Waterworth for instrumentation and data acquisition.

REFERENCES

Frizzell-Makowski, L., C.C. Sarabun, and D.G. Ondercin, 1994. Physical, optical and biological characteristics of thin homogeneous layers in the pycnocline of the Upper Chesapeake Bay. EOS Transactions of the American Geophysical Union

Phillips, O. M., J.H. Shyu, and H. Salmun, 1986, An experiment on boundary mixing: Mean circulation and transport Rates. Journal of Fluid Mechanics, 173: 473-499.

Sarabun, C.C. 1993. Observations of a Chesapeake Bay tidal front, 1993, Estuaries 16(1).

Sarabun, C.C., and D.C. Dubbel. 1990. High Resolution thermistor chain observations in the Upper Chesapeake Bay, Johns Hopkins APL Technical Digest, 11(1&2): 48-53.

Sarabun, C.C., A. Brandt , M.A. Tyler, and G.D. Smith 1985. Biological Transport, Internal Waves, and mixing in the Chesapeake Bay. John Hopkins APL Technical Digest.

Tyler, M.A. 1984. Dye tracing of a subsurface chlorophyll maximum of a red-tide dinoflagellate to surface frontal regions. Marine Biology 78: 285-300.

Toward a Sustainable Coastal Watershed:
The Chesapeake Experiment. Proceedings of a Conference
1-3 June 1994. Norfolk, VA
Chesapeake Research Consortium Publication No. 149

TRANSPORT OF CONSERVATIVE TRACERS IN THE CHESAPEAKE BAY WATER QUALITY MODEL

Lewis Linker
U.S. Environmental Protection Agency

Kurt Neumiller
Chesapeake Research Consortium

Abstract: Conservative tracers were used in the Chesapeake Bay Water Quality Model tracer scenarios to visualize the movement of material from major tributaries throughout the Bay. The tracer scenarios were run in order to better understand the reasons for the varied water quality response of the main Bay to the same nutrient load reductions taken at different tributaries. The analysis traced the three-dimensional movement of the conservative tracer in the mainstem. Dissolved conservative tracers were input continuously at the fall lines and ocean boundary at an arbitrary load of 100,000 kg/day. Particulate conservative tracers with a settling rate of 0.1 m/day were input continuously at the lower tributaries and ocean boundary at an arbitrary load of 100,000 kg/day. The average hydrology year of 1986 was used for this analysis.

The flux of tracer at main-bay transects is depicted as a three-dimensional picture showing the flux of each model cell with the hydrodynamic flux of seaward surface flow and up-bay bottom flow is rendered with considerable spatial detail. The analysis finds that tracers from northern Bay tributaries have greater retention in the Bay than southern Bay tributaries owing to hydrodynamic entrainment. The magnitude of the hydrodynamic accumulation of tracer material is variable throughout the Bay. The area of greatest accumulation is the mid-bay region of the Potomac. There is little up-bay transport of tracer from the James and York tributaries. Most of the up-bay transport of tracer from these tributaries is attributable to discharge of the tracer to the coastal ocean and its return to the Bay by coastal ocean mixing.

INTRODUCTION

Conservative tracers were used in the Chesapeake Bay Water Quality Model to visualize the movement of material from major tributaries throughout the Bay. The tracer scenarios were run to better understand the reasons for the varied water quality response of the mainstream of the Bay to nutrient load reductions in different tributaries. Dissolved conservative tracers were input continuously at the major tributary head of tide and at the ocean boundary at an arbitrary load of 100,000 kg/day. Particulate conservative tracers, with a settling rate of 0.1 m/day, were input continuously at the mouth of major tributaries and the ocean boundary at an arbitrary load of 100,000 kg/day. An average hydrology year (1986) was used for this analysis.

The dissolved tracer flux was quantified over seven main-bay transects, with the tracer flux of each transect model cell being calculated. Deposition of the particulate tracer flux was quantified in eight main-bay regions and the ocean region. The analysis quantifies the influence of dispersion and estuarine circulation on estuary load inputs.

METHODS

The Three-Dimensional Eutrophication Model of Chesapeake Bay (3D model) was used in this analysis (Cerco and Cole 1994). Hydrodynamic input for the 3D model is from a three- dimensional, time-varying hydrodynamic model of the Chesapeake Bay (Johnson et al. 1991). The timestep of the hydrodynamic model is 5 min, which is aggregated into 12hr (intertidal) current, salinity, and elevation by a postprocessor for use by the 3D model. In the tracer scenarios, water

quality dissolved and particulate state variables were used with all chemical kinetics turned off to render the tracers completely unreactive.

The 3D model was calibrated for three hydrodynamic years, 1984-1986. The tracer simulation was run by splicing a 10- year sequence of the 1984 (wet), 1985 (dry), and 1986 (average) years that most closely represented the sequence of hydrology over 1980 -90. The average hydrology year (1986) in year nine of the simulation was used for the analysis.

An arbitrary load of 100,000 kg/day of dissolved conservative tracers was input continuously at the head of tide of major tributaries and at the ocean boundary. An arbitrary load of 100,000 kg/day of particulate conservative tracers was input continuously at the surface layer of the tributary mouths and ocean boundary. Conservative particles had a settling rate of 0.1 m/day, which is consistent with the rate of living suspended particles (algae) in the model. The tributaries with releases of dissolved and particulate tracers include the Susquehanna, Patuxent, Potomac, Rappahannock, York, James, Pocomoke, and Nanticoke, and the ocean boundary. Figure 1a depicts the points of input for the dissolved and particulate tracers. The tracers were allowed free exchange between the Bay and the coastal waters through the model's ocean boundary simulation. The dissolved tracers from the Susquehanna, Potomac, James, Patuxent, Rappahannock, and York are described in this paper, as are the particulate tracers of the Susquehanna, Potomac, James, and the ocean boundary, with the primary focus on the Susquehanna, Potomac, and James tracers.

Analysis of dissolved tracers is by the flux of load at main-bay transects. Figure 1a shows the location of the transects. and figure 1b shows the 3D model surface cell grid. The flux of tracer at any transect can be depicted as a three-dimensional picture showing the flux of each model cell. Figure 2 depicts the flux of tracer material across the face of transect 5. Note from figure 1 that transect 5 dissects 10 surface cells into an up-bay and down-bay orientation. In figure 2, the 10 surface cells are rendered, along with all other cells on the transect face, each cell with an annual average up-bay or down-bay flux in units of kg/day.

This is the second series of the tracer scenarios completed by the Chesapeake Bay Program. This second series builds on the methods and findings of the first tracer scenarios, which are documented in Thomann et al. (1994).

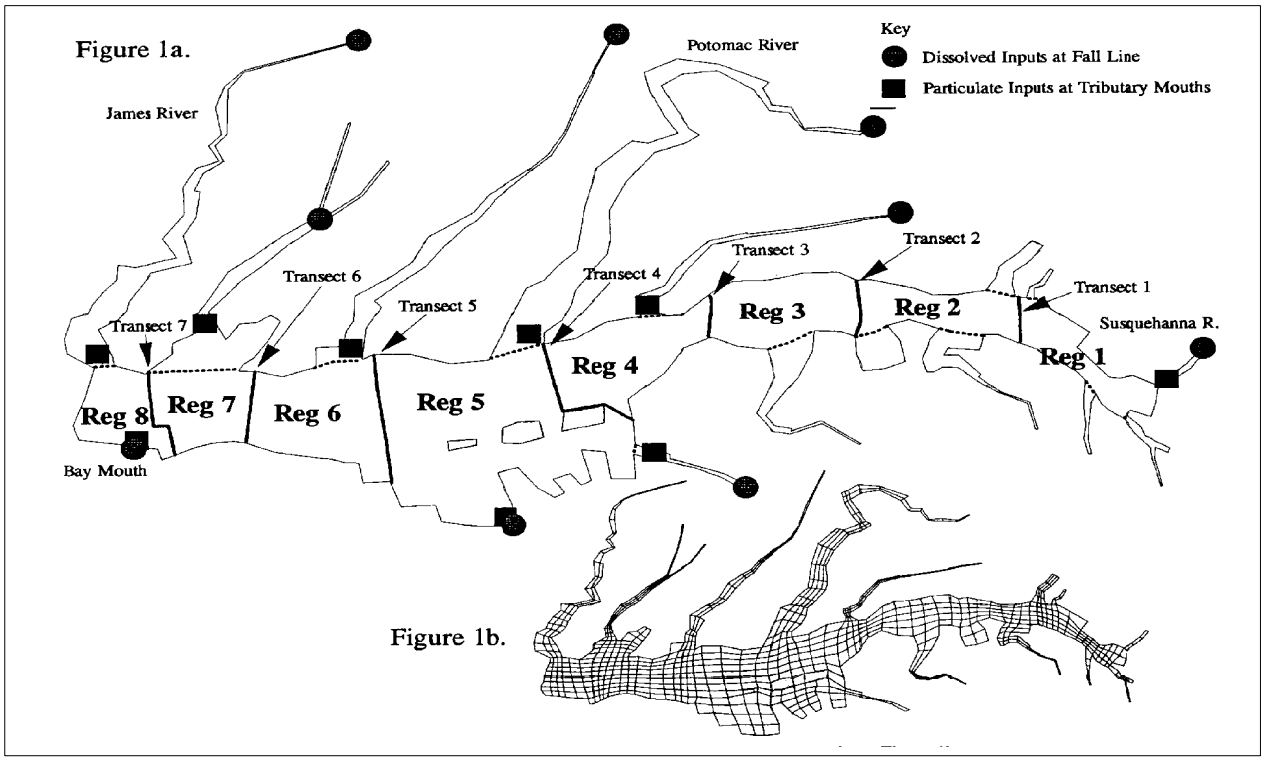

Figure 1. Use of the Chesapeake Bay water quality model. 1a: tracer analysis transect, regions, and discharge points. 1b: surface cells.

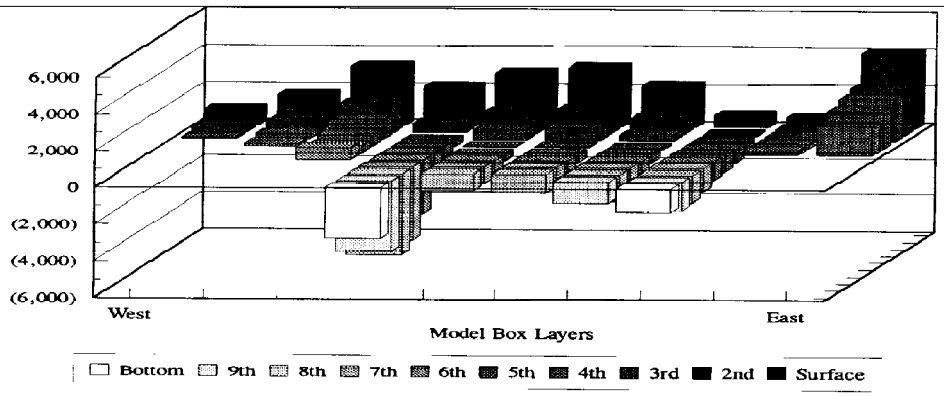

Year 9 Average Flux Kg/Day

	West								East	
Surface Layer	882	1,650	3,228	2,150	2,924	3,206	2,272	683	554	4,077
	274	601	1,605	527	1,191	1,324	838	(81)	293	2,532
	86	298	1,058	(368)	561	631	314	(490)	262	2,346
		155	619	(1,212)	25	31	(112)	(800)	245	2,070
			432	(1,992)	(393)	(452)	(442)	(946)	235	1,620
			677	(2,943)	(711)	(939)	(816)	(1,004)		
				(4,029)	(886)	(1,230)	(1,221)	(1,288)		
				(4,403)	(937)	(1,061)	(1,480)	(1,558)		
				(3,843)			(1,203)	(1,590)		
Bottom Layer				(2,786)				(1,280)		
Up Bay Transport										(42,496)
Down Bay Transport										42,477
Net										19

Figure 2. James River dissolved tracer at transect 5. Units of dissolved tracer flux are given in average kg/day. The transect face is from the ocean side of the Bay facing up-bay (north).

DISCUSSION

As summarized by Thomann and Mueller (1987), a steady state, infinitely long, one-dimensional (in the longitudinal) estuary with constant load inputs and a constant cross sectional area can be described by

$$Ed^2s/dx^2 - Uds/dx - ks = 0$$

where E is the dispersion or mixing coefficient which includes tidal flow oscillations, density currents, and other lateral and vertical velocity gradients, and U represents the net nontidal velocity (net estuarine flow). The parameters s and k are respectively, the concentration of the material input into the estuary, and its first -order decay constant. The longitudinal position within the estuary is represented by x.

Assuming the material "s" is a conservative tracer, then k = 0 and the equation reduces to:

$$Ed^2s/dx^2 - Uds/dx = 0$$

The tracer scenarios approximate the steady state condition in the unreactive state of the tracers, the constant input tracer input load, and in the use of an annual average condition for flux or deposition. For a downstream boundary condition of s_o, the solution of s for $x \leq 0$ (the case for a position up-estuary from the discharge point of the tracer) is

$$s = s_o \exp(Ux/E)$$

And for $x \geq 0$, the solution is

$$s = s_o = W/UA$$

In other words, at any discharge point x of a load W, in cross section A, the load will be dispersed up estuary of the discharge point by dispersion and the net discharge load down-estuary will be the same as the steady state input load-indeed the downstream steady state discharge load must be the same as the input load for any conservative material. The steady state flux for $x<0$ is therefore equal to zero.

Graphically, figure 3 indicates the Potomac tracer input point in the estuary that would represent x = 0. Up-bay from the input point at transects 1 through 4, the tracer is influenced by mixing and transport and the up-Bay flux of tracer equals the down-bay flux of tracer. Down-bay

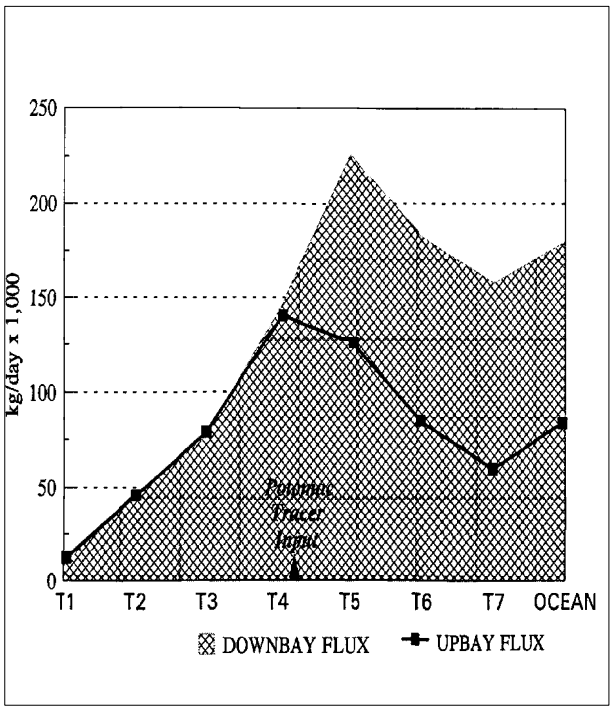

Figure 3. Potomac dissolved tracer flux.

from the input point at Transects 5 through 7, and the ocean transect, the net down-Bay flux (the difference between down-bay and up-bay flux) is equal to 100,000 kg/day, the load input at the tributary head of tide, a section of the graph is described by U, the net estuarine flow moving the input load down-bay.

Ideally, each transect up-bay of the input load would have a net discharge of zero, consistent with mixing across the transect, first up-bay and then down, and balanced by net transport in the downstream direction resulting in a net flux of zero (figure 2). Alternately, each transect down-bay of the input load (x = 0) should have a net discharge of 100,000 kg/day, consistent with the input load. Small variations from the ideal expected net value (such as in figure 2, n = 19 rather than zero) are attributable to transient load adjustments throughout the system as the system concentration adjusts to the dynamic hydrodynamics.

The flux of the Susquehanna dissolved tracer material throughout the mainstem is shown in figure 4. As there is no mainstem region up-bay of the Susquehanna (x is always greater than zero) the net flux at all transects and the ocean boundary approximate 100,000 kg/day, the discharge at the Susquehanna Fall Line. Interestingly, the main-bay transects of 4 and 5 have the highest level of up-bay movement of dissolved tracer material, as indicated by the total flux of Susquehanna tracer (figure 4).

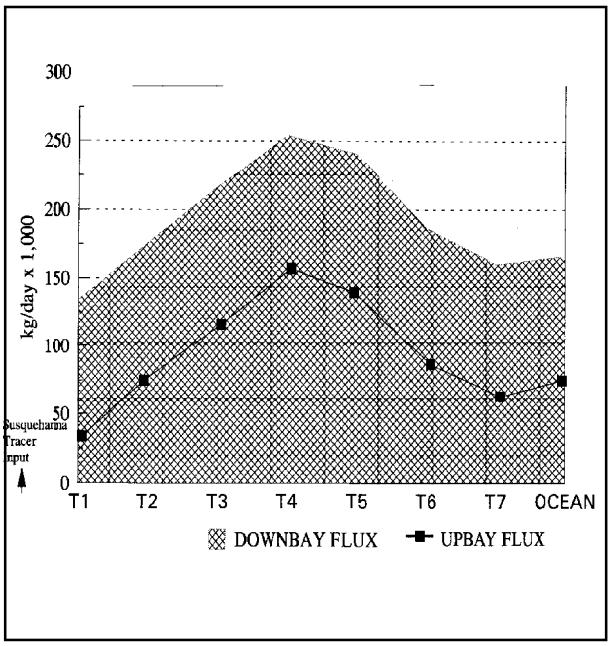

Figure 4. Susquehanna dissolved tracer flux.

The behavior of the James dissolved tracer is very different from that of the Susquehanna (figure 5). Except for the ocean transect, all of the main-bay transects are up-bay from the James mouth (x is always less than zero).

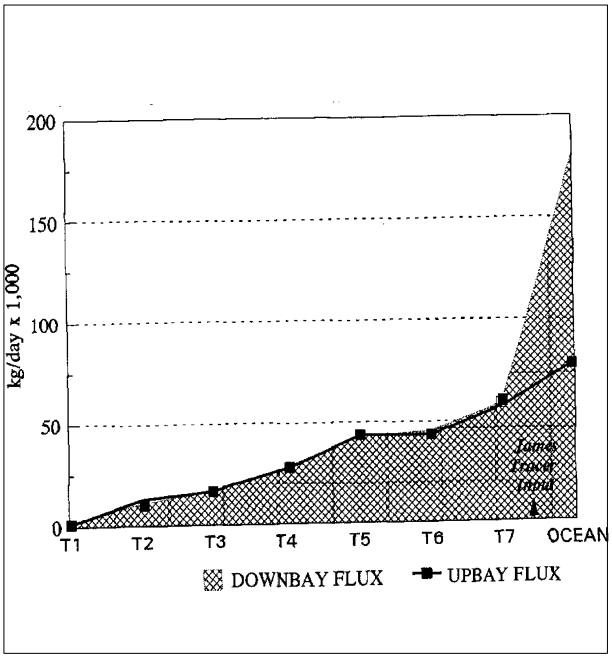

Figure 5. James dissolved tracer flux.

Interpretation of the Dissolved Tracer Fluxes

This analysis is based on a constant load of 100,000 kg/day. The absolute influence of a dissolved tracer from a tributary is attributable to the product of the tributary flow and the tracer concentration. This analysis examines the relative difference among the tributary inputs. To eliminate the influence of flow and to isolate the influence of tributary position in the Bay, a constant load was used. An additional caution must be exercised in the interpretation of these tracer scenarios, as the conservative tracers are not reactive. Nonconservative dissolved and particulate material will behave differently in the more complex water quality model. Nevertheless, these tracer scenarios provide guidance on the influence of different tributaries on the mainstream, and insight into the Bay water quality response to nutrient reductions in the different tributaries.

The tracer fluxes across the eight transects can be compared with respect to the down-bay movement of loads from all tracers (figure 6). The Susquehanna entirely dominates transect 1, with 83% of the total tracer loads coming from the Susquehanna, and 12% from the Patuxent and Potomac. The total tracer load across transect 3 is dominated by the Susquehanna, Patuxent, and Potomac tracers, which are 85% of the total tracer load.

Transect 5 is at the southern end of the deep trench. The flux of material across transect 5 has some importance, as tracer material crossing into region 5 has the potential for contributing to deep trench anoxia problems. The total tracer load across transect 5 (down-bay) is dominated by the Susquehanna (27%), Patuxent (27%), and Potomac (26%) tracers, yet the tracer load from the Rappahannock, York, and James make up 10%, 5%, and 5%, respectively,of the tracer load at transect 5.

Interpretation of the Particulate Tracer Fluxes

The total deposition in the eight main-bay regions and the ocean region is shown in figure 7. The sum of the particulate tracer deposition in all Bay and ocean regions is 100,000 kg/day. The tidal tributary deposition areas are not graphed. Where the total particulate tracer deposition does not equal 100,000 (i.e., the Potomac), deposition in the tidal tributaries is assumed to make up the unaccounted deposition mass.

In the cases of the Susquehanna, Patuxent, Potomac, and Rappahannock, at least 90% of the particulate tracer is deposited within about four

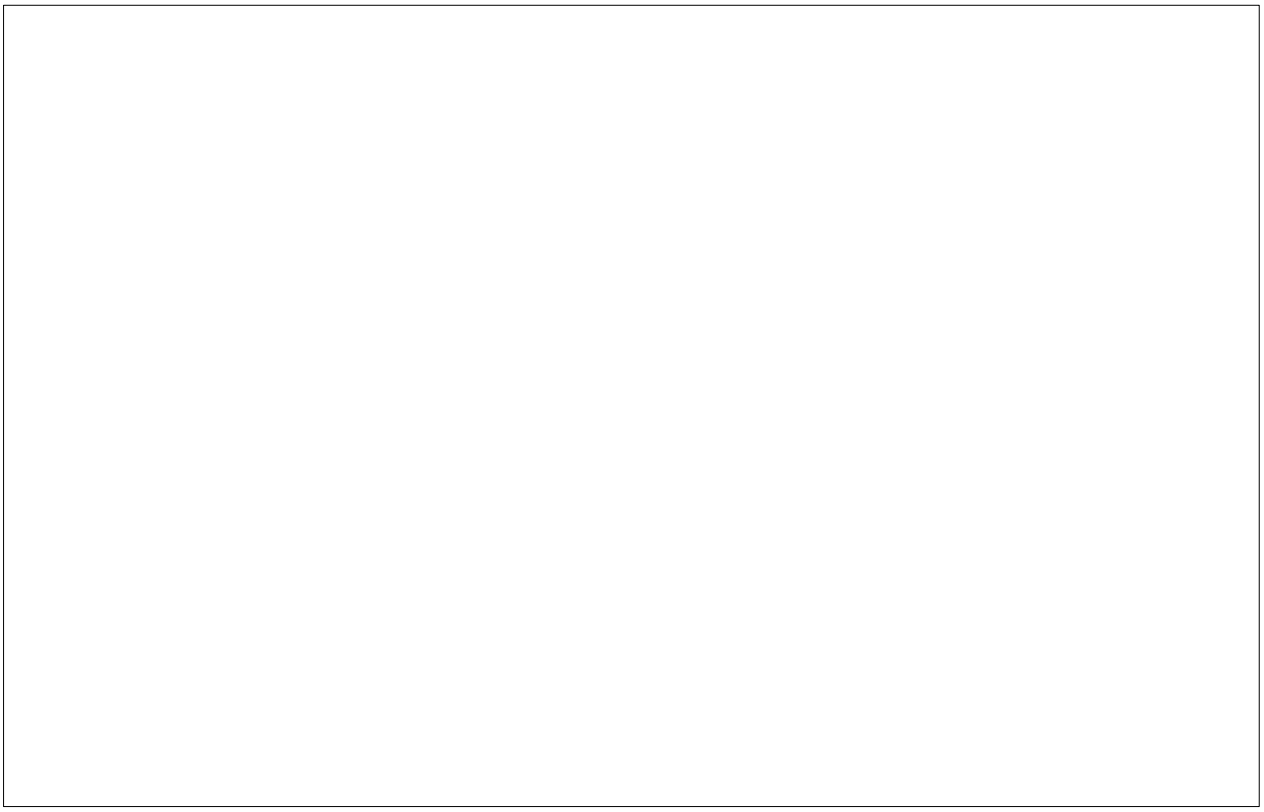

Figure 6. Dissolved tracer flux at all transects.

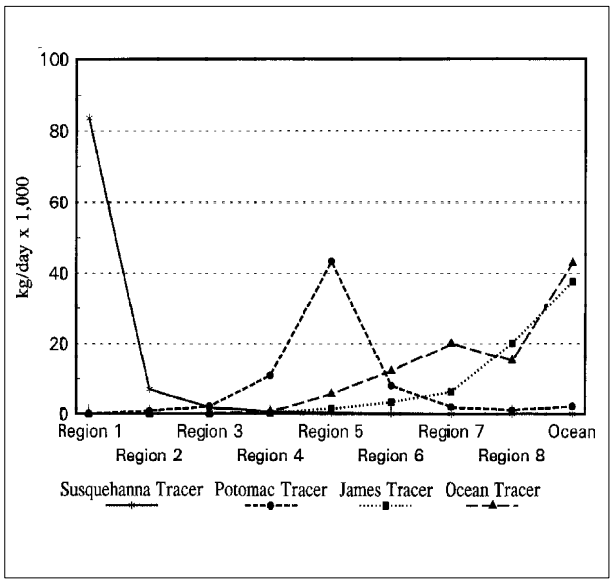

Figure 7. Particulate tracer deposition.

regions from the point of origin. For the York particulate tracer, 82% is deposited in the mainstream and tributaries, and 18% is lost to the ocean. For the James, only 63% of the particulate tracer is deposited in the mainstream and tributaries and 37% of the tracer is lost to the ocean. Particulate tracer released at the ocean boundary is widely dispersed well up into the middle Bay among regions 8, 7, 6, and 5.

CONCLUSION

Dissolved tracer released from major tributary fall lines were distributed throughout the Bay by mixing and transport. Generally, tributaries of the upper and middle Bay distribute greater mass of dissolved tracer throughout the mainstem Bay than lower Bay tributaries. Nevertheless, differences in the down-Bay tributaries can be seen. The Rappahannock is intermediate between the middle and the lower tributaries in the ability to disperse dissolved tracer mass in the mainstem. The Rappahannock tracer flux into region 5 is 38% that of the Potomac tracer in this deep trench region. The flux of the York and James tracer into region 5 is only about 18% that of the Potomac tracer into region 5.

In a program of nutrient reduction the question arises, "What is the efficacy of reducing a unit of nutrient mass in one tributary compared the same reduction of nutrients in another?" On the basis of the tracer analysis, the efficacy of nutrient reductions in the Rappahannock is about 38% that of the Potomac. The efficacy of nutrient reductions in the York and James are about 18% that of the Potomac.

Particulate tracers with a settling rate of 0.1 m/day usually settle within four regions of the point of release. For example, Potomac particulate tracer released at the mouth is transported up-bay into regions 4 and 3 and down-bay into regions 5 and 6. This implies that a reactive particle discharged from a tributary could influence sediment oxygen demand over several up-bay and down-bay regions.

Not surprisingly, the range of spatial influence of the particulate tracer with a settling rate of 0.1 m/day was intermediate between the spatial influence of a particulate tracer with a settling rate of 1m/day examined in a previous tracer study (Thomann et al. 1994) and the dissolved tracer.

ACKNOWLEDGEMENT

The authors wish to acknowledge the state, regional, and federal members of the Chesapeake Bay Program Modeling Subcommittee for their essential guidance and direction throughout the development of the Chesapeake Bay models. In particular, Dr. Thomann is acknowledged for his assistance in the analysis of the tracer scenarios and Drs. Cerco and Johnson are acknowledged for their key roles in development of the water quality and hydrodynamic models of the Chesapeake.

REFERENCES

Cerco, Carl F. and T.M. Cole. 1994. *Three-Dimensional Eutrophication Model of Chesapeake Bay, Vol.1: Main Rep.*. Vicksburg, MS. U.S. Army Corps of Engineers Waterways Experiment Station.

Johnson, Billy H., R.E. Heath, B.B. Hsieh, K.W. Kid, and L. Butler, 1991. *User's guide for a three-dimensional numerical hydrodynamic, salinity, and temperature model of Chesapeake Bay.* ,Vicksburg, MS.: U.S. Army Corps of Engineers Waterways Experiment Station.

Thomann, Robert V., J.R. Collier, A. Butt, E. Casman, and L.C. Linker, 1994. *Response of the Chesapeake Bay Water Quality Model to loading scenarios.* Annapolis, MD. U.S. EPA Chesapeake Bay Program.

Thomann, Robert V. and J.A. Mueller, 1987. *Principles of surface water quality modeling and control.*, New York. Harper and Row.

Toward a Sustainable Coastal Watershed:
The Chesapeake Experiment. Proceedings of a Conference
1-3 June 1994. Norfolk, VA
Chesapeake Research Consortium Publication No. 149

ESTUARY/SHELF EXCHANGE VARIABILITY DUE TO SYNOPTIC -SCALE WIND EVENTS AND FRESHWATER RUNOFF: IMPLICATIONS FOR BIOLOGICAL RECUITMENT

Glen H. Wheless
Old Dominion University

Abstract: The mechanisms by which biological and chemical materials are exchanged between Chesapeake Bay and the adjacent shelf are poorly understood. It is well-known that there is usually a net outflow of water from the Bay to the shelf in the surface waters of the Bay mouth and a net inflow from the shelf to the Bay in the lower levels. Rotational effects deflect the incoming, more saline shelf waters to the northern side of the Bay mouth region while the fresh, buoyant outflowing estuarine waters are moved to the southern reaches of the Bay mouth. A more detailed description of the effects of wind and runoff on the actual circulation in this boundary-dominated area remains to be completed.

A three-dimensional, semispectral primitive equation model was used to examine the effects of synoptic-scale wind variability and episodic runoff on the circulation in the mouth of a wide model estuary representing Chesapeake Bay and on an adjacent sloping shelf. The resulting transport of material from and to the estuary is shown to be strongly influenced by the magnitude and duration of synoptic wind events, much less so by the strength of runoff events. Downwelling favorable winds are shown capable of substantially changing the standard estuarine circulation pattern. Lagrangian trajectories of simulated drifters indicate that this wind-induced shelf/estuary exchange variability plays a large role in the ultimate fate of the larvae of shelf-spawning, estuarine-dependent species. The effects of vertical eddy diffusivity and eddy viscosity on the modeled circulation are also discussed.

INTRODUCTION

The Chesapeake Bay is the largest estuary in the United States and serves as nursery grounds or spawning areas for many commercially important species. A large annualized biomass coupled with convenient port sites has enabled an extensive fisheries industry to thrive in the Bay and adjoining coastal areas. Residential development and recreational activities are also economically and environmentally important to areas in and adjoining the Bay. The wide-ranging impact of these coastal activities places a high priority on developing a more complete understanding of the physical processes that control the overall circulation in the Bay and adjoining continental shelf waters.

Despite the obvious importance of the Bay, the mechanisms by which biological and chemical materials are exchanged between the Bay mouth and the adjacent shelf are poorly understood. Indeed, an accurate description of the overall circulation in this region has yet to be completed. The mean circulation may be described as a net outflow of water from the Bay to the shelf in the surface waters near the Bay mouth and a net inflow from the shelf to the Bay in the lower levels. Rotational effects deflect the incoming, more-saline shelf waters to the northern side of the Bay mouth region while the fresh, buoyant outflowing estuarine waters are moved to the southern reaches of the Bay mouth. Beyond this basic picture, a more detailed description remains to be completed regarding the actual circulation in the Bay mouth and adjoining shelf area and the effects of wind and tidal mixing in this boundary-dominated region. Also poorly understood are how these processes interact with the semipermanent frontal structures found in the Bay mouth region

and to what extent these processes control the transport of shelf-spawning, estuarine-dependent species into the estuarine nursery grounds of Chesapeake Bay.

This paper describes the results of a modeling project designed to develop a more complete understanding of the circulation in the lower Bay and on the adjacent shelf, and to investigate how physical forcing provided by variable wind stress and runoff directly influence the recruitment of shelf-spawning, estuarine-dependentbiological species. A three-dimensional, semispectral primitive equation model (SPEM) was used to examine the effects of synoptic-scale wind variability and episodic runoff on the circulation in the mouth of a wide-model estuary representing Chesapeake Bay and on an adjacent sloping shelf. The resulting transport of material from and to the estuary is shown to be strongly influenced by the magnitude and duration of synoptic wind events, much less so by the strength of runoff events. Downwelling favorable winds are shown to be capable of substantially changing the standard estuarine circulation pattern. Lagrangian trajectories of simulated drifters indicate that this wind-induced shelf/estuary exchange variability plays a large role in the ultimate fate of the larvae of shelf-spawning, estuarine-dependent species.

BACKGROUND

Outflowing buoyant water from a wide estuary or river usually exhibits an initial anticyclonic turn after exiting the coast and becomes a right-bounded coastal plume with an associated coastal current (Chao and Boicourt 1986, Garvine 1987 Chao 1988), the Bay being no exception. The near-field region just seaward of the buoyant outflow area is characterized by intense mixing as the fresh, buoyant outflow merges with the more-saline shelf water. There are often long-lived tidally produced frontal structures present in the Bay mouth, which serve as convergence zones for biological and chemical material. These frontal structures may often be seen well down the coast as they are advected by the coastal current. The mean, idealized description of flow in the Bay mouth and adjacent shelf is that of a standard rotationally affected flow, consisting of lighter fresh water outflowing at the surface along the southern reaches of the Bay and inflowing dense, saline shelf water confined to the northern side at depth. A view into the Bay mouth from the sea would show a tilt to the isopycnals owing to this density structure.

Observations from the Superflux study showed counterintuitive examples to this scenario (Boicourt 1980; see his (figure 14), possibly tied to sudden wind reversals (Wheless 1994). More recent observations across the Bay mouth from ship-towed acoustic Doppler current profilers indicate that extremely small spatial scales of variability and enhanced topographic effects combine to make the actual shelf/estuary circulation much more complex then the simplified idealization would indicate . This extreme variability is attributable to a wide spatial and temporal range in the controlling forcing, most notably that of precipitation and runoff, daily and seasonal wind stress patterns, the strength and duration of tidal mixing, and influences from the adjacent coastal shelf waters. A further complexity is that the circulation is strongly controlled by topography.

The shallowness and boundary-dominated nature of the Bay and adjacent shelf domain make them especially sensitive to wind mixing and forcing effects. Goodrich et al. (1987) demonstrated that the entire Bay may become unstratified owing to a strong fall wind event. It has been apparent for decades that wind forcing can increase or decrease the estuary/shelf exchange based upon direction. For example, it is intuitive to visualize the effect of an eastward wind as increased outflow through the mouth of the Bay and that of a westward wind as an inhibition of outflow. However, the actual response is much more complex. Elliot and Wang (1978) showed that the wind-driven response may also be a combination of local winds in the Bay mouth region and non-local winds over the shelf. In fact, the inner shelf region adjacent to the Bay mouth is dominated by wind-forced motion that may influence the flow in the Bay mouth to a great degree. There is a seasonal aspect to the forcing. Winter winds are mostly northerly and add a downcoast component to the outflowing Bay plume. The effects of this northerly stress on Bay mouth circulation is less well understood, but results from this study indicate a trapping of light water against the southern boundary of the Bay mouth on the Cape Henry side (Wheless 1994). Summer winds are mostly southwesterly, providing conditions favorable for coastal upwelling and offshore transport of the buoyant estuarine plume water. Bay mouth flow is also affected, an increase in the volumetric outflow owing to drift effects being the primary result.

The salinity structure of the Bay is an important indicator of the variability of the circulation there, as well as being a dynamically important driving force through the effects of the resulting density field. The salinity differential between the Bay and the shelf is driven primarily from freshwater runoff, less so by short-term rainfall events although large-scale storms can contribute large amounts of fresh water through the river cachement system (Schubel et al. 1976). In addition to the structure of the estuarine outflow, movement of water through the mouth of a large estuary is partially governed by the history of freshwater discharge through the estuary's tributaries. The strength of nontidal currents as well as the salinity of the estuary waters exiting onto the shelf are affected by the recent characteristics of the fresh water added to the estuary. An increase in freshwater runoff would theoretically increase the strength of the estuarine plume signal as well as the amount of mixing phenomena at the fresh/saline water boundary. The majority of the fresh water entering the Bay comes from the Susquehanna system, with the James, York, and Rappahanock Rivers also contributing substantial amounts of fresh water. Fluctuations in this input owing to changes in rainfall or drainage cause systemic changes to occur throughout the shelf/estuary system. During especially dry years, saline shelf water intrusions have been found as far inland as the city of Hopewell, far up the James River. As with wind forcing, estuarine circulation owing to the changes in runoff values and the associated density structure in the Bay mouth region is also seasonal. Well-mixed conditions prevail in winter, with the velocity structure being reasonably represented via thermal wind equations. Conversely, highly stratified conditions exist in summer and fall, with the resulting dynamics being strongly baroclinic. The upper and lower layers are usually decoupled, and the resulting flow is not easily described.

Biological Recruitment Issues

Clearly, the annual population variability of shelf-spawning, estuarine-dependent biological species is dependent upon both biological as well as physical factors. The links between circulation and species distribution are critical to the survival and subsequent recruitment of a yearclass (Govoni et al. 1989). The larval stages of shelf-spawning, estuarine species are usually widely varied horizontally. Biological behavior such as motile ability, buoyancy charcteristics and affinity for light or water mass characteristics, all contribute to the location of the larvae on fairly small spatial scales. Equally important, yet operating on larger scales, is the advection of the larvae owing to hydrodynamic flow fields and physical hydrography. The complex circulation features in the Bay mouth/shelf region are ephemeral by nature. However, the semipermanent frontal structures located in the mouth and the downcoast-flowing estuarine plume are features that are fairly persistent. These features and their temporal behavior are of potentially great importance to the transport of larval stages into the Bay or their retention on the shelf (Dustan and Pinckney 1989, Govoni et al. 1989, Wheless 1994).

The forcing provided by wind and runoff contributes to and interacts with biological behavior to control the early life ecology of certain species. Variance from the optimum runoff or precipitation amounts can negatively impact the necessary salinity structure necessary for growth and successful recruitment. Wind forcing in the estuary and over the shelf can drive flow that will advect the organisms to or away from preferred nursery areas. Tidal forcing may act in a similar manner, as well as creating areas of convergence in the semipermanent frontal zones found in the Bay mouth. To completely describe all aspects of an entire life cycle of an estuarine-dependent species and the effects of all forcing would be a daunting task indeed. Thus, this study concentrates on the transport phase of an estuarine-dependent organism and examines the effects of external forcing on this transport by calculating Lagrangian particle paths from modeled hydrodynamic flow fields. Early attempts to model larval transport were one- and two-dimensional efforts that did not include vertical migratory behavior (Flierl and Wroblewski 1985). Later efforts have utilized three-dimensional (3D) hydrodynamical models coupled with Lagrangian particles, with vertical behavior based upon biological observations (Hofmann et al. 1991, Werner et al. 1993). This study uses a passive particle strategy with no preordained vertical cycling behavior. Although model limitations coupled with the great differences between advective and biological length scales make this approach somewhat unsatisfying, it enables one to study the effects of basic forcing processes on the shelf-to-estuary transport of an organism and, ultimately, on species mortality rates.

The Model

Field studies have shown that the circulation in the Bay mouth and on the adjacent inner shelf is extremely complex with an inherent three-dimensionality to the motion and a nonlinearity to the dynamics. This fully turbulent, boundary-dominated region is characterized by strong frictional effects, short length and time scales, and frontal structures. To realistically model this domain requires the use of a 3D circulation model with a sufficiently dense grid in both the horizontal and vertical axes as well as accurate boundary and initial conditions, preferrably derived from observations. Recent advances in computational resources now allow highly complex 3D numerical models to be run with reduced grids cales, the resulting high-resolution results not being overly expensive in terms of computing time.

The model used to examine the circulation in the lower Bay was the 3D semispectral primitive equation model (SPEM), which solves a system of primitive hydrodynamic momentum, density, and continuity equations on a horizontal finite difference grid with spectral approximation using Chebyshev polynomials in the vertical. A vertically stretched, sigma-coordinate system is used. Further details regarding the model formulation and usage may be found in Haidvogel et al. (1991).

The model domain used to simulate the Chesapeake Bay was a 116 by 154 km basin, comprised of a flat 20 m deep estuary connected to a linearly sloping shelf by a 22 km wide estuary mouth as shown in figure 3. A constant horizontal grid spacing of 1.2 km was used. Nine sigma levels were used for vertical resolution. The time step was 43 sec. The model was initially quiescent and unstratified, with a constant reference density of 1,026 kg/m^3. A buoyancy flux was turned on at the northern end of the model Bay and ramped up to a maximum outflow velocity of 20 cm/sec and a density anomaly of 10 sigma-T, yielding an internal radius of deformation, R_i, of O (10 km). The density anomaly and outflow velocity were varied linearly from a maximum at the surface to zero at the bottom. This forcing is held constant throughout the simulations. The forcing scenario simulates a large runoff event, or the reformation of a buoyancy flux after an up-estuary wind stress event. Figures in this article show a subdomain of the full model domain used in the calculations.

SPEM allows one to choose between mixing along either *insitu* density surfaces or geopotential surfaces. Vertical diffusivities of momentum and density (via temperature and/or salinity) may be allowed to vary horizontally and vertically according to Richardson number dependence. However, in an attempt to simulate the highly frictional inner shelf environment, values for vertical eddy diffusivity for both momentum and temperature were held constant at $8 \times 10^{-4} m^2/s$. Values for vertical eddy viscosity of momentum and temperature were set at $5 \times 10^{8} m^4/s$, also constant through the water column. Horizontal mixing was provided by biharmonic sub grid scale mixing along sigma surfaces. Linear bottom friction was used and was allowed to decrease offshore from an initial value of 5.0×10^{-4} m/s. Nonlinear advection of momentum and density was allowed.

One would like to have a classification system whereby certain physical parameters would allow a particular system to be related to specific dynamical behavior. A convenient parameter for classifying a buoyant outflow system and its related dynamics is the Kelvin number, K, a ratio of the internal Rossby radius, R_i, and the system length scale, L, usually the outflow width or plume length scale (Garvine 1994). For $K > 1$, rotational effects are important to the dynamics of the system, the outflow becoming a coastal current system. Small K indicates the decreased importance of rotation and the increasingly nonlinear behavior of the system. Using the width of the model Bay mouth as the length scale, the Kelvin number is therefore larger than one, signifying the importance of rotation on the dynamics of this modeled system.

RESULTS

After 6 days of simulation, the estuarine buoyancy flux has moved down the western wall of the estuary and out of the estuary mouth to form a buoyant plume (figure 1a). The plume rotates anticyclonically as it exits the estuary (figure 1b) and the turning region just offshore the estuary mouth scales in width with the internal radius. A coherent coastal current is also beginning to form. Vertical velocities are positive in the turning region, with significant downwelling near the nose of the plume, caused in part by the overrun of the decelerating nose by faster water behind in addition to the downwelling motion caused by the impact of the plume with the coastal sidewall. Near-bottom flows in the estuary mouth show areas of flow reversal (figure 1c), indicative of strong vertical velocity shear. In a view looking back into the estuary mouth, a classic estuarine circulation

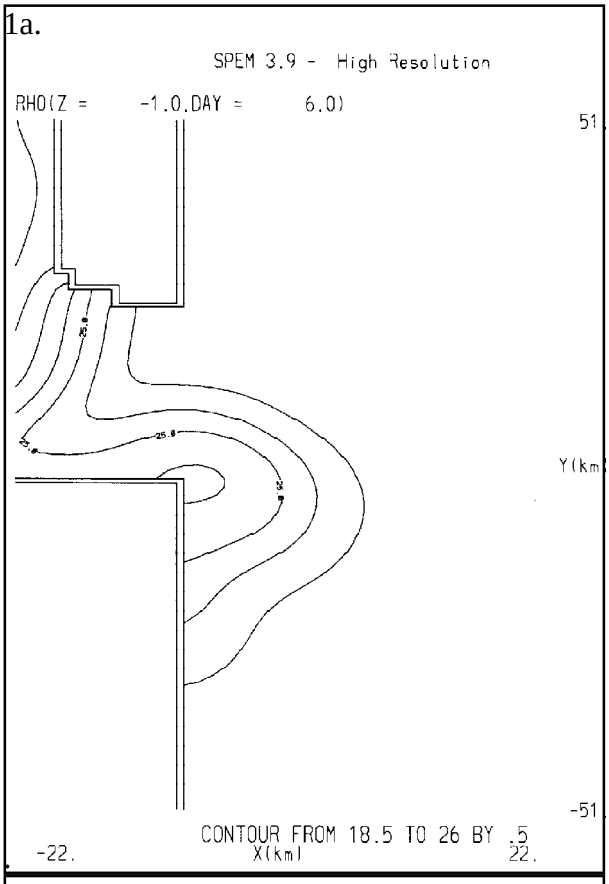

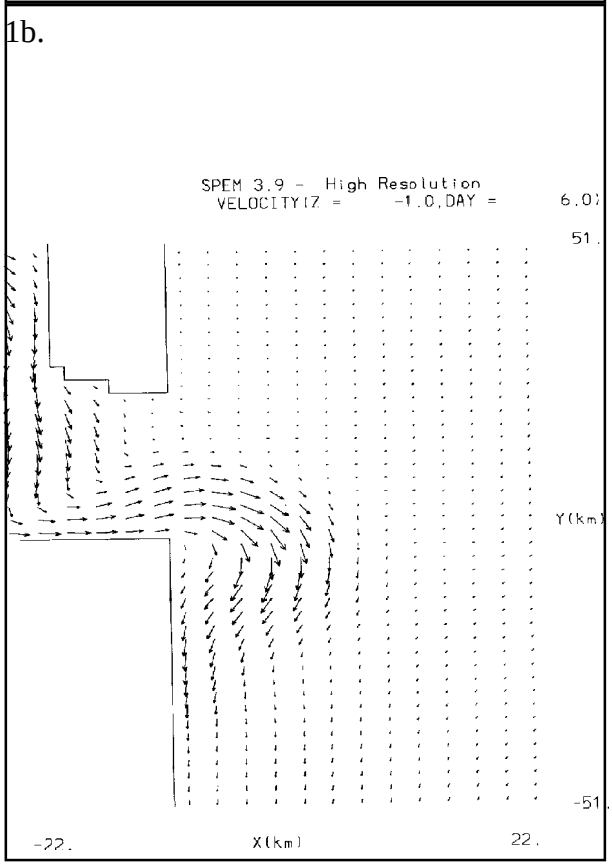

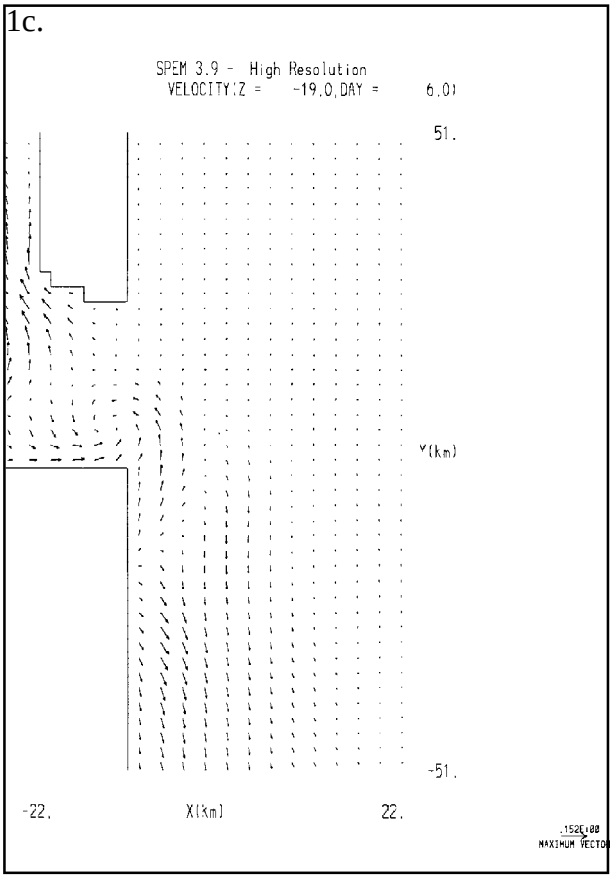

Figure 1. Surface density (1a) and velocity (1b) and near-bottom velocity (1c) fields after 6.0 days of constant outflow from a 20 km wide estuary. Rotational effects have confined the outflow to the southern reaches of the estuary, with inflow occurring in the north.

pattern has developed, with the outflowing buoyant water confined to the righthand area of the estuary mouth and a weak return subsurface flow of saline shelf water on the opposite side of the estuary mouth (figure 2).

After 6.5 days of simulation, a temporally varying wind stress field, constructed from an observed wind climatology, was applied to the evolving model solutions. The model wind stress field was constructed from observations taken from the Chesapeake Light Tower (located offshore of the Chesapeake Bay mouth) and Diamond Shoals Light (located approximately 120 km to the south of the Bay mouth) during February of 1988. For both stations, there are minimal breaks in the data. Missing values were filled using a simple averaging between adjacent temporal data points. Wind speeds in m/sec were converted to stress values using the standard quadratic law with a

drag coefficient of 1.3 x 10^-3. The observations were 40hr low-pass filtered and spatially averaged and then allowed to increase linearly offshore to a value approximately 1.5 times the measured value. This particular segment of observations was chosen as a representative cold front passage, with a complete wind reversal over a period of approximately 5 days (figure 3).

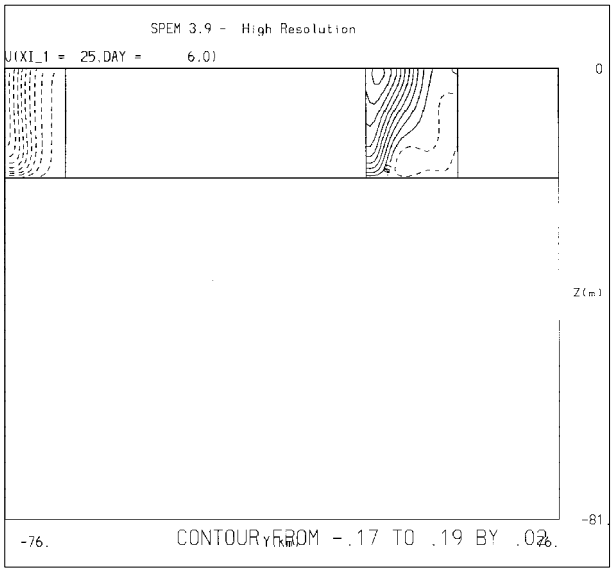

Figure 2. Velocity field in the Bay mouth at 6.0 days. Classic estuarine flow pattern has developed, with buoyant outflow confined to the southern reaches of the Bay mouth and a weak subsurface saline shelf return flow.

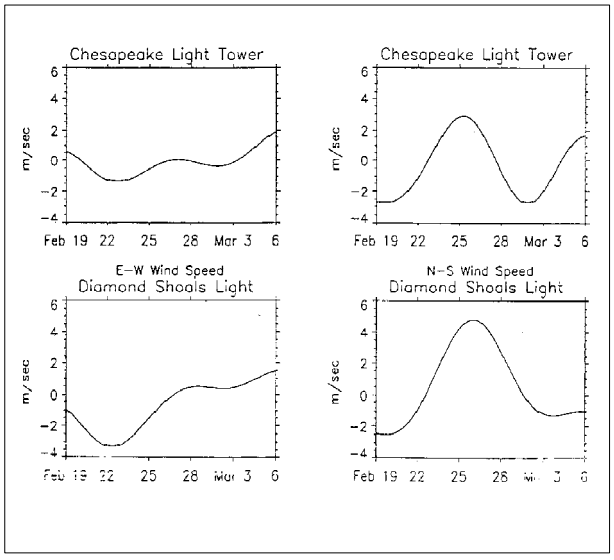

Figure 3. Time series of filtered wind speed components observed at Chesapeake Light Tower and Diamond Shoals Light in February 1988 and used as model forcing.

After 12 days of simulation, just before the time of maximum upwelling-favorable wind stress, the turning region is still evident but expanded in area. Northward spreading of the buoyant water in the Bay mouth may be seen, with the maximum outflow now located near the northern reaches of the Bay mouth. The plume is spread well offshore owing to Ekman drift, and the dynamics of the turning region are now controlled by the effects of the wind stress rather than by that of geostrophy. The coastal current has been decreased in magnitude and there is slight offshore flow present (figure 4a) in the region south of the Bay mouth. Very close to the bottom in the Bay mouth, saline shelf water with positive potential vorticity flows into the estuary (figure 4b) and there is a strong northerly-flowing subsurface jet.

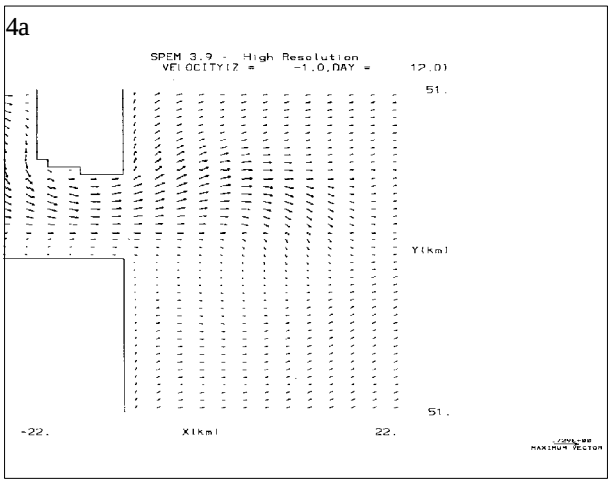

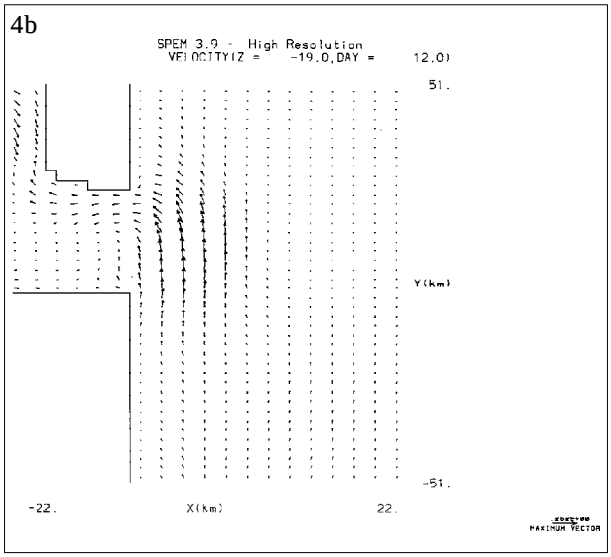

Figure 4. Surface velocity (4a) and near-bottom velocity (4b) fields after 12.0 days of constant outflow with maximum upwelling-favorable wind stress.

At 15 days the winds have now fully reversed to be downwelling favorable. Surface flow is once again in the form of a strong down-coast jet, the effects of the wind augmenting the geostrophic effects in the re-emergent turning region figure 5a). Near-bottom flows just outside the estuary mouth are opposite in direction to those at the surface (figure 5b). There is a large amount of vertical shear found in this region with correspondingly high amounts of mixing. Density contours near the bottom are now more closely aligned with the isobaths (figure 5c), allowing the density-topography interaction associated with the JEBAR (Joint Effect of Baroclinicity and Relief) effect to be more important as a flow driving mechanism (Shaw and Csanady 1983, Wheless and Klinck 1994). Circulation in the Bay mouth consists now of two regions of flow directed into the estuary (figure 6), a situation found in the mouth of Chesapeake Bay several times during the Superflux experiment (Boicourt 1980).

Lagrangian floats released near the surface track with the coastal current and clearly show the effects of the wind as they move offshore with the Ekman drift, then back onshore (figure 7a). Floats released near the bottom are less affected by the coastal current and act much differently (figure 7b). Bottom floats initially released near the southern boundary of the Bay mouth (the righthand wall looking seaward) are initially ejected from the estuary and then are advected back into the Bay owing to the strongly reversing bottom currents. In contrast, those bottom floats initially released near the northern side of the estuary mouth are immediately advected into the estuary, are lifted in the rising flow and then ejected out of the estuary in the near-surface seaward flow. Bottom floats released well offshore show little motion.

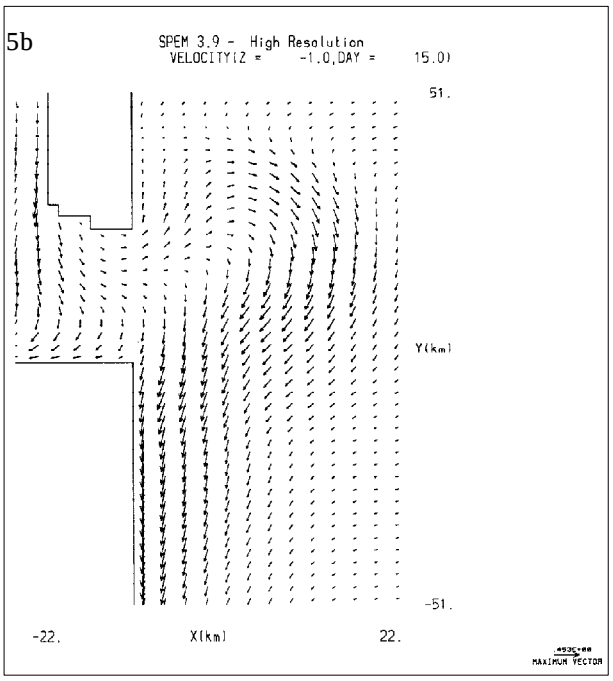

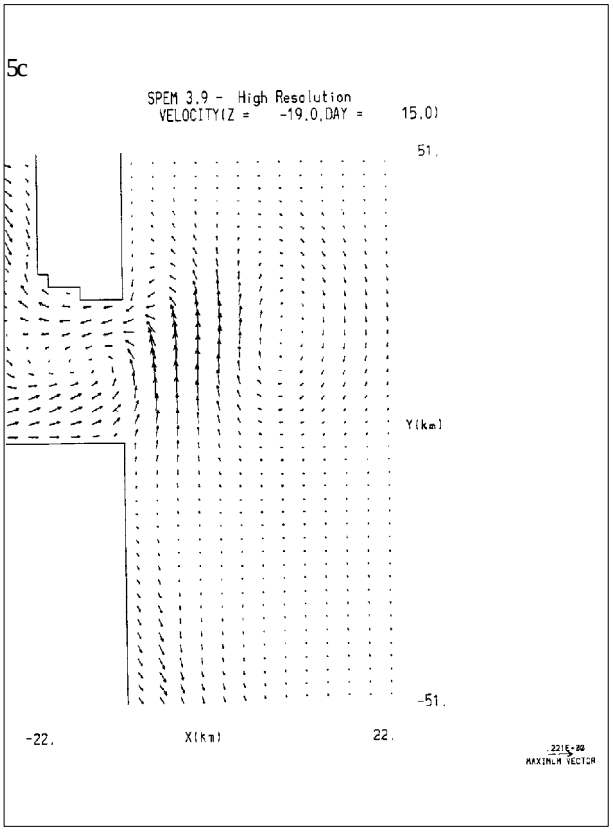

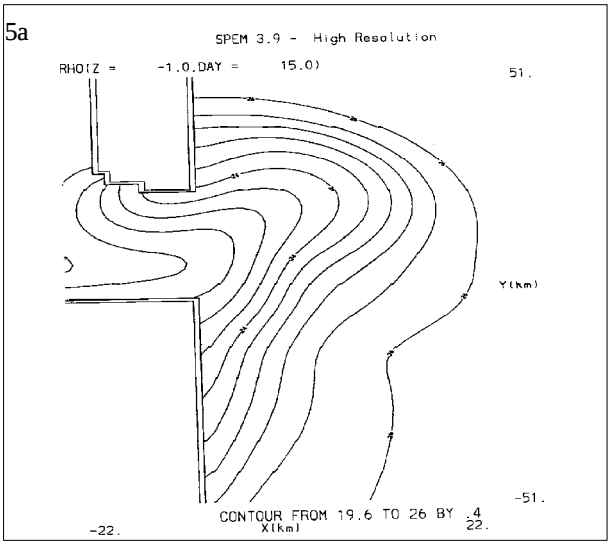

Figure 5. Surface density (5a) and velocity (5b) and near-bottom density (5c) and velocity (5d) fields after 15.0 days of constant outflow and at time of maximum downwelling-favorable wind stress.

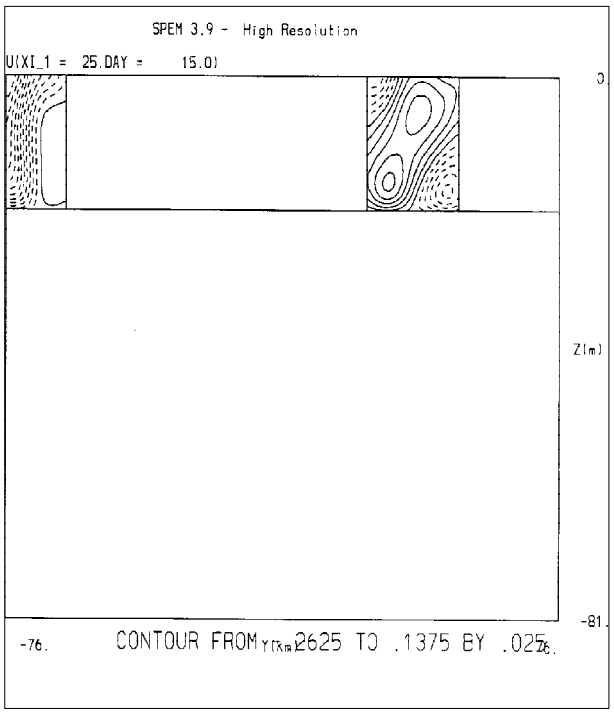

Figure 6. Velocity field in the Bay mouth at 15.0 days. Classic estuarine flow pattern has given way to a bimodal velocity distribution, attributed to wind reversal associated with frontal passage.

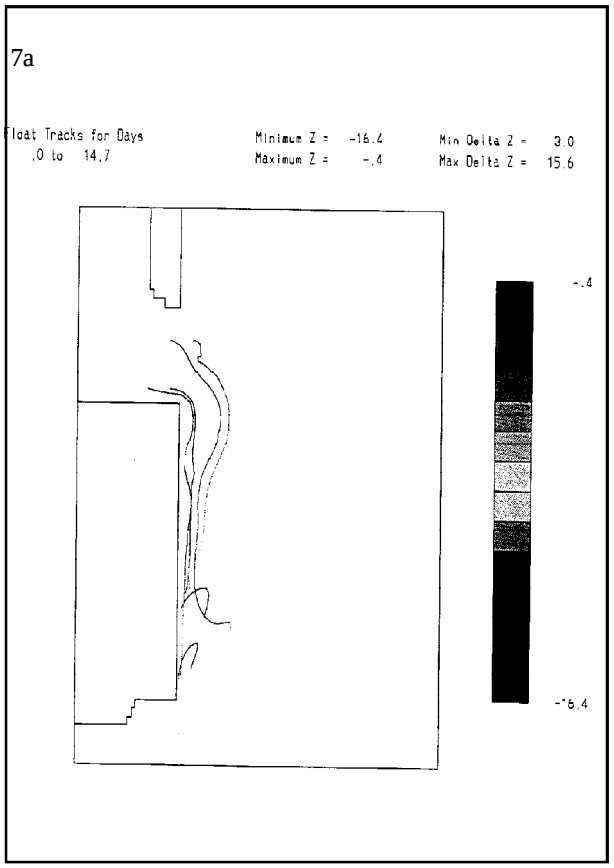

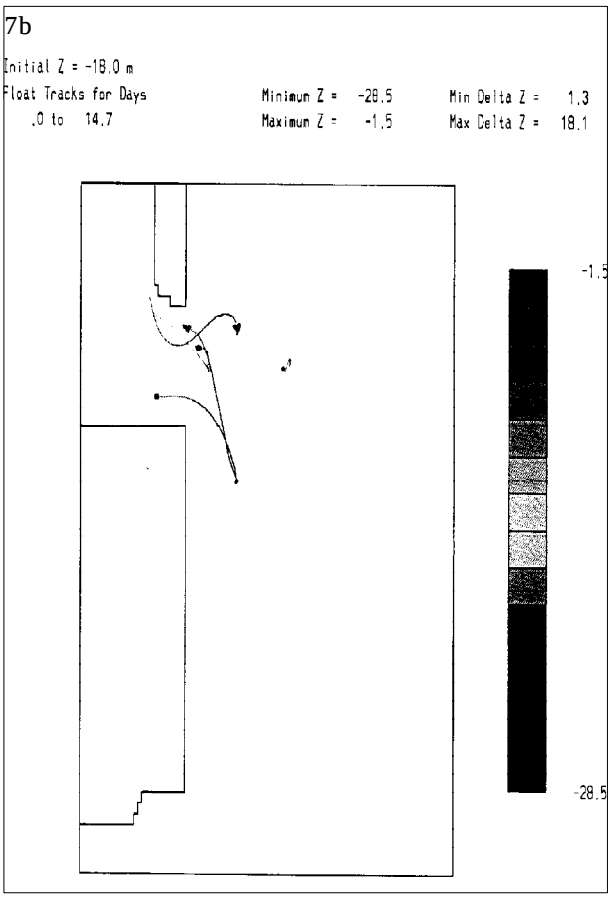

Figure 7. Particle tracks for surface-released drifters (7a) and those released near the bottom (7b). Solid plotting denotes shallow surface locations; stippling indicates deeper depths. The black dot shows start positions of the drifters.

DISCUSSION

In the absence of wind stress, the model reproduces the standard rotationally controlled circulation pattern of a wide estuary, that is, a buoyant plume and associated coastal current. The width of the plume and the turning region scale well with the internal radius of deformation. Strong vertical velocities and mixing are found in the nose of the plume as well as in the turning region. After the plume and coastal current are generated owing to buoyancy inputs as described in the previous section, the model plume responds at first order to the effects of the variability of the synoptic-scale wind stress as does much of the observed subtidal current variability in the Mid-Atantic Bight (Beardsley et al. 1979).

The effects of wind forcing on the behavior of estuarine outflow are clearly shown in the results of this study. Along-coast, downwelling-favorable wind stress augments the effects of rotation in the Bay mouth to keep the fresh, more buoyant estuarine water located in the southern reaches. Additionally, it thins the buoyant plume and accelerates the coastal current. Coastal sea surface height is augmented in this case, the resulting geostrophic current component complementing the coastal current. In contrast, upwelling-favorable wind stress broadens the area of fresh water in the Bay mouth, spreads the plume owing to Ekman drift, and retards the coastal current. The decrease in surface height at the coast and the corresponding upcoast geostrophic component combines with the upcoast wind drift to counter the down-coast-flowing coastal current. Crossshore wind stress effects are primarily Ekman drift effects.

In the context of biological recruitment, wind-forced variability exerts strong control on the transport of passive particles. In particular, the behavior of the near-bottom floats highlights the great difficulty in quantitatively describing the fate of estuarine-dependent larval stages. In addition to wind drift of the particles in the near-surface layer, the strong circulation cells found throughout the water column in the mouth of the Bay serve to advect neutral floats in unexpected ways, the initial location of the floats controlling their fate. Those initially released in the Bay mouth near the surface are invariably transported down the coast by the strong coastal current. Motion of bottom-released floats is less easily described. The direction, duration, and timing of wind events controls the eventual transport of the bottom floats as the water column undergoes strong shearing, both vertically and horizontally. For those larvae whose position in the water column is based on an active repsonse to an estuarine salinity signal, wind forcing clearly will exert control over their ability to enter the estuary indirectly through the dynamic variability of the salinity structure as well as directly via drift.

The strength and depth of the northern Bay buoyancy flux controls the non-wind-forced flow in the Bay mouth as well as on the adjacent shelf. There are basic physical differences between the behavior of a thin, surface plume and the coastal outflow that remains connected with the bottom over a substantial portion of its length. A surface-to-bottom inflow, simulating a strong runoff event or the flow in a well-mixed winter estuary, has a strong barotropic response to forcing. The vertical velocity profile of the coastal jet south of the Bay mouth in this case satisfies thermal wind relations referenced to the bottom and is bottom-diminished; maximum flow magnitudes occur at the surface and decrease with depth, in some areas reversing direction. Conversely, experiments with a thin surface inflow (not shown) show a primarily decoupled, two-layer velocity structure, similar to the results of Garvine (1987) and O'Donnell (1990). Surface-to-bottom buoyancy flux may also remain in contact with the bottom and be subject to a density-topography interaction as the mass field interacts with the sloping shelf. This so-called JEBAR effect is a locally important flow generation mechanism for the surface-to-bottom plume, yet not for the thin, surface plume which essentially remains uncoupled from topographic effects. Frictional dissipation owing to bottom drag strongly controls the maximum advective speed of the surface-to-bottom plume. A thin plume experiences much less control from bottom drag. Vortex tube stretching effects are also different for the two scenarios. As Munchow and Garvine (1993) point out, the thin plume gains anticylonic vorticity owing to layer thinning at the edge of the plume while cyclonic vorticity is induced in the surface-to-bottom plume as the bottom depth increases over the sloping shelf.

CONCLUSION

This paper has discussed results from a 3D modeling study of circulation in Chesapeake Bay induced by strong surface-to-bottom buoyancy forcing and the effects of wind forcing on this flow and on the transport of neutrally buoyant Lagrangian floats. Rapid wind reversals that often characterize the passage of winter cold fronts have been shown to control the strength and structure of the circulation in the Bay mouth and the exchange between the estuary and the shelf. Vertical velocities in the Bay mouth proper are shown to be quite variable owing to the boundary-dominated nature of the region. The initial horizontal and vertical positioning of particles released in the mouth of the Bay controls their ultimate fate. Implications for biological recruitment are clear. Larvae able to control their position in the water column owing to motile ability and triggered by environmental cueing are much more likely to become part of the successful recruited yearclass.

REFERENCES

Beardsley, R. C.., and W. C. Winant. 1979. On the mean circulation in the Mid-Atlantic Bight. J. Phys. Oceanogr. bf 9: 612-619.

Boicourt, W. C., 1980. Circulation in the Chesapeake Bay entrance region: Estuary-shelf interaction. In : Campbell, J. W. and J. P. Thomas, eds. Chesapeake Bay plume study: Superflux 1980. NASA conference publication 2188.

Chao, S.-Y., 1988. River-forced estuarine plumes. J. Phys.Oceanogr. 18: 72-88.

Chao, S.-Y., and W.C. Boicourt. 1986. Onset of estuarine plumes. J. Phys. Oceanogr. 16: 2137-2149.

Dustan, P., and J. L. Pinckney Jr. 1989. Tidally induced estuarine phytoplankton patchiness. Limnol. Oceanogr. 34(2): 410-419.

Elliot, A. J., and D. P. Wang. 1978. The effect of meteorological forcing on the Chesapeake Bay: The coupling between an estuarine system and its adjacent coastal waters. In Nihoul, J. C. J., ed. Hydrodynamics of estuaries and fjords, pp. 127-245, New York: Elsevier Publishing.

Flierl, G., and J. S. Wroblewski. 1985. The possible influence of warm core Gulf Stream rings upon shelf water larval fish distribution. Fish. Bull.83: 313-330.

Garvine, R. W. 1987. Estuary plumes and fronts in shelf waters: A layer model. J. Phys. Oceanogr. 17: 1877-1896.

Garvine, R. W. 1994. A classification system for buoyant coastal discharge (abstract). EOS 75(3).

Goodrich, D. M., W. C. Boicourt, P. Hamilton and D. W. Pritchard. 1987. Wind-induce destratification in Chesapeake Bay. J. Phys. Oceanogr. 17: 2232-2240.

Govoni, J., D. Hoss, and D. Colby. 1989. The spatial distribution of larval fishes about the Mississippi River plume. Limnol. Oceanogr., 34(1): 178-187.

Haidvogel, D. B., J. L. Wilkin, and R. Young. 1991. A semi-spectral primitive equation ocean circulation model using vertical sigma and orthogonal curvilenar horizontal coordinates. J. Comp. Phys. 94: 151-185.

Hofmann, E. E., K. S. Hedstrom, J. R. Moisan, D. B. Haidvogel, and D.L. Mackas. 1991. Use of simulated drifter tracks to investigate general transport patterns and residence times in the coastal transition zone. J. Geophys. Res. 96: 15,041-15,052.

O'Donnell, J. 1990. The formation and fate of a river plume: A numerical model. J. Phys. Oceanogr. 20: 551-569.

Munchow, A., and R. W. Garvine 1993. Dynamical properties of a buoyancy driven coastal current. J. Geophys. Res. 98: 20,063-20,077.

Schubel, J. R., H. H. Carter, and W. B. Cronin. 1976. Effects of Agnes on the distribution of the salinity along the main axis of the Bay and in contiguous shelf waters. In: The effects of Tropical Storm Agnes on the Chesapeake Bay estuarine system pp.33-56. Chesapeake Research Consortium, publication no. 54. The Johns Hopkins University Press.

Shaw, P. T., and G. T. Csanady. 1983. Self-advection of density perturbations on a sloping continental shelf. J. Phys. Oceanogr. 13: 769-782.

Werner, F. E., F. H. Page, D. R. Lynch, J. W. Loder, R. G. Lough, R. I. Perry, D. A. Greenberg and M. W. Sinclair. 1993. Influences of mean advec tion and simple behavior on the distribution of cod and haddock early life stages on Georges Bank. Fish. Oceanogr. 2:2: 43-64.

Wheless, G. H. 1994. Effects of variable wind stress on the behavior of a buoyant estuarine plume. EOS 75(3) and in preparation for submission to J. Geophys. Res.

Wheless, G. H., and J. M. Klinck. 1994. The evolu tion of density drivencirculation over sloping bottom topography. Elsevier Publishing. J. Phys. Oceanogr.